Outdoor testing station for solar cells

Sakari Lepikko

School of Science

Thesis submitted for examination for the degree of Master of Science in Technology.
Espoo 30.01.2017.

Thesis supervisor:

Prof. Peter Lund

Thesis advisor:

D.Sc. (Tech.) Kati Miettunen

Aalto University
School of Science

AALTO UNIVERSITY
SCHOOL OF SCIENCE

ABSTRACT OF THE
MASTER'S THESIS

Author: Sakari Lepikko

Title: Outdoor testing station for solar cells

Date: 30.01.2017 Language: English Number of pages: 60+16

Department of Applied Physics

Professorship: Energy Systems Code: SCI-3056

Supervisor: Prof. Peter Lund

Advisor: D.Sc. (Tech.) Kati Miettunen

The focus of this work is on the preparation and testing of a measurement system for real life outdoor testing of emerging photovoltaic devices, namely dye-sensitized solar cells and perovskite solar cells. While laboratory level accelerated aging tests for solar cells are a powerful tool for studying the stability of the cells in longtime operation, such tests do not cover all environmental variations present under real outdoor environment. Hence, when going forward in lifetime testing, outdoor testing of the emerging solar cell technologies becomes critical in evaluation of their suitability for commercialization.

The new station was designed according to ISOS standards for organic solar cell outdoor aging tests: it is capable to monitor the current-voltage characteristics of the tested cells, provide adjustable electric load for the cells, and record weather values. A short aging test was performed with this new station for dye-sensitized solar cells during late autumn in Finland, when the weather varied from mildly warm autumn weather to freezing and snowy. The lightly encapsulated cells did suffer from degradation during the test since their short circuit current decreased. The degradation did not occur during the frosty period but instead during the warmer, rainy periods so the cause of degradation was most likely moisture.

Additionally, the tested cells were able to generate current at sub-zero temperatures about as well as in warmer environments, which has not been previously reported in literature for dye-sensitized solar cells.

Keywords: aging, degradation, efficiency, solar cell outdoor testing, dye-sensitized solar cell, perovskite solar cell

AALTO-YLIOPISTO
PERUSTIETEIDEN KORKEAKOULU

DIPLOMITYÖN
TIIVISTELMÄ

Tekijä: Sakari Lepikko

Työn nimi: Aurinkokennojen ulkotestausasema

Päivämäärä: 30.01.2017 Kieli: Englanti Sivumäärä: 60+16

Teknillisen fysiikan laitos

Professuuri: Energiatieteet Koodi: SCI-3056

Valvoja: Professori Peter Lund

Ohjaaja: Dosentti Kati Miettunen

Tämän työn aiheena on kehittyvien aurinkokennojen, etenkin väriaineherkistettyjen ja perovskiitti-aurinkokennojen, ulkotestausaseman rakentaminen ja testaaminen. Laboratoriotason aurinkokennojen kiihdytetyt ikäännytyskokeet ovat tehokas työkalu tutkimaan kennojen vakautta pidemmän ajan käytössä, mutta nämä kokeet eivät kata kaikkia oikeassa ulkoilmassa esiintyviä vaihteluita. Tästä johtuen, kehittyvien aurinkokennoteknologioiden testaaminen ulko-olosuhteissa on tärkeä vaihe, kun niiden soveltuvuutta kaupallistamiseen arvioidaan.

Laitteiston suunnittelussa huomioitiin ISOS standardit orgaanisten aurinkokennojen ulkoikäännytysmittauksille: se mittaa testikennojen virta-jännite yhteyttä, kuormittaa kennoja sähköisesti sekä tallentaa sääarvoja. Uudella laitteistolla suoritettiin myös lyhyt ikäännytyskoe väriaineherkistetyillä aurinkokennoilla myöhään syksyllä, jolloin sää vaihteli lämpöisestä syyskelistä lumisiin pakkaskeleihin. Kevyesti suojatut testikennot kärsivät kulumisesta testauksen aikana, koska niiden oikosulkuvirta laski. Kuluminen ei kuitenkaan ajoittunut pakkasjaksoon, vaan lämpöisempiin sadejaksoihin, eli kulumisen syy oli mitä luultavimmin kosteus.

Testatut kennot pystyivät lisäksi tuottamaan virtaa pakkasessa kutakuinkin yhtä lailla kuin lämpöisemmässä kelissä, mistä ei ole aikaisempaa tutkimusta kirjallisuudessa väriaineherkistettyjen aurinkokennojen alalla.

Avainsanat: ikääntyminen, kuluminen, hyötysuhde, aurinkokennojen ulkotestaus, väriaineherkistetty aurinkokenno, perovskiitti-kenno

Preface

I thank D.Sc. Kati Miettunen, the instructor of my thesis, for guiding me throughout the thesis work, and especially for giving valuable tips for writing the thesis. I also thank Prof. Peter Lund, the supervisor of my thesis, for giving a chance to make the diploma thesis in the New Energy Technologies group that had provided inspiring and supporting working environment. Especially, the coffee break discussions have given positive mood boost to keep working during the last working hours afternoons. The whole group deserves great thanks.

I give special thanks for Aapo Poskela, a colleague and a friend, for teaching me to not only to assemble solar cells but also for teaching me to do the characterization of the cells. It has been a great help. Armi Tiihonen, a colleague and friend, too, deserves also thanks for giving guidance in many questions, especially in the early steps of my work.

Lastly, I thank my family and friends for offering possibility to shift from work life to leisure time. Without good rest the quality of my thesis work would not have been on this level.

The work has been funded and made possible by Academy of Finland through SOLID project.

Contents

Symbols and abbreviations

Symbols

FF	Fill factor
I	Current
I_o	Diode dark current
I_{cell}	Output current of solar cell
I_{mpp}	Maximum power point current
I_{ph}	Photo current
I_{sc}	Short circuit current
K	Acceleration factor
$k_{accelerated}$	Solar cell degradation rate in accelerated aging test
K_B	Boltzmann's constant
$k_{outdoor}$	Solar cell degradation rate in outdoor environment
m	Diode ideality factor
P	Power
P_{max}	Solar cell maximum power point
P_{sun}	Solar irradiance
q	Elemental charge
R_{CE}	Charge transfer resistance of counter electrode
R_D	Mass transport resistance of counter electrode
R_s	Ohmic series resistance
R_{se}	Operating cell resistance
R_{sh}	Shunt resistance
R_{TiO2}	Photoelectrode film resistance
T_K	Absolute temperature
V	Voltage
V_{cell}	Output voltage of solar cell
V_{mpp}	Maximum power point voltage
V_{oc}	Open circuit voltage
η	Solar cell efficiency
η_{COL}	electron collection efficiency
η_{INI}	electron injection efficiency
η_{IPCE}	total incident photon-to-electron conversion efficiency
η_{LH}	light harvesting efficiency

Abbreviations

ACN	Acetonitrile
c-SI	Crystalline silicon solar cell
DSSC	Dye-sensitized solar cell
EIS	Electrochemical impedance spectroscopy
e^-	Electron
ETL	Electron transport layer
FTO	Fluorine doped tin oxide
h^+	Hole (positive charge carrier in semiconductor)
HOMO-level	Highest occupied molecular orbital
HTL	Hole transport layer
IPCE	Incident Photon-to-electron Conversion Efficiency
IP	Power-voltage
IV	Current-voltage
LUMO-level	Lowest unoccupied molecular orbital
Omh-PSC	Organometal halide perovskite solar cell
PV	Photovoltaic
S	Dye molecule (any)
SMU	Source measure unit
TBA	Tert-butylalcohol
TCO	Transparent conducting oxide
UV	Ultraviolet light
VI	Virtual instrument sub program in LabVIEW

1. Introduction

The world energy production is facing a dramatic challenge: how to provide an increasing amount of electricity for people around the world while giving up the fossil fuels as an energy source? Furthermore, the new capacity to produce electricity should preferably be low-cost so that the world economics can withstand the massive investments on new energy technologies. This has driven the scientific communication looking for alternative energy sources and a variety of possibly utilizable ones have been found. Out of these sources, sun light has proven to be the most easily accessible globally. The use of sun light as a direct energy source has grown rapidly, especially in electricity production where the growth has been exponential [1]. For example, in 2006 the cumulative installed photovoltaic (PV) capacity was between 6 and 7 GW, in 2010 around 40 GW and in 2014 almost 180 GW.

However, PV accounts only for one percent of electricity generation worldwide at the moment [1] and its installation pace has started to decrease after 2011. There are several limiting factors that are behind the slowing of the PV installations. One important limitation is the high investment cost for PV panels. The most mature photovoltaic technology, crystalline silicon solar cells (c-Si), has become quite well developed and decreasing its price further is difficult. There are challenges regarding the price of c-Si panel systems for both commercially operating electricity suppliers and private households. Currently, the price of c-Si panel array with inverter and installation included is about 2.5 €/nominal power of the panel (W_p) for household-scale [2]. The grid parity is achievable with this price level, but the 10 to 20 €k cost of typical household sized array is easily considered too high. The high initial investment means that the payback time of the array is 10 to 25 years. For utility-scale c-Si arrays the price is lower, about 1.7 €/W_p [2], but the hindrance on the utility side is that the electricity suppliers have to be able to match the electricity generation to the demand. Photovoltaics have highly variating power output so the suppliers have to invest in fast adjustability of their other power sources in addition to the PV arrays if they already have a significant share of photovoltaics or wind power in their power portfolio.

The high price of crystalline silicon solar cells has steered the development of photovoltaics for looking for alternative, cheaper PV technologies. One such promising technology is dye sensitized solar cell (DSSC). Currently, it is still under development and has not yet penetrated to the markets but its price estimation in large scale production is relatively low, less than 0.75 €/W_p, due to two reasons [3]. Firstly, its material costs could be smaller than c-SI cells since the dye sensitized cell type requires only small amounts of expensive materials. Furthermore, there are several alternative material options for DSSCs, which makes it possible to economically optimize the ratio of cost and performance [3]. Secondly, the whole panel could be assembled by printing or roll-to-roll technology, which reduces the equipment and time needed for the panel assembly [3].

DSSCs have also two performance related advantages compared to c-SI solar cells. Their electricity production decreases less than c-SI when light intensity decreases [4] and their electricity production may even slightly increase

when temperature rises from warm to hot (> 60 °C) whereas the electricity production of silicon solar cells decreases significantly [5]. These two features are very good since they also stabilize to some extent the electricity production levels of DSSCs.

One main reason why dye-sensitized solar cells have not yet penetrated to the consumer markets is their limited lifetime. The DSSC operation principle is based on repeatable electrochemical reaction cycle. Grätzel pointed out that during a 20-year operation time (corresponds to the lifespan of c-SI panels) the chemical reaction cycle (see Chapter 2) occurs roughly 100 million times [6]. Hence, the probability for any alternative reaction per cycle should be much less than one per 100 million if a 20-year lifespan is desired. Another issue for the stability is high temperature. Under intensive sun light, the cell temperature may exceed 80 °C, which, in addition to slight performance increase, may cause also adverse issues for the cell such as evaporation of the electrolyte solvent. This leads to reduced conductivity of the electrolyte that again means reduced output power of the cell and often eventually the complete failure of the device.

Understanding the degradation phenomena of solar cells has been an issue for the scientific community. Typically, stability studies for solar cells are performed in laboratory conditions using accelerated aging tests. This improves comparability of different stability studies, but also keeps in the investigations fast paced. Whilst these tests have been proven to be extremely fruitful in the development of the solar cell, at the end, outdoor testing is still needed to verify that the cells survive the real life conditions outdoors. Usually, the accelerated aging test are performed in stable conditions so they cannot predict the effects of weather variations.

To improve the quality of solar cell studies, the cells and materials that performed successfully under simulated conditions should be tested under real outdoor conditions to see, whether the tested cells or materials are stable or not outdoors, too. For this comparison, a proper testing system is needed and developing one is the goal of this study. The testing system will be developed for the New Energy Technologies group in Aalto University. The group has already good facilitates for indoor aging studies but they lack an outdoor testing station. There are several tasks and requirements that the testing system should fulfill:

- Automatic monitor and record current and voltage output of the cells
- Enable aging under different operation regimes (open circuit, maximum power, and short circuit)
- Simultaneous support for multiple and different cell types
- Weatherproof components such that no cover structures are not needed
- Record key weather parameters: solar irradiance, temperature, and humidity
- Compatible with other measurement devices such that additional, semi-manual measurements are easy to do when needed.

The new station will be designed according to so-called ISOS standards that define how solar cell aging studies should be carried out. In addition, good ideas and practices of other outdoor aging studies are looked for in a review and they are applied when preparing the new system.

The new station was tested with a set of DSSC solar cells. The test was performed in autumn in Espoo, Finland (60.2°N, 24.8°E) at very humid and partly freezing conditions. The test was performed to confirm that the station is working correctly and to study the real-time performance of the cells in harsh pre-winter conditions that have not been reported previously in literature.

2. Theory and methods

In the beginning, the outdoor testing station will facilitate mainly the study of dye-sensitized solar cells, which have been for a long time the primary research focus of the New Energy Technologies group at Aalto University in their solar cell studies. However, the group has recently expanded the research on so-called organometal halide perovskite solar cells. Hence, the station should work with both cell types thought the initial test is performed with more mature DSSCs. Next, both technologies are presented.

2.1. Operation principle of DSSC

Fig 1 shows the schematic of a DSSC. It has three main components: a photoelectrode, a redox electrolyte and a counter electrode. Hence it is a photoelectrochemical cell. Next, the functions of each three components are presented.

The photoelectrode (anode) contains a transparent conducting oxide (TCO) layer (typically fluorine doped tin oxide, FTO) on a glass substrate, a nanoporous film of semiconducting oxide nanoparticles (typically titanium dioxide particles, TiO_2) and a monolayer of dye-molecules attached on the surface of the nanoparticles. The photoelectrode is responsible of producing the current of the DSSC. First, the photons of light excite electrons of the dye-molecules from a so-called HOMO energy-level (highest occupied molecular orbital) to a so-called LUMO energy-level (lowest unoccupied molecular orbital) (1). The LUMO-level is located energetically slightly above the conduction band of the semiconducting oxide, which drives the electrons to jump from the dye molecules to the nanoparticles (2). The jumped electrons begin to diffuse towards the TCO layer since the light excites continuously new electrons to the conduction band of the semiconducting oxide material.

The shift of electrons from the LUMO-level to the conduction band leaves the dye-molecules positively charged. Before the dye molecules can liberate more electrons to the semiconducting oxide, they need to be reduced back to neutral state. This is the task of the electrolyte (3). In typical DSSC, the electrolyte is composed of a so-called redox couple (typically an iodide-tri-iodide pair, I^-/I_3^-) in a liquid solution. The redox couple liberates electrons for the dye molecules in the following reaction:

$$3I^- + 2S^+ \rightarrow I_3^- + 2S \qquad (1)$$

where S stands for the dye-molecule. In simple, the dye molecules oxidize part of the iodide ions by reducing themselves back to neutral charge state. In the process, the neutralized iodide atoms bind with one non-oxidized iodide ion to form a tri-iodide molecule.

After the dye recover reaction, the tri-iodide molecules diffuse away from the photoelectrode towards the last component, the counter electrode. There, the

tri-iodide molecules are re-reduced back to separate iodide ions by receiving electrons from the TCO layer on the glass substrate of the counter electrode (4):

$$I_3^- + 2e^- \rightarrow 3I^- \quad (2)$$

However, this is a slow reaction and therfore a catalyst is needed. Typically, a thin layer of platinum (Pt) is used for that purpose. To electrically close the loop, the TCO layer of the counter electrode is connected to the external circuit whereof it can receive electrons to replace the ones given for the redox electrolyte.

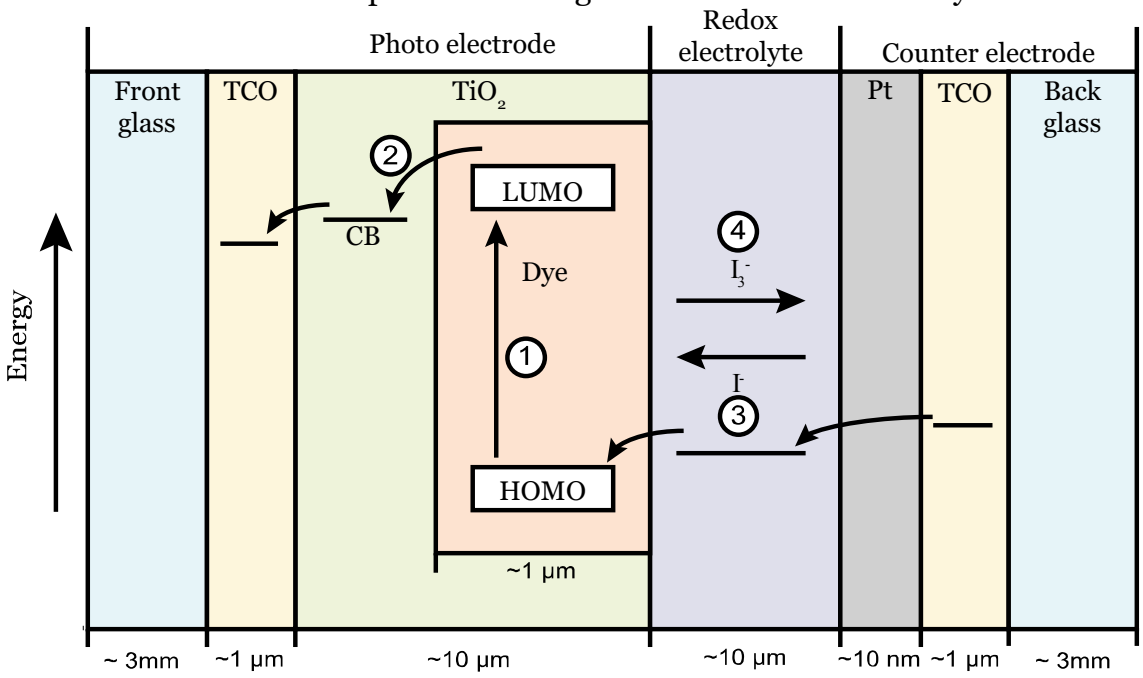

Figure 1. Schematics of a DSSC with typical materials and dimensions.

2.2. Operation principle of Omh-PSC

The bottleneck of DSSCs is that the dye absorbs effectively only photons with certain wavelength ranges. Thus, a large share of photons passes the dye without absorption and does not generate electricity. For example, the current record DSSC with a 13 % efficiency is able to absorb photons with wavelengths near 450 nm, which corresponds only to blue light [7]. Therefore, it has been a hot topic to find a better structure of photoelectrodes for photoelectrochemical solar cells.

Akihiro Kojima *et al* found in their study [8] that perovskite-structured nano-crystalline $CH_3NH_3PbX_3$ particles, where X is either Br or I, worked as photosensitizers for TiO_2. They prepared a cell containing the new photoelectrode, a lithium halide and halogen redox couple electrolyte and a Pt coated FTO-glass counter electrode. The cell reached an efficiency of 3.8 %. Since then, numerous different solar cell structures utilizing $CH_3NH_3PbX_3$ particles as light sensitizers have been shown to work and a common name, organometal halide perovskite solar cell (shortly perovskite solar cell or Omh-PSC) have been

given for them. At the moment, the top efficiency of Omh-PSCs has reached 20.1 % [9].

The structure of Omh-PSC has also developed since the pioneering cells. Many different materials and preparation techniques have been used but the basis of the perovskite cells is quite common for them, see Fig 2. The perovskite material acts as the light absorber. A photon generates an electron hole pair into the perovskite by exciting an electron from HOMO to LUMO (1). The electron is injected into electron transport layer (ETL) (2) and holes are injected into hole transport layer (HTL) (3). ETL and HTL are semiconducting materials such that ETL rejects holes and HTL electrons, which prevents the electron-hole pair from direct recombination after excitation. The electron is further driven into the FTO contact of the photoelectrode and the hole is driven into the back contact of the counterelectrode. Lastly, the electron and hole are recombined in the external circuit connecting the electrodes, which brings the cell in its original state. [10]

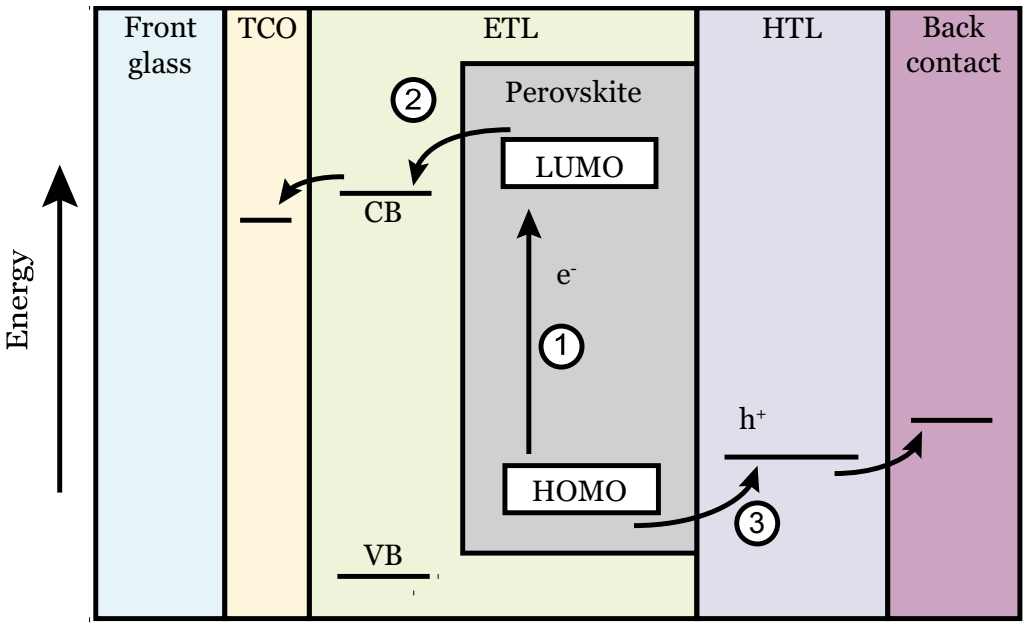

Figure 2. Schematics of a typical perovskite solar cell structure.

There are also other architectures for perovskite solar cells than the one presented in Figure 2, which shows the schematics of a so-called planar architecture of perovskite solar cell. One such is otherwise similar as the planar architecture but it has no separate HTL. Instead, the perovskite layer acts also as hole transporting medium [11] and this architecture is simply called HTL free architecture. Another used structure is a so-called inverted structure where ETL and HTL are in opposite positions [12]. A yet another architecture is a one that has two layers of TiO_2, a mesoporous and compact layer, as ETL [13]. All these structures are slightly different but the basic operation principle of each is the same as described above.

2.3. Solar cell characterization methods

Characterization of solar cells is important for comparing cell-to-cell variation between similar cell types, and comparing them to other PV technologies. The key method to characterize them is current-voltage (IV) measurement. It gives the main parameters describing the operation performance of the solar cell. The new outdoor aging setup records automatically the IV curve with certain interval during the aging test. Another important characterization method is electrochemical impedance spectroscopy (EIS), which gives the impedances of the different components of the cells. However, performing good quality EIS data requires short measurement cables, which was not possible with the new setup, and analyzing the data requires manual work time so it was decided to exclude the EIS from automatic measurements. Instead, EIS can be performed indoors in the process when the cells are characterized from time to time under standard measurement conditions to track the level of aging in the cell. The indoor setup is capable for both IV and EIS measurements.

Other important characterization methods are incident photon-to-electron conversion efficiency (IPCE) measurements, saturation current measurements, and cell photographing. These methods provide additional detailed information of the cell operation and bring insight to the degradation phenomena. The new setup cannot perform these characterization measurements since they require special equipment. Like with EIS these measurements can be performed separately with regular intervals. Next, the above-mentioned characterization techniques are presented shortly.

2.3.1. Current-voltage (IV) measurement

Current-voltage (IV) measurement is the most used method to characterize different solar cells. In IV-measurements, one applies a range of bias DC voltages to the cell and records the corresponding DC currents. As a result, one receives an IV and power (IP) curves like in Fig 3a. The IV curve represents all the possible operation points of the cell, or in other words, the cell cannot operate with other voltage-current combinations. It also tells the basic performance characteristics of the cell: open circuit voltage, short circuit current, maximum power point, fill factor (FF), and efficiency (η). In the following, they are presented shortly.

The open circuit voltage (V_{oc}) can be read from the cross-point of the IV-curve and voltage (horizontal) axis. It describes how large a potential difference the cell is able to generate when no current is drawn from the cell. The short circuit current (I_{sc}) can be read from the cross-point of the IV-curve and current (vertical) axis. It describes the maximum current that can be obtained from the cell when the potential difference across the cell terminals is forced to zero.

The power output at these two points of curve is zero, since $P = VI$, so they are not suitable operating points of the cell. Instead, the most efficient operating point is at the maximum power point (P_{max}). It is located at the point where the product of the current and voltage along the IV curve is at its maximum, i.e. where the power curve reaches its maximum. Graphically, this point can be found by maximizing the area of the rectangle **I** between the axis and the IV-curve. The fill factor (FF) is defined as

$$FF = \frac{P_{max}}{V_{oc}I_{sc}} = \frac{V_{mpp}I_{mpp}}{V_{oc}I_{sc}} \quad (1)$$

Thus, the fill factor defines the ratio of maximum power output and theoretical maximum power output without any resistive losses. Graphically presented it is the ratio of areas **I** and **II**. It is always between zero and one and the larger the value the better the cell is.

The efficiency (η) of a solar cell is defined as the ratio of maximum electrical output power and solar irradiance

$$\eta = \frac{P_{max}}{P_{sun}} \quad (2)$$

The efficiency describes how well the cell is capable to convert sunlight into electricity. Like the fill factor, the efficiency is a number between zero and one and the higher the value the better the cell is.

If a diode model (see Fig 3b) is fitted to the IV curve more parameters can be obtained from the measurement. The diode model,

$$I_{cell} = I_{ph} - I_0\left(e^{\frac{-q(V_{cell}+I_{cell}R_{se})}{mK_BT}} - 1\right) + \frac{V_{cell} + I_{cell}R_{se}}{R_{sh}} \quad (3)$$

describes the relation between the current and voltage of a solar cell mathematically [14]. In the equation 3 I_{cell} is the output current of the cell, V_{cell} is the output voltage of the cell, I_{ph} is the current that the absorbed light generates and it is called photocurrent, I_o is a so called dark current of the diode of the model, R_{se} is the series resistance of the cell, R_{sh} is the shunt resistance of the cell, q is the elemental charge, m is the diode ideality factor, k_b is the Boltzmann's constant, and T_K is the absolute cell temperature. Out of these parameters, the most interesting ones are the series and shunt resistances. Series resistance describes how well the current runs through the cell (the lower R_{se} the better) and shunt resistance describes how much current is lost inside the cell (the higher R_{sh} the better).

The diode model (3) is derived for p/n junction solar cells, not for electrochemical solar cells. Nevertheless, it applies usually well for DSSCs and Omh-PSCs but there is a non-ideality in the model: their series resistances are not constant as function of current [15] as it is for p/n junction solar cell. Therefore, to get deeper knowledge about the electrical and electrochemical performance of the DSSC and Omh-PSCs electrochemical impedance spectroscopy (EIS) is needed. It is not only able to reveal the series resistance as function of current but also identify the significance of different resistances contributing to the overall series resistance. Nevertheless, determining R_{se} is interesting as it gives more information than merely looking at FF, which usually tells about changes in resistances, but which can also change due to variation in photovoltage and photocurrent and is therefore an incomplete measure of differences in resistances. Looking at R_{se} will give indication if there are appears

variation namely in the resistances and detailed investigation e.g. using EIS is called for.

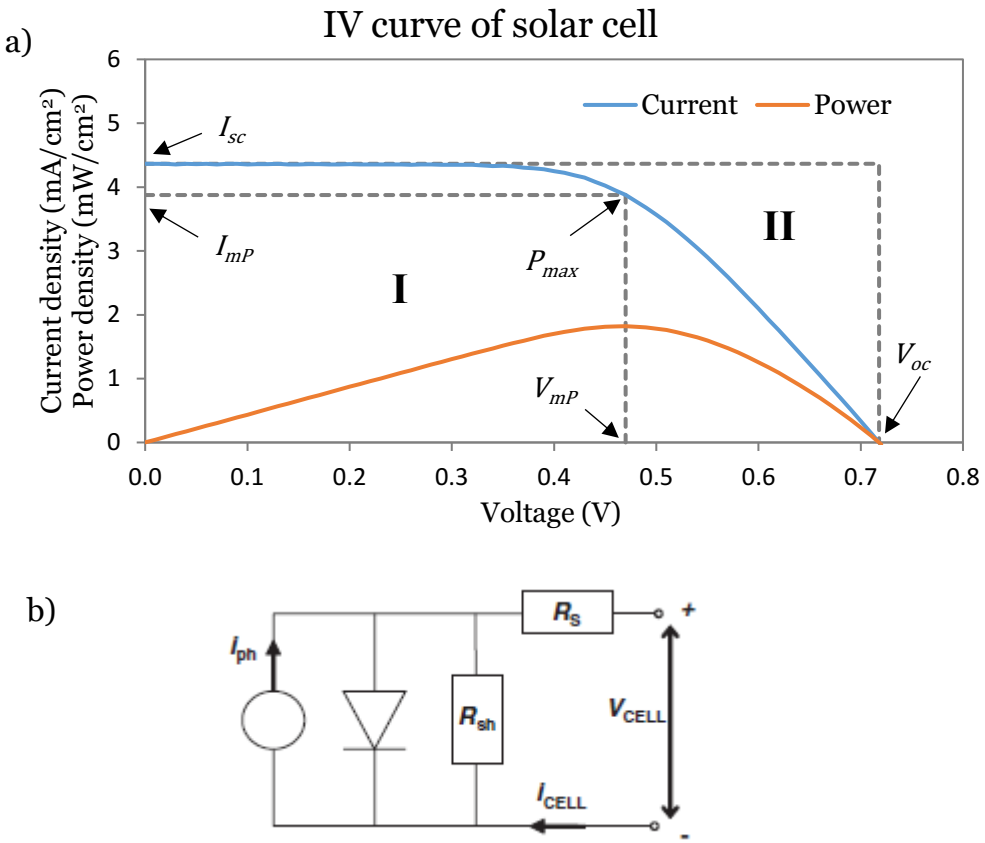

Figure 3. a) Typical IV and IP curves of a solar cell and some characterizing values of the curve. b) A simple one diode mode describing the electrical behavior of a p/n junction. R_s corresponds to R_{se} in this work. Figure b from [14]

2.3.2. Electrochemical impedance spectroscopy (EIS)

In EIS, the solar cell under examination is set to operate at some operating point along its IV-curve. An alternating current –voltage (AC) with certain frequency is superimposed over the operation direct current-voltage (DC) and the resulting current is measured. The process is repeated over a certain range of frequencies, and from the obtained measurement results, the frequency dependent impedance and phase shift can be solved. From these obtained values, one can separate the real and imaginary parts of the impedance. Finally, plotting a so-called Nyquist and Bode plots (see Fig 4) reveal internal resistances of the cell. Additionally, the EIS scanning can be repeated for a range of operating voltages to see how impedance values change when different amount of current is drawn from the cell. [14]

Each component of a solar cell has unique response to AC signal. Fortunately, the components typically response to the signal only within certain frequency range so the different components of the solar cell can be often, though not always, distinguished from the EIS spectrum. Since different cell structures contain different

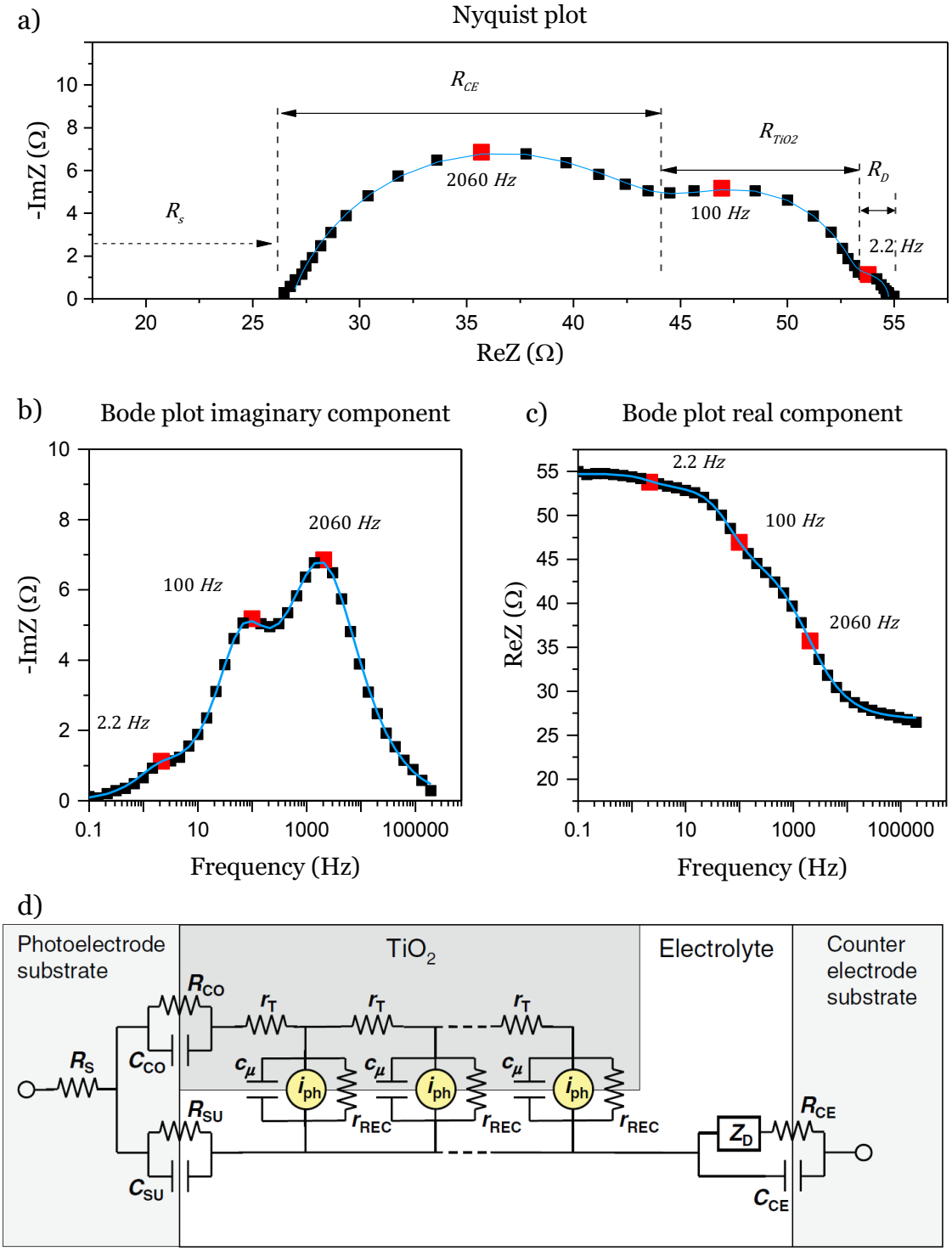

Figure 4. EIS spectrum of a DSSC at open circuit conditions. Nyquist plot (a) shows imaginary part of the impedance as function of the real part and Bode plots (b,c) show the imaginary and real parts of the impedance as function of AC. The highlighted data points show the peak positions of the different components of the DSSC. The blue line represents a fit that was made with the equivalent circuit (d). Figure d obtained from [14]

components, like a liquid electrolyte or a solid electrolyte, the spectra for these structures look different. Next, the EIS spectrum of typical DSSC is presented.

In the Nyquist plot, the width of the semicircle nearest to the origin represents the charge transfer resistance at the counter electrode/electrolyte interface (R_{Ce})[1], the width of the semicircle in the middle represents the resistance of photoelectrode film/electrolyte interface (R_{TiO_2}), and the width of the last semicircle represents the mass transport resistance of the counter electrode (R_D). These components are also visible as peaks in the Bode plot from the imaginary component of the impedance. Locations of the peaks shows the characteristic frequencies of each component. Lastly, the gap between the origin and the spectrum equals to the Ohmic series resistance (R_s) of the cell. This series resistance includes only Ohmic resistances (wiring, TCO, and electrolyte resistivity) while the R_{se} includes all four resistance components shown here:

$$R_{se} = R_S + R_{TiO_2} + R_D + R_{Ce} \quad (4)$$

Often, the semicircles overlap each other and it is difficult to estimate their accurate widths directly from the spectrum. To overcome this problem, an equivalent circuit model can be fitted to the spectrum (see Fig 4d). The circuit is based on the charge kinetics and its parameters describe resistances and capacitances of different components and their interfaces, see ref. [14] for a comprehensive representation of a widely used equivalent circuit model for DSSCs. In summary, the fitting of the equivalent circuit to the spectrum gives values for the parameters what reveals information how well each component of the solar cell works in terms of electrical performance. [14]

2.3.1. Incident photon-to-electron conversion efficiency

IV and EIS measurements cannot reveal all important factors affecting the solar cell performance. Especially, they cannot provide deep insight into current generation of the cell. Normally, not all the generated electron-hole pairs reach the external circuit in solar cells, instead a share of them recombine already inside the cell. This means that the cells have a limited incident photon-to-electron conversion efficiency (IPCE). For solar cells, it is defined as ratio between electrons reaching external circuit per time unit and incident photons per time unit:

$$IPCE = \frac{electrons\ from\ SC\ output/time\ unit}{incident\ photons/time\ unit} \quad (5)$$

Typically, IPCE is measured as function of wavelength, which generates IPCE spectrum, see Fig 5. The spectrum shows how well solar cell generates current with different wavelengths of light.

[1] The abbreviations correspond to the ones used in ref [14]

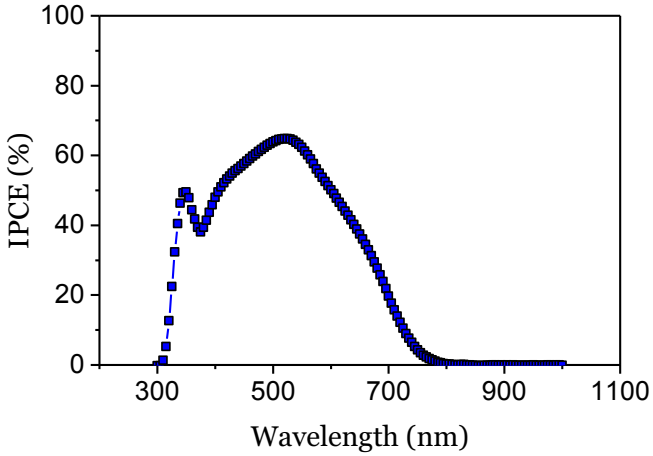

Figure 5. An IPCE spectrum of DSSC.

In case of DSSCs and Omh-PSCs, the IPCE is divided into three components: light harvesting efficiency (η_{LH}), electron injection efficiency (η_{INI}), and electron collection efficiency (η_{COL}) [14]. The light harvesting efficiency describes how large share of incidents photons excites electrons in the dye molecules, the electron injection efficiency describes how large share of the excited electrons moves to the TiO_2 particles, and the electron collection efficiency describes how large share of the moved electrons finally reach the external circuit, see Fig 6 for schematics. The product of the three factors forms the total IPCE (η_{IPCE}):

$$\eta_{IPCE} = \eta_{LH}\eta_{INI}\eta_{COL} \tag{6}$$

Since the total IPCE is product of its components, the values of all components have to be as high as possible for good solar cell, otherwise the cell cannot produce current efficiently.

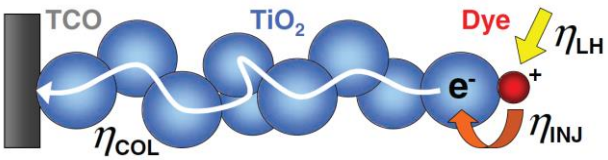

Figure 6. Different components of the IPCE. Figure from [14].

2.3.2. Cell photographing

When DSSCs degrade, there are often visual changes in the appearance of the cell, for instance bleaching of the electrolyte due to loss of charge carriers. Therefore, monitoring the cell with photographing can reveal crucial information about the state of the cell. In fact, it has been studied in the New Energy Technologies group that the iodine concentration of the electrolyte can be measured with photographing and image analyzing [16]. It was found that the blue pixel value in the RGB color space is nearly linearly dependent on the iodine concentration. It

was estimated that the increase of blue pixel value by one (in 0 to 255 scale) corresponds to decrease of $7.35 \cdot 10^{-4}$ M in iodine concentration in the electrolyte when the concentration is between 0.025 and 0.1 M.

The result holds only in the very same light conditions that was used in study [16]. There, the light conditions were stabilized by performing the photographing in a dark box lit by four led lamps and by having the camera fixed into one position. In addition, the image should always be taken with the same settings, i.e. exposure time, aperture size, light sensitivity, white balance, and other color settings should be the same. For that purpose, the camera is every time calibrated with a color checker passport.

In this study, the aging of the electrolyte is monitored with the same setup that was used in a previous study [16]. In addition, photographing is used for monitoring any other visible changes in the cells. For example, freezing of the cells may cause mechanical damage to their sealing, which might by visible.

2.4. Solar cell degradation mechanisms

The parameters describing the solar cell performance are not constant. Instead, they tend change their values so that the efficiency of the solar cell decreases over time. This means that the solar cell degrades gradually, and its maximum output power decreases. For DSSCs, and especially for perovskites, the degradation is one of the main issues preventing them from widespread commercialization. There are several reasons why these cell types degrade, and next the most important ones for both DSSCs and perovskite solar cells are presented.

2.4.1. Degradation mechanisms of DSSCs

One main hindrance of DSSC is its redox electrolyte since it is sensitive for high temperatures and UV-light that are both present under real outdoor operation conditions. Asghar *et al.* found in their review that both of these degradation factors is found to decrease tri-iodide concentration [17]. This decreases directly the ability of the electrolyte to transport charge, which again increases the total cell resistance and thus decreases the fill factor of the cell. The reduction of charge carriers also affects the maximum current that the cell can generate, and via that the loss of charge carriers may eventually reduce the photocurrent as well. In addition, some possible electrolyte solvents, such as acetonitrile, may boil at elevated temperatures causing internal damage to the cell. On the other hand, the liquid form of the electrolyte enables it to leak out from the cell if encapsulation is not perfect.

Another major issue of DSSC is its dye. There are numerous different dyes that have been used in DSSCs [18], but many of them tend to separate from the TiO_2 nanoparticles especially at high temperatures. Asghar *et al.* found several competing hypotheses for this phenomenon, so the issue is still under debate. Nevertheless, the dye desorption decreases IPCE of the cell since less excited electrons are able to transfer from dye molecules to the TiO_2 nanoparticles. In addition, the dyes may undergo chemical transformations, which may disable the

dyes functionality totally. These degradation mechanisms decrease the short circuit current of the cell.

A third problem is the formation of recombination sites at the TiO_2 and TCO layers. Typically, these sites are formed due to impurities. There are several routes where the impurities can enter these two layers. Firstly, the impurities can enter the cell during its assembly if the used materials are not pure. Secondly, the impurities may enter the cell through a poor sealing. Lastly, catalyst desorption from counter electrode may introduce recombination sites on the photoelectrode [19]. Especially, the last issue is difficult since it effects on the operation of both electrodes, and it cannot be solved by more thorough sealing of the cell. The increase of recombination in photo-electrode decreases the open circuit voltage since the dark current of the cell increases.

2.4.2. Degradation mechanisms of perovskite solar cells

The modern perovskite solar cells have very different materials compared to DSSCs and have no liquid electrolyte so their degradation mechanisms are also different. However, there are only few common degradation mechanisms of Omh-PSCs since there are many different architectures for them and each has unique degradation mechanisms. More information about these mechanisms can be found from refs. [10, 20, 21].

One very common reason for aging of Omh-PSCs is the degradation of the perovskite sensitizer. There are several aging mechanisms for the perovskite material. Wang *et al.* found in their review that many perovskite materials, such as methylammonleadiodide ($CH_3NH_3PbI_3$), are sensitive for moisture. The molecules react with water losing their function to work as photosensitizer [20]. Berhe *et al.* found in their review that another problem is UV-light. It generates halogen free radicals that react with the perovskite molecules breaking their functionality [10]. In addition, Niu *et al.* found in their review that elevated temperature may cause degradation of the perovskite material [21]. There are several hypotheses how high temperature breaks down the perovskite material but they are not yet proven. Nevertheless, the effect of the breakdown of the perovskite for solar cell performance is similar as the dye desorption: the short circuit current decreases. The perovskite may cause stability issues for other cell components, too. Leijtens *et al.* found that the perovskite materials react with a common counter electrode material silver. [22]. This forced them to use more expensive gold as a counter electrode material.

2.5. Indoor testing methods of solar cell aging

Usually, the degradation of the solar cells is studied with three types of aging tests in indoor laboratory conditions: dark storage test, constant illumination test and cycling test. In dark storage test, the tested solar cells or solar cell materials are kept in dark either at room temperature or at elevated temperature. In addition, humidity may be controlled. In constant illumination test, the solar cells are kept at constant illumination under a solar simulator. Additionally, temperature and humidity may be controlled like in the dark tests. Lastly, the aging conditions may

be varied periodically in the cycling test. The cycling can be done for all three condition variables or for part of them. In all testing types, the solar cell performance is tested periodically for monitoring the development of the solar cell degradation over time.

The set of different possible combinations of these condition variables is vast. Therefore, several standardized testing methods for solar cell aging have been presented [23]. These ISOS standard measurement conditions are based on IEC 61646 standard that define what kind of conditions commercial thin-film solar panels should withstand. The difference between the two standard systems is that the ISOS concentrates on solar cell material stability whereas the IEC focuses on stability of single panel.

The ISOS standards were originally presented for organic photovoltaic cells but they are adopted by many other photoelectrochemical technologies as well since the environmental causes of degradation are usually very similar for each technology. The standards list rather explicitly how the different aging temperatures should be conducted and in which environmental conditions. In addition, the ISOS standards have three different level of "tolerance" for the aging test equipment, condition control, and measurement parameter reporting.

The first level called "Basic" is designed so that it can be performed with minimal equipment and minimal environmental control. It is enough to monitor just open circuit voltage and short circuit current of the cells with a multimeter. The temperature control of the cells can be made with simple hot plate, and humidity controlling is not required. The light source used for the measurements should match the IEC standard AM 1.5G spectrum as well as possible, though testing of the spectrum is not required. The next level, "Intermediate" requires more advanced measurement equipment and environmental conditioning. The cells should be monitored by measuring IV curves with regular interval. The temperature of the cells should be controlled but humidity can be ambient. The light source must match closely to AM 1.5G spectrum. The last level "Advanced" is otherwise similar as "Intermediate" but it also requires IPCE measurements and humidity control of the environment. Next, the testing conditions of the three aging test types and the special requirements to reach the three ISOS levels in each of them are presented. For recommended practice of reporting the study results, see [23]. After that, the common practices for making these kind of aging studies is shortly reviewed and how they compare to the ISOS standards.

2.5.1. Dark storage tests

The standardized aging conditions are listed in Table 1. If a certain standard level is desired the characterization of aging should follow at least the same standard level. The degradation of the cell or material should be measured with certain intervals that match the expected lifetime of the cell. The standards advice to have denser measurement interval in the beginning of the test since typically aging due to thermal annealing occurs already in the beginning.

2.5.2. Constant illumination tests

The constant illumination test standards are listed in Table 2. The temperature and humidity conditions are almost the same as in standardized dark tests. Like with dark tests, to achieve certain standard level the characterization of the cell should be performed at least with the same standard.

2.5.1. Cycling tests

Standardized aging conditions for cycling tests are shown in Table 3. At the moment, standards only for temperature cycling are established. There are two cycling standards, dark and constant illumination, the latter standard conditions are presented in parentheses in Table 3 if the values differ from the ones for dark cycling test. Like with dark and constant illumination tests, to achieve certain standard level the characterization of the cell should be performed at least with the same standard.

Table 1. Standardized measurement conditions for dark storage aging test.

	ISOS-D-1	ISOS-D-2	ISOS-D-3
Storage temperature	Ambient	65 or 85 °C	65 or 85 °C
Storage humidity	Ambient	Ambient (low)	85 %
Temperature control	Monitor	Control (± 2 °C)	Control (± 2 °C)
Humidity control	Monitor	Monitor	Control (± 3 %)

Table 2. Standardized measurement conditions for constant illumination tests.

	ISOS-L-1	ISOS-L-2	ISOS-L-3
Test temperature	Ambient	65 or 85 °C	65 or 85 °C
Test humidity	Ambient	Ambient	50 %
Irradiance level	400 – 1200 W/m²	600 – 1200 W/m²	600 – 1200 W/m²
Irradiance uniformity	Preferably uniform	Max ± 10 %	Max ± 10 %
Temperature control	Monitor	Control (± 2 °C)	Control (± 2 °C)
Humidity control	Monitor	Monitor	Control (± 3 %)
Irradiance control	Monitor	Control	Control
Load of test cells	Preferably P_{max}, Open circuit optional	Preferably P_{max}, Open circuit optional	P_{max}

Table 3. Standardized measurement conditions for constant temperature cycling tests. The table have values for both dark and illuminated cycling tests. The optional values in parentheses are used in the illuminated test if they are not the same as are in dark test.

	ISOS-T-1 (ISOS-LT-1)	ISOS-T-2 (ISOS-LT-2)	ISOS-T-3 (ISOS-LT-3)
Test temperature	Room temp to 65/85 °C	Room temp (5 °C) to 65/85 °C	-40 °C (-25 °C) to 85 °C (65 °C)
Test humidity	Ambient	Ambient (Ambient, at over 40 °C set to 50 %	Ambient (Ambient, at over 40 °C set to 50 %
Ramping type	Step or linear	Linear	Linear
Humidity control	Monitor	Monitor (Control)	Control
Irradiance control	Monitor	Control	Control

All the above-mentioned tests are called as accelerated aging tests. All of them simulate different environmental conditions, which takes them to a much more demanding level than the real outdoor conditions. For example, the cell temperature may stay above 65 °C for just couple of hours daily during hot seasons. Therefore, the cells degrade in these conditions much faster than in typical outdoor conditions. Usually, a so-called acceleration factor K of the test is estimated. This factor connects the measured degradation rate ($k_{accelerated}$) to the real degradation rate under outdoor conditions ($k_{outdoor}$):

$$k_{outdoor} = \frac{1}{K} \cdot k_{accelerated} \tag{7}$$

This equation is very approximative since the degradation rate in outdoor conditions is location dependent. Moreover, defining the factor K itself is difficult. For visible and UV light, the cumulative irradiance of the test is simply calculated and then estimated how long it takes to reach the same light doses outdoor. For temperature and humidity there are not any standardized way to estimate the factor. Lastly, estimating acceleration factor for test where there are more than one aging source present is very difficult or even impossible in practice [24, 25].

In general, a solar cell is considered as stable if it lasts long enough in all the above-mentioned tests. Typically, this means that the cell has maintained at least 80 % of its initial efficiency measured after possible initialization use. What is long enough is basically defined by the end user. For comparison, commercialized silicon solar cell manufacturers typically guarantee that their cells have an operation life of 25 years, which means that the cell should maintain at least 80 % of its initial efficiency after 25 years of outdoor operation [26].

2.5.2. Short review on indoor aging studies

To get an idea how the indoor aging studies are performed in practice a short, non-comprehensive review was performed. The goal of the review is to compare the methods used in actual studies to the ISOS standard practices. Studies [27-38] focused on dark storage tests, [20,30,31,33,35,39-44] on constant illumination tests and studies [30,38] on cycling thermal test. The dark storage and constant illumination tests were both common but cycling thermal tests seems to be rare since only two were found with quick search. The studies were picked otherwise randomly from Google Scholar searches but newer studies were favored and picking many studies from same research group was avoided to get best possible idea what kind of facilities and practices solar cell research groups have. The review includes only DSSC and Omh-PSC studies.

First notice was that none of the checked studies [20,27-44] completely followed the ISOS standards. Mostly, humidity values in the studies were totally omitted if the humidity level was not a central topic in the study. Especially, studies on DSSCs omitted humidity controlling in 15 cases out of 16. The Omh-PSC field was more rigorous with humidity values, 5 out of 8 studies controlled measurement environment humidity. The reason for this difference is that moisture is major source of degradation for Omh-PSC but not such for DSSCs. Most likely, if humidity was not reported it has been at ambient level, which means that the relative humidity at elevated temperatures has been quite low.

A more severe problem found in the review was how temperature of the experiment was reported, especially under strong illumination. Only one study reported both environment and cell temperatures [42] and they found that the cell temperature under 1000 W/m^2 irradiation was 30 °C higher than the environment temperature. Others measured either cell temperature [30,33] or environment temperature [39 ,44]. Moreover, some studies did report temperature values but did not specify which temperature [22,31,40] and some studies did not report temperature values at all [35,41,43]. Since temperature is reported with such different methods, actual insight about material stability is very difficult to obtain. For example, Fig 7 shows how much cell temperature was noticed to affect the performance of a single DSSC[2] measured in study [5]. Therefore, the studies without proper temperature reporting are difficult to compare in other studies in literature.

The used light sources in both aging and characterization seem to be of rather high standard. Only 3 out of 19 studies [27,33,35] did not report to use simulated AM 1.5 G spectrum. However, couple of studies filtered UV component of the spectrum during the aging tests [31,39]. UV is known to cause degradation of DSSCs and Omh-PSCs so it would be good to have at least reference measurements under complete AM 1.5 G spectrum to see, whether UV is causing degradation for the cell materials or whether there is another reason. Complete removal of UV radiation in long term operation is difficult so the used materials should last UV radiation at least to some extent. Fortunately, there are also studies that particularly focus on UV aging of cells [33,41].

[2] Study [5] had several different test cell structures with liquid and ionic-liquid electrolytes, but they did not specify, which of them was tested in Fig 9.

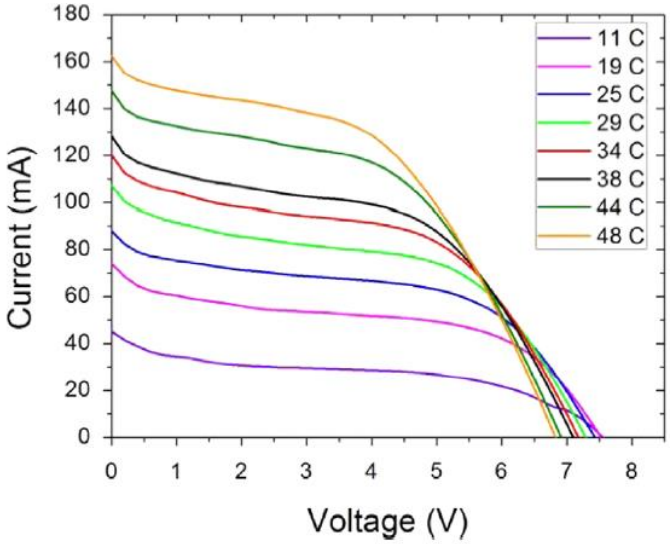

Figure 7. The effect of temperature on IV curve of a DSSC. The graph from [5]

Last important note about general practices concerning constant illumination tests is that the cells are mostly aged under open circuit conditions. Thus, these tests cannot unquestionable state how stable the materials are under power generation. There is evidence that at least short circuit conditions are more demanding than open circuit conditions [45] and also with closed circuit aging under UV illumination [41].

Characterizing the cells under the tests and reporting the results are usually done well: the ISOS standards have slightly narrow recommendations for cell characterization (it mainly focuses on cell efficiency and partially on IPCE) but often groups report more than the standards require. Most commonly not only the cell efficiency but also open circuit voltage, short circuit current density and fill factor are monitored over the aging period. In addition, EIS analysis is also typically included into the study.

As conclusions, Table 4 shows how the ISOS procedures are generally followed and what kind of differences are between the standards and general practices. Most common issue is poor temperature and humidity monitoring, especially in constant illumination tests. Without proper environment condition reporting, the results are not well comparable to the results of other studies. On the other hand, it is good to see that advanced level testing is reached in the other categories of Table 4, even in this sample type review, though it has to be mentioned that none of the reviewed studies followed exactly all the ISOS advanced level processes. On the contrary, many studies included other measurement methods, such as EIS, that are not required in any ISOS standard level in their studies to improve the depth of their studies.

Table 4. Typical followed levels of the ISOS standards for dark storage and constant illumination tests within the review studies in the review sample.

	General level	Best level	Comments
Dark storage	Intermediate (2)	Advanced (3)	Most problems with humidity reporting
Temperature control	Advanced (3)	Advanced (3)	Sometimes other temperatures than suggested 65 °C or 85 °C used
Humidity control	Intermediate (2)	Advanced (3)	Humidity reporting often omitted. Sometimes other humidity than suggested 85 % used
Constant illumination	Basic (1) to Intermediate (2)	Intermediate (2)	Commonly problems with temperature and humidity reporting.
Light source	Basic (1) and Advanced (3)	Advanced (3)	AM 1.5 G spectrum often followed but in some studies either different spectrum is used or UV is filtered
Temperature control and monitoring	Not suitable to Advanced (3)	Advanced (3)	Much variation especially on temperature reporting.
Humidity control and monitoring	Intermediate (2)	Advanced (3)	Humidity reporting often omitted
Load	Intermediate (2)	Advanced (3)	Typically open circuit aging only

2.6. Outdoor aging methods

Final estimation of solar cell stability has to be done outdoors. One simply cannot determine acceleration factor K that would predict universally the degradation rate of the solar cell. Fortunately, the ISOS protocols as well as IEC standards cover also outdoor testing [23]. For all levels of testing (see Section 2.5), at least ambient and cell temperature, relative humidity, and solar irradiance have to be recorded. The test cells should face towards the equator and be at tilt angle corresponding to the latitude of the test location. A sun tracking system may also be used. The “Advanced” level standard also requires monitoring of wind speed and direction. The cell characterization practices of the cell parameters are listed in Table 5. The outdoor characterizations should be performed at least once in an hour and the indoor characterizations weekly.

Table 5. Standardized operation regimes of solar cells and characterization techniques and intervals for outdoor aging tests.

	ISOS-O-1	ISOS-O-2	ISOS-O-3
Load	P_{max} preferred, Open circuit optional	P_{max} preferred, Open circuit optional	P_{max}
Cell characterization	Indoors	Outdoors	Indoors and outdoors
Measurement interval	Weekly to monthly	15 min to 60 min	Outdoors: 15 min to 60 min, indoors: weekly to monthly

2.6.1. Review on outdoor aging studies of DSSCs and Omh-PSCs

After Grätzel introduced the DSSC technology only a handful of studies have actually tested DSSC outdoors [4,5,45-55][3]. Omh-PSCs are tested even less due to their novelty: only two studies were found [56,57]. Mostly, the DSSC outdoor studies demonstrate manufacturing a module with larger size and its ability to function in power generation, but there are also small, single cell studies. The typical aging time scale is several months [4,45,47-51] but there are also studies where cells have been outdoors for only few days to weeks [5,46,52,53,56,57] or one to 2.5 years [54,55]. Locations of the studies limit on rather narrow longitude range from 21°N to 48°N (see Table 6 and Fig 8) and studies are mostly rather close to sea level with maximum altitude around 300 m. The typical climate conditions are subtropical and from dry to humid and mostly sunny.

Studies report the weather conditions in varying degrees. Only five studies out of 15 report recording irradiance [5,45-47,53] and temperatures [5,45,46,49,56]. Sometimes, only average, maximum, and minimum temperature of cells [47,48,54] during the measurements are presented. Humidity is reported only in studies [5,56]. Continuous recording of weather is actually important in outdoor tests. If degradation of the tested cell is found to occur, one could try to detect when and in which conditions the degradation occurred. In addition, continuous recording of irradiance is important for calculating the cumulative irradiance. This value is useful when comparing the outdoor data to indoor data from constant illumination tests.

A major deficiency of many studies is that they do not report the operation regime of the tested cell or panel during the test. This was the case in six studies [5,49,50,52,56,57]. On the other hand, eight studies [4,45,46,48,51,53-55] had the cells or panels operating at maximum power point and two of them [45,48] had another set of cells at open circuit. Thus, many studies represent the actual stability of the DSSCs under real operating conditions. However, neither of the Omh-perovskite studies reported the operation regime.

[3] Not totally comprehensive: some studies were excluded since they did not perform properly enough outdoor tests (e.g. too short for aging) and some might have been accidentally left out.

Table 6. Descriptions of the study locations. Altitude data received from [59] and climate descriptions from [60]. If time of study is reported, the climate description is limited for that time of the year. Otherwise the description is average of the year.

Location	Coordiantes	Altitude	Climate description	Times and lengths of study	Studies
Freiburg im Breisgau, Germany	48°N, 8°E	200 - 300	Inland, warm, slightly humid, sunny	Summer 3 months	47
Ljubljana, Slovenia	46°N, 14°E	200 - 300	Inland, warm, humid, sunny	Apr to Oct	45
Turin, Italy	45°N, 7°E	200 - 300	Inland, warm, humid, partly cloudy	Feb to Apr	49
Rome, Italy	41°N, 12°E	0 - 100	Coastal, warm, dry to humid, sunny	-	46,48
Porto, Portugal	41°N, 8°W	0 - 100	Coastal, warm, dry, sunny	Summer 47 days	53
Cheonan, South Korea	37°N, 127°E	50 - 200	Coastal, warm, very humid, part cloudy	-	52
Toyota, Japan	35°N, 137°E	0 - 100	Coastal, warm, very humid, part cloudy	4 months to 2.5 years	4,54, 50,51
Hefei, China	32°N, 117°E	0 - 50	Inland, warm, humid, part cloudy	Full year	55
Abi Dhabi, UAE	24°N, 55°E	0 - 50	Coastal, hot, dry, very sunny	-	5
Hong Kong, China	22°N, 114°E	0 - 300	Coastal, very warm, very humid, partly cloudy	-	56
Jeddah, Saudi Arabia	21°N. 39°E	0 - 50	Coastal, hot, dry, very sunny	Sep 1 week	57

Typically, the cells were quite well encapsulated from the environment, in some cases perhaps too much. In four studies [45,51,54,56] the cells were placed into waterproof, UV filtered containers or other waterproof encapsulations. These covers do not let rainwater get close to the cells and may have strong greenhouse effect on ambient temperature. In studies [4,47,48,52,52,55] the sealed cells were “sandwiched” between two glass plates to form panels. This type of encapsulation is the same or very similar as commercial solar panel

encapsulation. Only in studies [5,46,49] cells were exposed for outdoor conditions with minimal weather protection that just enables measuring the cell also during rainy conditions. Two studies did not report how they protected cells from weather [50,57]. Reporting the level of encapsulation is important since highly encapsulated cells show less degradation than minimally encapsulated cells where moisture and other impurities enter faster into the cells. When thinking of encapsulation, it is important, which level of encapsulation is viable for commercial devices, e.g. 10 mm thick external casing is not viable in practical applications for cells planned to be lightweight and flexible. In contrast, filters and capsulations should represent what could be realistically used in actual products. To get insight to degradation mechanisms, other type of sealing configuration may be interesting as well, but the end goal should not be forgotten. It should be also considered that even though some of the encapsulation was meant for keeping the rain water from entering the contacts, the encapsulation could also significantly affect the light spectrum, e.g. filtering of UV light. If the cover is of commercially viable level, additional benefits such as UV filtering is not an issue, but with overly thick coverage, it may be that further problems arise in more fields than merely issues with moisture.

The level of reporting aging during the outdoor exposure is on moderate level: most studies perform regularly and often enough IV measurements for the cells or panels [5,45-50,53-57]. However, due to lack of weather recording, some studies were not able to state why the cell degraded if it encountered aging in the first place. Moreover, IPCE measurements are rarer in outdoor studies than in indoor ones, for some reason: only one study executed IPCE in outdoor studies [49]. For these reasons, cell/panel characterization does not reach the highest level in any study.

As a summary, very different types of aging studies have been reported for DSSCs and Omh-PSCs in literature: the range of study lengths is from weeks to years and the devices range from small study cells to large panel arrays. The largest issues in the study methods are the poor weather monitoring and the lack of IPCE measurements, see Table 7. On the other hand, some studies used very strong encapsulation for the cells, which may not be commercially feasible for the end product. Thus, the studies may overestimate the stability of their devices under real outdoor operation conditions. A positive finding was that rather many studies kept their cells under load.

Table 7. Typical practices for outdoor aging measurements.

	Typical level	Best level	Comments
Weather monitoring	Not suitable to Intermediate (2)	Advanced (3)	Not all parameters are monitored. Most severely irradiance is not monitored
Cell/panel characterization	Intermediate (2)	Intermediate (2)	IPCE required for Advanced level is not measured
Operation regime	Advanced (3)	Advanced (3)	Many studies focus on aging under maximum power point.
Encapsulation	Not ISOS standardized		Three levels of encapsulation are used: "Greenhouse" type, panel encapsulation and no extra encapsulation

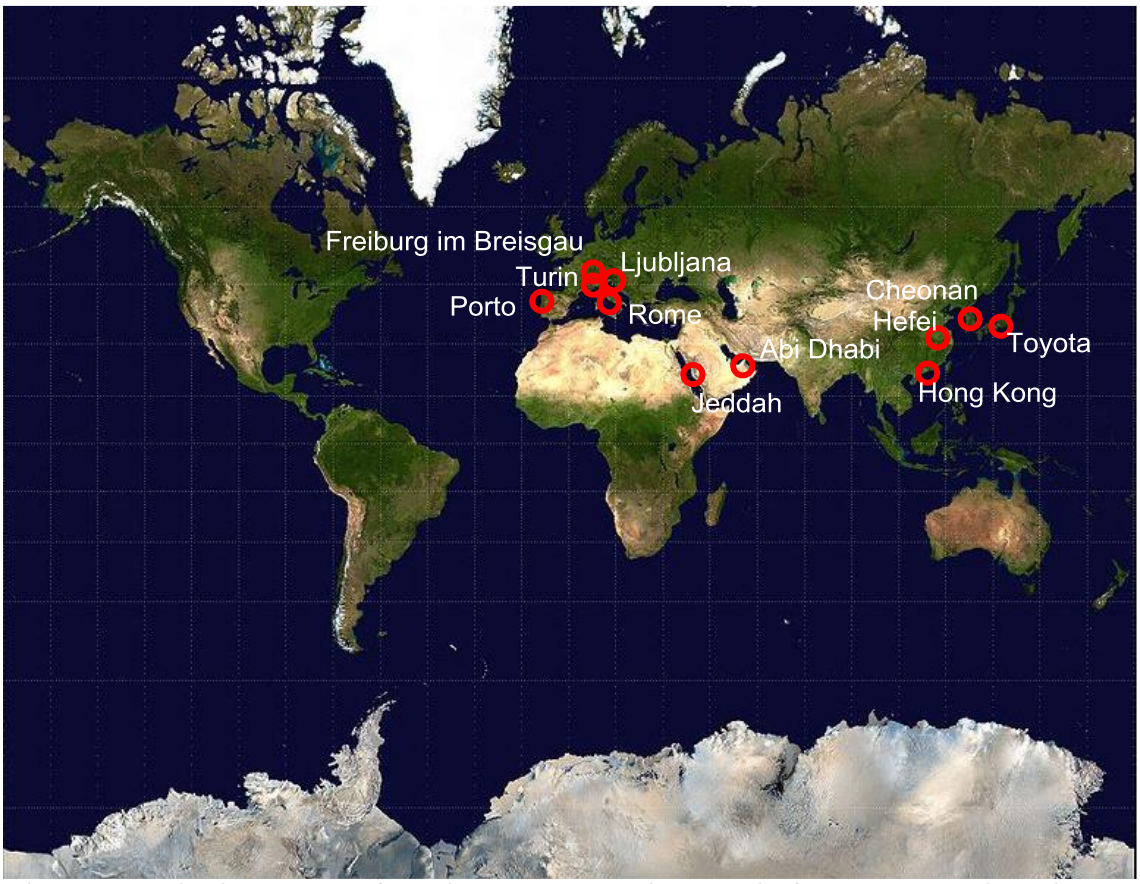

Figure 8. The locations of outdoor aging studies made for DSSCs and Omh-PSCs. Background map from [58]

3. Experimental section – new outdoor testing station

The New Energy Technologies group set five design requirements for the new outdoor testing system:

1. It should meet ISOS-O-3 standards.
2. It should support the group's current cell design.
3. The cells should be as bare as possible under the outdoor conditions, i.e. no extra encapsulation by default.
4. The new system should be able to execute different measurements simultaneously.
5. In future, the system should have support for larger 10 by 10 cm cells.

The first requirement was set since the group wants to execute state-of-the art outdoor measurements. For the second requirement, there are multiple reasons. Most important one is there is no need to build one cell design for indoor aging and other for outdoor aging. Similar cells ensure consistency between the performances of individual cells. Secondly, some of the group's characterization systems are only compatible with the current cell design. The third requirement was set for ensuring maximal comparability between outdoor and indoor aged cells. The fourth requirement is needed since outdoor aging tests may last months or possibly even years. Therefore, multiple tests will be executed simultaneously. Lastly, the system should be designed such that it is easily modified for larger cells in future. Small cells are criticized since they do not suffer as much as larger cells from the high resistivity of the TCO layer. For that reason, the efficiency of a small cell does not represent the efficiency of similar, larger cell.

A good starting point for the design of the new outdoor testing station is the group's current indoor aging system [61]. It is capable for making constant illumination tests and illuminated thermal cycling tests up with ISOS-L-2 and ISOS-LT-2 levels, respectively. This system is compatible with the group's characterization systems and provides also support for multiple simultaneous measurements. Hence, the new outdoor system can be built by copying the existing indoor system with slight modifications. Next, the indoor system is presented in short and after that the required modifications and additions are discussed in more detail. More detailed information about the system can be found from Appendix A.

3.1. Indoor aging system

The indoor testing station is composed of five main components: a lightning setup for simulating sunlight (optionally environment chamber with possibility to install lights), a BioLogic SP-150 potentiostat, an Agilent 34980A switch unit, a cell platform, and a computer. The lightning unit is composed of eight halogen lamps that produce a light spectrum close to the AM 1.5G spectrum and 1000 W/m^2 intensity. The environment chamber is capable of controlling the test

temperature and humidity. The cells are placed on the cell platform that is again placed underneath the halogen lamps or in the chamber. The distance of the platform and the lightning source is set such that the light intensity corresponds to one sun illumination. The cell platform can hold up to 16 cells at once. These cells are connected by custom-made spring connectors into 44 pin D-sub cable, see ref [62] for details. The stand is connected into one of the measurement banks of the switch unit. In this bank, the 44 pin D-sub cable is separated into 16 different cable pairs (each having the positive and negative terminal of a cell) and the pairs are connected into separate measurement channels (see manual [63]). The task of the switch unit is to connect each cell one-by-one with the potentiostat that performs IV and EIS scans for the cell. The whole switching and measuring process is controlled by a custom-made LabVIEW program [61].

3.2. Modifying the cell platform weatherproof

The first task was to make a weatherproof version of the cell platform, but without using an overall coverage so that the encapsulation of the cells can be decided on case by case. The problem of the platform design is that the spring connectors are bare and rain water can short circuit them. This disables the possibility to measure the cells and force the cells into short circuit state, which increases the cell aging rate inappropriately.

A solution for protecting the spring terminals from water was to build a comp like structure around them, see Fig 9a. Firstly, underneath each plastic beam was added a plastic wall that separated the positive and negative terminals. This disables the possibility of short circuiting the cells. Then, each terminal was separated from a neighboring one with a partition plastic wall. Without the partition wall, measuring one channel could possibly collect current from multiple cells if the neighboring cells were electrically connected by rainwater. All the walls were sealed with silicon paste so that water cannot pass through the gaps between the walls and the platform.

Next, the “rooms” of each spring terminal were closed with a detachable plastic sheet see Fig 9d. These sheets must be easily detachable since the cells have to be easily removed and reconnected from the platform. The rubber sealant stripes ensure that water cannot penetrate to the spring loads through any gap. The walls can be pressed against the beam and comp structure with wedges, see Fig 9c. The rubber is elastic enough material, which makes the seal watertight around the copper tape of the solar cell, see Fig 9b. Alternate outer walls were made slightly taller than what is the depth of the gap between the beams holding the solar cells. There is just a practical reason for that: it is very difficult to get the outer walls away from the gap if there are no place to get grip from the wall. The wall is also low enough that it is not shading the cells unless the elevation angle of the sun relative to the platform is too small. This does not happen any time of the year as long as the tilt of the platform is between 25° and 65°. Of course, the platform can be more horizontal during summer and more vertical during winter. Lastly, a removable back cover was added to the platform so that the connections between spring terminals and the measurement wires are protected from water and dirt.

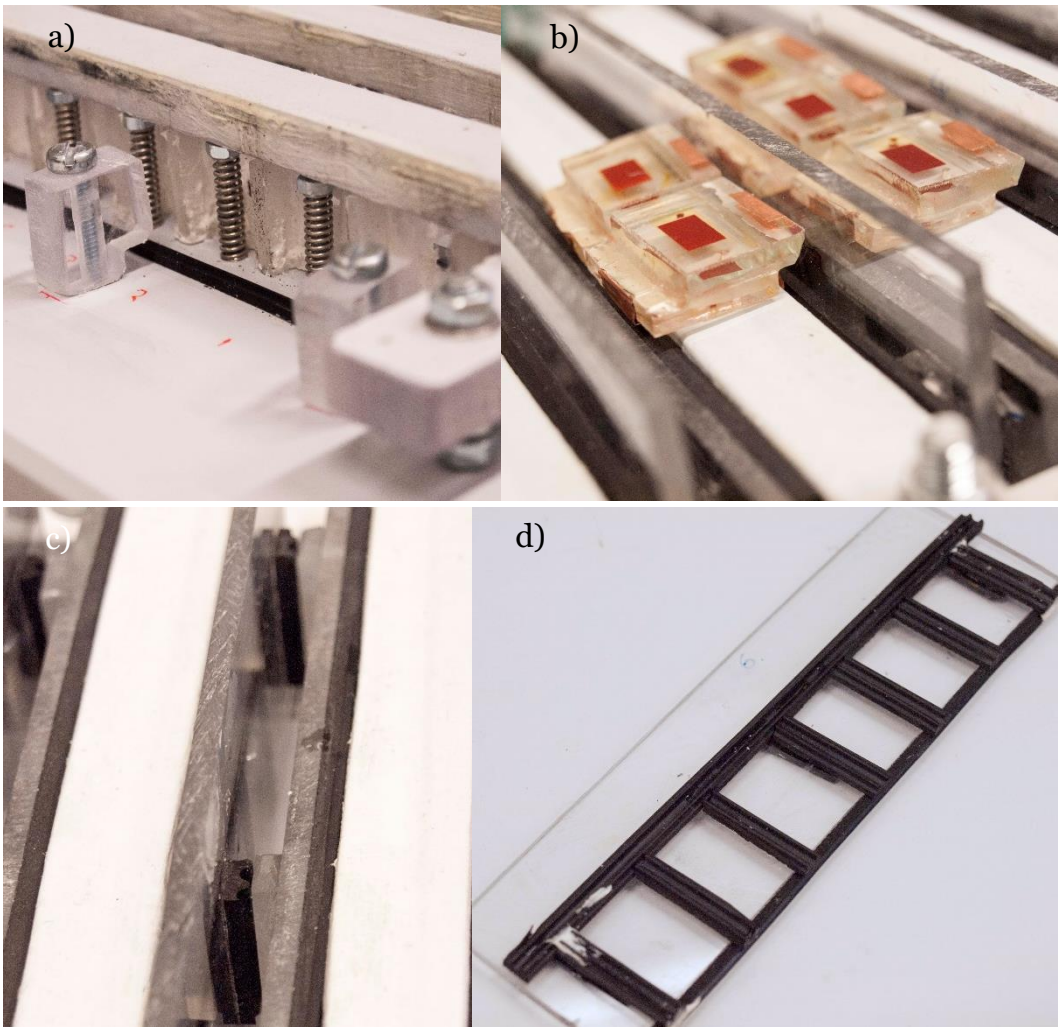

Figure 9. a) Comp structure around the spring terminals b) Cells connected to spring terminals with weather protection c) Ledges press the outer walls tightly against the platform beams. d) A detachable outer wall

3.3. Stand for the solar cell platforms

Next task was to develop a proper measurement place for the solar cells. Luckily, there was a free, unused aluminum stand on the roof of the group's faculty, see Fig 10. The stand has adjustable tilt angle so it is ideal for solar cell measurements. Unfortunately, a new building was constructed southwest of the faculty during this work and it became tall enough to shadow the aluminum stand when the elevation of the sun is approximately below 15°. Thus, the cells are shadowed during noon and afternoon from mid-November to beginning of February.

The modified cell platform is connected to the aluminum stand with custom made plastic, hook-like holder. The holder is connected with screws to the back cover of the cell platform so the platform cannot drop from the holder even with high tilt angles due to wind. The holder itself is simply hanged to the aluminum stand. The gravity will keep the holder attached to the stand with all tilt angles.

3.4. Connecting the cell platform to measurement devices

The measurement instruments and the computer are not weatherproof equipment so they have to be located indoors in a lab. Unfortunately, the available lab is not directly below the measurement stand on the roof. This makes it very difficult to connect the cell platform to the switch unit. Therefore, it was decided to make a separate, stationary connector terminal next to the measurement stand on the roof, see Figs 10 and 11. The user can simply hang the measurement platform to the stand and connect the cell platform to the terminal, just like the platform would be connected to the switch unit in the indoor setup.

The connector terminal is connected to the measurement equipment with 18 m long 44 wire D-sub extension cables. The cable wires are solid copper, which retains the total wire resistance small enough even if the setup was modified in future to support slightly larger solar cells. Additionally, the cables have aluminum foil shielding so electrical noise should not enter the cables along the extension wires even though the wires pass some technical spaces with 50 Hz 230 V grid electricity wires.

Figure 10. Roof station of the measurement setup. The cell platform is hanging on the stand and the connector terminal is on the plywood on the left.

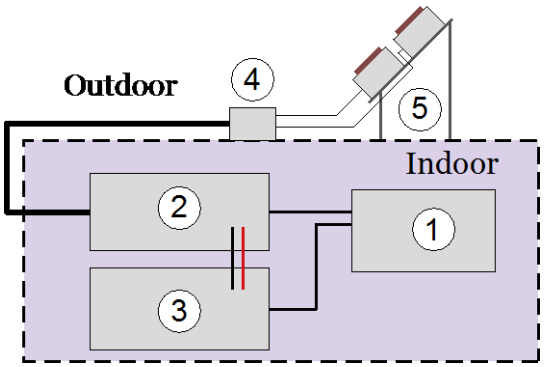

Figure 11. The computer (1) and measurement devices (2-3) are indoors. The Switch unit (2) is connected with extension measurement cables to the outdoor connector terminal (4). The solar cell platforms and weather sensors (5) are connected to the connector terminal.

3.5. Weather recording

Weather recording is important in outdoor measurements and is required in the ISOS-O-3 standard. The installed sensors are pyranometer (SP Lite2, Kipp & Zonen) for recording solar irradiance, humidity sensor (HM1500LF, TE Connectivity) and T-type thermocouples for measuring ambient and cell temperature. The pyranometer is positioned in the same tilt angle as the cells, see Fig 12. The humidity sensor is connected to the stand such that it is not exposed for rain. The thermocouples measuring air temperature are positioned close to the cells such that they are constantly in the shadow. The thermocouples measuring cell temperature are not physically connected to the cells themselves. Instead, they are positioned to the sun light next to the cells and let heat up due to the irradiation, see Fig 12. According to an infrared camera (InfraCAM Wester, FLIR) the thermocouples are approximately in the same temperature than the cells (± 2 °C, measured on a sunny day October 6th). This would provide more accurate cell temperature measurements. Thermocouples were not directly connected to the cells since their weather encapsulation would had limited the heat flow from the cells to the sensors. However, in future a thermocouple could be tried to be fitted inside a similar solar cell that will be tested for improved accuracy. At the moment, there are two thermocouples measuring each temperature for the sake of reliability since thermocouples have limited lifetime.

The ISOS-O-3 standard requires also monitoring wind speed and direction. However, wind speed is a very time and location dependent parameter. For that reason, studying the effect of wind on solar cells requires much manual analyzing. Wind influences cell temperature and humidity, but both parameters are recorded separately. In addition, the solar cells are quite well protected from the wind due to the shape of the cell platform. As a conclusion, an anemometer was not yet installed to the measurement system though it can be easily added later to the system.

Figure 12. The outdoor station. The cell platform is on the left and pyranometer and one cell temperature simulating sensor is on the right.

3.6. The measurement instruments

The cell performance monitoring system is kept almost similar as the existing monitoring system for indoor measurements. The only difference is that the expensive potentiostat is replaced by five-fold cheaper source measure unit (SMU) (Keysight U2722A). The switch unit is same model (Agilent 34980A) and both instruments are controlled by computer with LabVIEW environment (see Section 3.7). During the measurements the operation principle of these devices is the same: the switch unit connects the cell terminals to the terminals of the SMU that performs the measurements. The data is stored to the hard drive of the computer.

One larger difference between the new setup and the existing setup is that the new setup is only capable for IV measurements. EIS measurements were thought to be too time consuming for outdoor conditions. A typical EIS scan lasts several minutes and having stable weather conditions for such long time is not guaranteed, especially during partly cloudy days. Moreover, EIS should be performed with short measurement wires to minimize their effect on the impedance values. The 20 m cables might be too long for that[4]. For these two reasons, it was decided that a SMU is enough for the measurements and five times more expensive potentiostat is not needed.

Another larger difference is that the new setup was configured to support aging under different loads. The SMU has in total three measurement channels. The first one was labeled for IV measurements and the rest were labeled for sinking current with adjustable voltage difference. These two channels are connected also to the switch unit. When a cell is not measured the switch unit connects it to either of the current sinking channels. For aging simultaneously multiple cells under load the cells are connected first in parallel and the formed cell array is connected to the current sinking channel of the SMU, see Fig 13 for a schematic. The SMU channels are all separate and they can operate individually so there can be two different cell arrays under load at the same time.

[4] EIS was not tested with the extension cable. The impedance of the cable could possibly be filtered from the data but this is beyond the scope of this work.

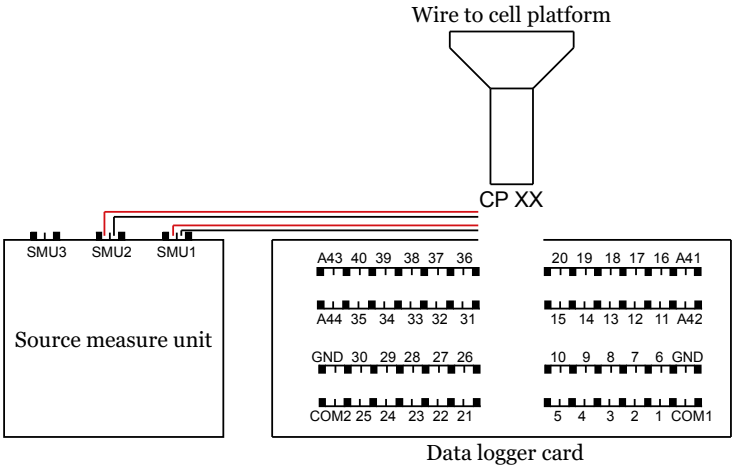

Switching procedure during measurements

1. Start: every channel open
2. Close channels 22 - 36 and 40
3. Close channels 1 and 20
4. Perform measurements
5. Open channels 1 and 20
6. Close channel 21
7. Open channel 22
8. Close channels 2 and 20
9. Repeat the procedure for every channel
10. Open channels 16 and 20
11. Close channel 36
12. Open channel 21
13. Move to step 3

Connection scheme

1 -> CP 01	21 -> CP 01
2 -> CP 02	22 -> CP 02
3 -> CP 03	23 -> CP 03
4 -> CP 04	24 -> CP 04
5 -> CP 05	25 -> CP 05
6 -> CP 06	26 -> CP 06
7 -> CP 07	27 -> CP 07
8 -> CP 08	28 -> CP 08
9 -> CP 09	29 -> CP 09
10 -> CP 10	30 -> CP 10
11 -> CP 11	31 -> CP 11
12 -> CP 12	32 -> CP 12
13 -> CP 13	33 -> CP 13
14 -> CP 14	34 -> CP 14
15 -> CP 15	35 -> CP 15
16 -> CP 16	36 -> CP 16
17 -> (free)	37 -> (free)
18 -> (free)	38 -> (free)
19 -> (free)	39 -> (free)
20 -> SMU 1	40 -> SMU 2 (3)
A41 -> (free)	A43 -> (free)
A42 -> (free)	A44 -> (free)
COM1 -> (free)	COM2 -> (free)
GND -> CP GND	GND -> (free)

Figure 13. The schematics represents how cells are connected to the channels of the SMU, and the order in which the channels switched. Every cell is connected to two channels in the switch unit: the channels with smaller numbers connect the cell to the measurement channel 1 of the SMU and the channels with larger numbers connect the cell for loading to the SMU channels 2 or 3 when it is not being measured.

3.7. Creating program for measurement execution

The new outdoor testing station requires a software for measurement execution. The station uses the same LabVIEW environment as the indoor aging system. Hence, the new program follows the style of the old program, for convenience [61]. Fig 14 shows the simplified schematics of the program (more detailed figure in Fig A6 in Appendix A).

The measurement software is launched by opening the “Start window” sub program called virtual instrument (VI) in the LabVIEW environment. The user may set some general settings, such as pyranometer sensitivity value, or determine the switch unit channels that are connected to solar cells. The actual measurement execution is started by moving from the “Start window” to “Measurement initialization” section. At this point, user will define different measurement parameters for the first set of measurements. The parameters include information such as measurement interval and IV scan rate. In addition, user will determine, which switch unit channels are included into the test and whether the test cells will be kept under load or not. At later point, more measurement sets can be added to the program if another aging study is wished to start.

After initializing the measurements, the software starts executing the measurements by moving to the “Main program” section. This section is the core of the software: it handles the sub programs controlling the measurement instruments and offers interactive user interface. The sequence in which order the “Main program” progress is shown in Fig 15. First, it checks whether user wishes to make modifications to the measurement sets. For example, if user wants to end a measurement set it is removed from the program at this point. Next, the program loads the measurement parameters given for the first set (or the oldest still running set if the first set is ended) and starts taking measurement for the test cells of this set. After these measurements are finished the program moves to the next set if there is one.

The commands that user can give for the program are: pause measurement, continue measurement, update measurement, add measurement or end measurement. The pause ability was included to the program so that the execution of single set can be suspended temporarily. It enables removing the cell or cell platform from the station so that extra measurements like EIS can be performed with different measurement setup while other sets are kept running. The update command lets the user to modify the measurement parameters and the amount of test cells of an existing set. The add command lets the user add a new measurement set to the program and the end command removes a measurement set from the program.

The user interface of the “Main program” contains all the above mentioned commands. In addition, it also shows the state of the program, latest IV data from all cells, weather charts, and an event log. The event log lists all the non-regular events, such as pausing, and it also shows if the program has crashed due to error. All the events are time stamped so that the time of the event can be located afterwards, too.

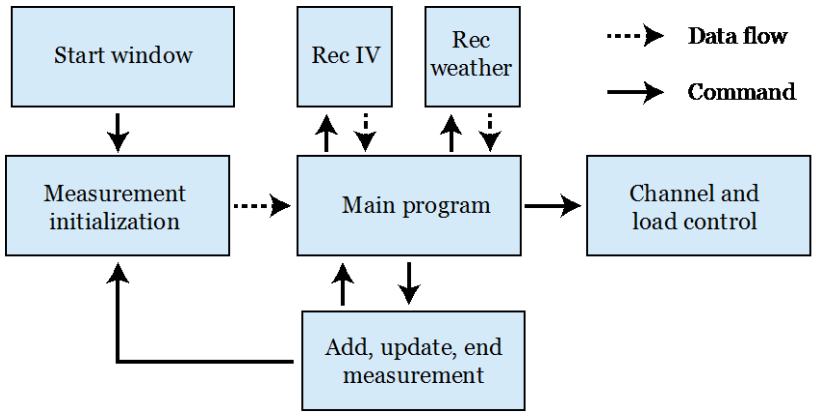

Figure 14. The simplified structure of the program. The program starts by measurement initialization section after which the main program section activates. The main program section controls the measurement execution and launches different sub-programs that executes measurements, switch channels of the switch unit, and etc.

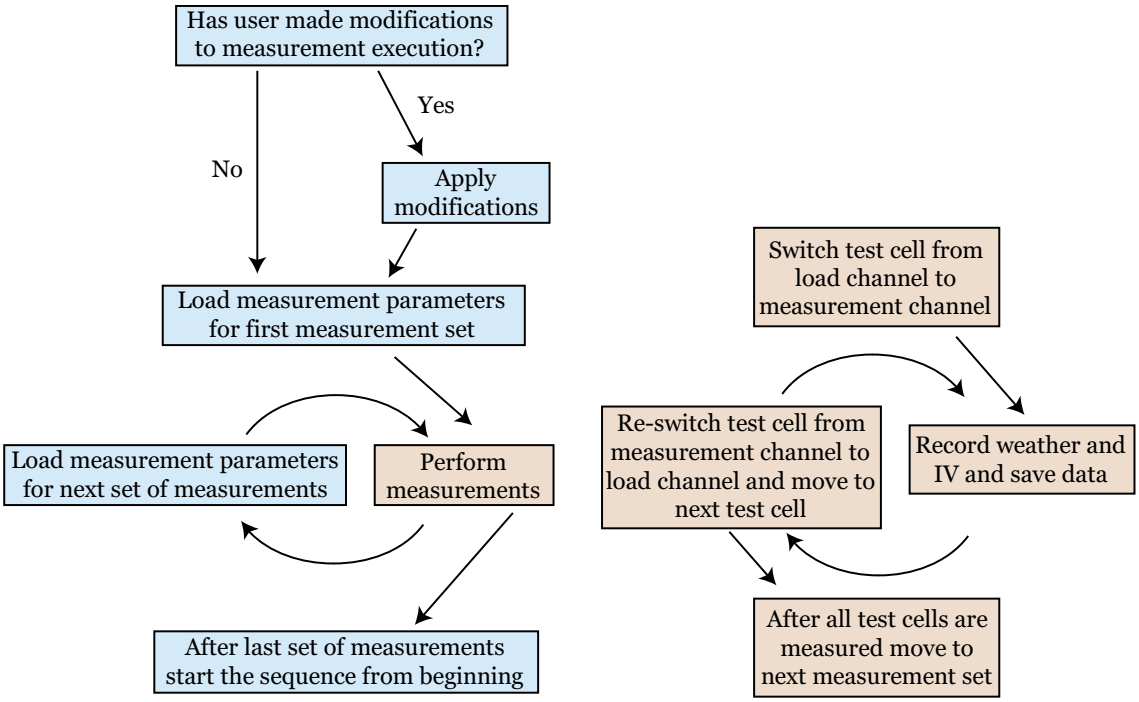

Figure 15. The measurement execution sequence. The program loop starts with the interactive part of the VI. If user wishes to make modifications to the measurement execution (e.g. update measurement parameters of an existing measurement or add a new one) the modifications are performed at this point. Next, the VI starts taking measurements a channel by channel, a set by set.

3.7.1. Minimum interval time for measurements

Electrochemical solar cells have limited response speed to load voltage changes, i.e. the current output of the cells takes some time to stabilize after the voltage change. For this reason, the IV scan cannot be performed very fast. For DSSCs, the scan can be performed about in 30 s to 60 s per scan direction depending on cell structure and degradation state of the cell. Otherwise, hysteresis will occur between the forward and reverse scans. For Omh-PSCs, the scan has to be even slower, sometimes several minutes to avoid hysteresis. This limits how many cells the system can measure during the set interval. For example, if 15 DSSCs are to be measured a 30 min interval for the measurements should be selected, at minimum. With shorter interval lengths, the measurement time of the first cells occurs before the system has completed measuring the remaining cells. In this kind of situations, the system continues directly to the next measurement round.

3.7.2. *Effect of varying irradiance on IV scans*

The IV scan is performed twice in the program: forward and reverse. This is a normal practice when measuring IV curve of a solar cell. Typically, the reason is to see whether the cell has been stable during the measurement. If the cell has been unstable, the forward and reverse scans do not match each other completely. In this system, there is also an additional reason for performing both scans: to see whether the measurement conditions have remained stable. Especially, on partly cloudy conditions, the irradiance level varies often quickly. This varies the output current of the solar cell, which can be seen easily from an IV scan, see Fig 16. For this reason, both scans are saved so that these kinds of failed scans can be filtered out with least squares method, for instance.

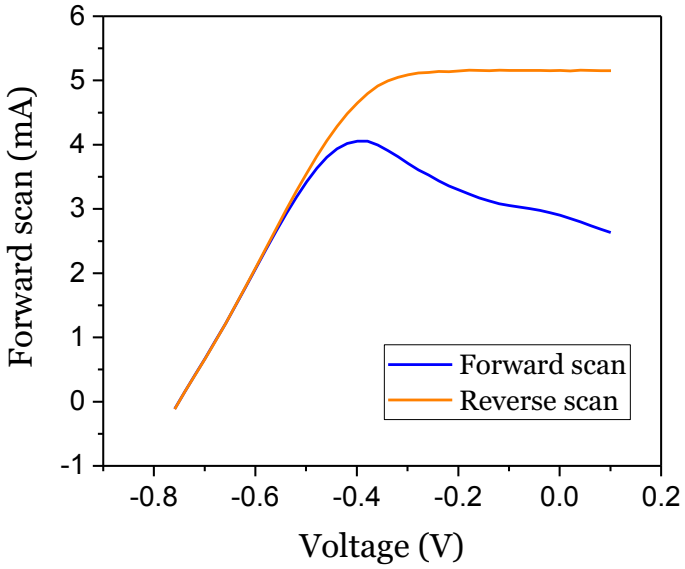

Figure 16. An example of an IV scan where cloud covered sun in the beginning of a scan but not anymore in the end.

3.7.3. *Effect of cable resistance*

The resistance of the measurement cables was measured to be 4.5 Ω on average for each channel. This resistance introduces a voltage difference between the cell terminals and SMU terminals. Therefore, the controlled SMU voltage (V) does not match the cell voltage (V_C) when current (I) runs through the system:

$$V_c = V + IR_W \tag{7}$$

where R_W represents the total resistance of the measurement cables. With small currents (< 1 mA) the difference between the two voltages is negligible but with higher currents there is more significant difference. For example, with 100 mA output current the voltage loss in the wires is already 0.45 V.

Typically, this problem can be solved by using 4-wire measurement setup. However, it would require large, additional modifications to the test station so the problem was decided to solve with programming. In IV recording, the scan voltage is replaced by the actual cell voltage that is obtained with Eq 7 during the

data analysis. In load voltage controlling (see Section 3.8) the effect of cable resistance is removed real time with the LabVIEW program.

3.8. Maximum power point tracking

There are numerous different methods to track the maximum power point of the solar cell [64]. Since the setup has computing power, a so-called perturb and observe (P&O) algorithm was implemented to the LabVIEW program for tracking the maximum power point during the aging. The P&O method involves varying the aging voltage of the cell array and recording its output power round-by-round, see Fig 17. If the aging voltage is increased (decreased) and the output power of the array increases, the voltage is further increased (decreased) on the next round. On the other hand, if the increase (decrease) in aging voltage decreases the output power, the voltage is decreased (increased) on the next round. The summary of the possible events in P&O algorithm is shown in Table 8.

The algorithm is updated every 10 seconds and the perturbation size is 0.01 V by default in the LabVIEW program though it can be modified easily in future experiments. However, due to communication limits between the SMU and the computer, the tracking cannot be performed during the IV scans. Therefore, the tracking is performed between each scan, and it is repeated until the perturbation direction changes, i.e. the maximum power point is found. This slight modification prevents that the operation voltage does not lag too long behind the maximum power point.

Table 8. Possible events in P&O algorithm and their effect on next round.

Voltage perturbation	Change in output power	Next perturbation
Increase	Increase	Increase
Increase	Decrease	Decrease
Decrease	Increase	Decrease
Decrease	Decrease	Increase

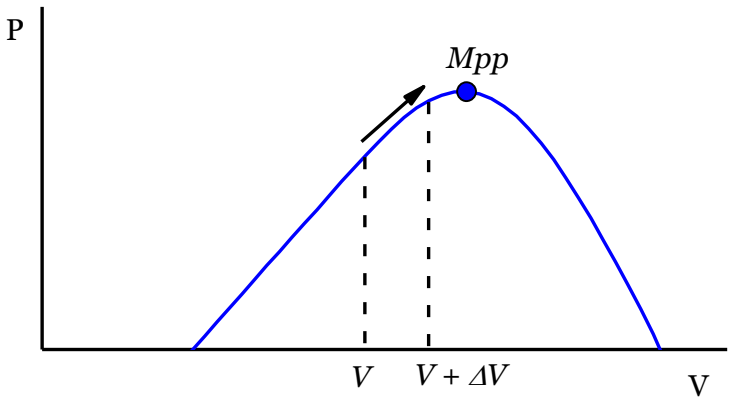

Figure 17. The P&O algorithm varies the aging voltage such that the aging voltage follows the maximum power point voltage.

4. Full-scale test of new measurement setup

4.1. Test solar cell assembly

Five laboratory scale solar cells were fabricated for testing the new aging system (named R1, R3, R4, R6, and R7). The active area of the cells was 0.4 cm^2 and the total area around 4 cm^2, see Figs 18 a-b. The dark red square is the photoanode of the cell (the active area) and the light yellowish part is the electrolyte. In addition, the cell contained transparent oxide layers on both electrodes and a transparent layer of platinum catalyst on the counter electrode. To prevent the two electrodes touching each other directly, there is an insulating plastic layer of Surlyn® (20 μm thickness, DuPont) between them, which also seals the liquid electrolyte into the cell. The copper tapes are the terminals of the cell, and they are attached with silver paint and epoxy glue on the conductive oxide layers of the electrodes. Next, the preparation process and more precise description of the used materials of the cell is presented.

The photoanode of the cell was prepared with screen printing method. First, a 4 mm borosilicate glass plate with one side coated with TCO layer was cleaned thoroughly with washing detergent, ethanol and acetone. In addition, the plate was placed under strong UV light for 20 min in UV-ozone device (UV/Ozone Pro Cleaner, BioForce Nanosciences) and then into ultrasonic bath of ethanol for 8 minutes. The cleaned plate was inserted into a solution of titanium(IV) chloride tetrahydrofuran complex (1 w-%) in de-ionized water and heated for 30 minutes at 70 °C. Next, three rectangle layers of TiO_2 were screen printed on the conductive side of the glass plate. The first two layers contained particles of average size 20 nm (DyeSol, 18NR-T) and the third layer contained particles of size 150 to 250 nm (DyeSol, WER2-O). The smaller particles are effective to absorb light and the larger particles are effective to scatter light. This configuration increases the light absorption of the electrode since the last layer scatters photons back to the first layers.

The screen-printed glass plate with TiO_2 layers was sintered for 30 minutes at 450 °C. After the plate had cooled down, it was inserted again into the solution of titanium(IV) chloride tetrahydrofuran complex in de-ionized water and heated for 30 minutes at 70 °C. Next, the glass plate was rinsed with de-ionized water, ethanol, and with both again. The cleaned glass plate was cut into single cell pieces with glass cutters so that each piece was 16 x 20 mm. The pieces were sintered again for 30 minutes at 450 °C. Finally, the pieces were placed into a liquid solution for dying. The solution was prepared earlier by Aapo Poskela and it contained Z907 dye (cis-Bis(4,4'-dicarboxy-2,2'-bipyridine)di-isothiocyanato-Ruthenium(II)) and aceto-nitrile (ACN) and tert-butylalcohol (TBA) as solvent. The pieces were kept in the dye solution for 24 h in dark, airtight container at room temperature. After that, the cells were moved into acetonitrile tert-butyl-alcohol solution (1:1 vol-%) waiting for cell assembly.

The counter electrodes were also prepared on 4 mm borosilicate glass with one side coated with TCO. Unlike the glass used for photoanode, the glass for

counter electrode contained small drilled holes for filling the electrolyte in the assembly process (described in next paragraph). The counter electrode glass plate was cleaned and cut into smaller pieces similarly as the photo electrode glass plate. Next, 4.0 µl of 5mM H_2PtCl_6 in 2-propanol solvent was spread with micro-pipette evenly over the conductive side of the glass piece. The coated pieces were sintered for 20 minutes at 390 °C.

For the liquid electrolyte, 1-methyl-benzimidazole (NMBI), 1-propyl-3-methylimidazolium (PMII), and iodine (I_2) were all dissolved into 3-methoxypropionitrile (MPN). The ratios of the three compounds were 5:5:1 (mol-%), respectively, and the ratio of the three compounds to the MPN was 11:10 (mol-%).

The cells were assembled after all the required components were ready. First, the photo and counter electrodes were dried from moisture and acetonitrile-alcohol solution. Next, they were attached to each other with the help of a Surlyn® plastic sealant. The rectangular sealant was placed around the photoanode and the counter electrode was placed on top of that sealant. Then, the "sandwich" was pressed for 1 min at 120 °C, which made the sealant melt and glue the glass pieces together. Next, the cell was let cool down and the electrolyte was added through one of the holes in the counter electrode. Capillary forces spread the electrolyte quickly into the empty space while excess air escaped through the second hole. Then, the holes were sealed with a thin cover glass and a Surlyn® sheat. The cover glass was again attached on the counter electrode by quick hot pressing. Next, copper tape terminals were attached to the cells. The electrical contact between the electrodes and the tape pieces were improved with silver paint. Lastly, the cell was sealed with epoxy to prevent the electrolyte from leaking and to ensure the mechanical strength of the copper tape terminals.

Since moisture may cause degradation of the solar cell materials the cell assembly should be performed in dry atmosphere. However, there were no such facilities available at the time of the assembly so it was completed in normal laboratory room with relative humidity between 40 and 50 %. For that reason, some moisture may have entered the cell during the assembly, which may have lowered the initial cell performance.

a)

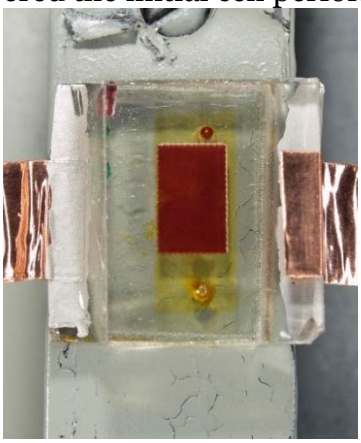

b)

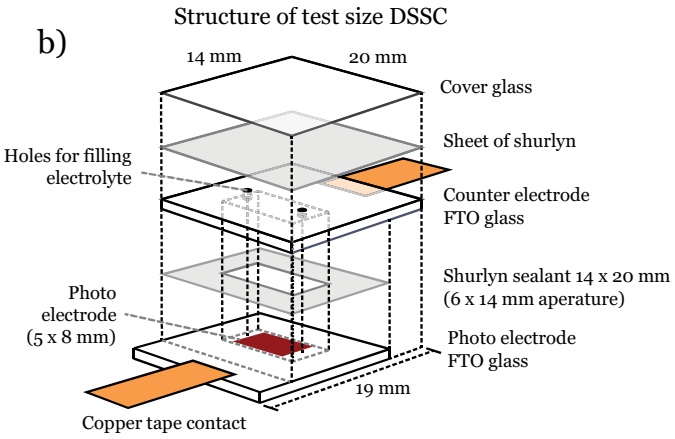

Figure 18. a) Photo of a test solar cell and b) schematic structure of the cell. The red rectangle is the photoanode that is the active area of the cell, and the yellowish area around and beneath the photoanode is the electrolyte of the cell. Surlyn® sealant is used to encapsulate the liquid electrolyte between the electrode glass substrates.

4.2. Cell characterization methods

In addition to monitoring the IV curves outdoor, the cells were characterized with different methods in standard indoor conditions, either with weekly basis or just initially before the outdoor test and afterwards it. See Table 9 for summary of the characterization methods and parameters. Before characterization the cells were let dry and warm up until they reached room temperature.

The characterization light source for IV and EIS was Peccel PecL01 class A solar simulator. The characterization light for saturation current was in-house built LED light, which intensity can be varied from 0.4 sun to 9 sun equivalent. Opaque tape mask was used with IV and EIS measurements to prevent diffuse light reaching the active area of the cell during the measurements, see Fig 19.

The IV measurement was quick enough that the cell temperature remained close to room temperature, but the EIS measurement was slower and was performed after the cell had stabilized to around 40 °C temperature. The cell temperature under the in-house built LED light was kept close to the ambient temperature with strong PC desktop fan: the cell temperature rose approximately 5 °C higher than the ambient temperature. Other characterization methods were performed at room temperature.

Table 9 Summary of characterization methods.

IV	Interval	Weekly
	Device	Keithley 2401
	Light spectrum	AM 1.5 G, 100 mW/cm²
	Temperature	25 °C ± 3 °C
	Voltage range	-0.3 V to 0.8 V
EIS	Interval	Weekly
	Device	Zhaner Zennium
	Light spectrum	AM 1.5 G, 100 mW/cm²
	Temperature	40 °C ± 5 °C
	Frequency range	100 mHz to 4 MHz
	Bias DC voltage	Open circuit
Cell photographing	Interval	Weekly
	Device	Olympus E620
	Other settings	See [16]
IPCE	Interval	Initial and final
	Device	PV Measurements QEX7
	Temperature	22 °C ± 3 °C
	Light range	400 nm to 1000 nm
Saturation current	Interval	Initial and final
	Device	Autolab PGSTAT N302
	Light spectrum	White LED
	Light range	0.4 sun to 9 sun equivalent
	Temperature	27 °C ± 3 °C
	Voltage range	-0.3 V to 0.8 V

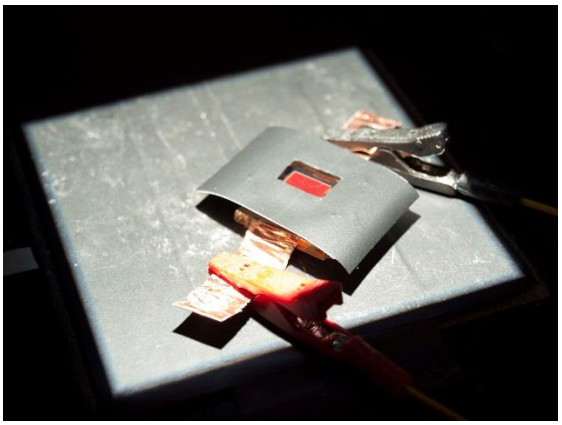

Figure 19. Rectangular tape mask was used to prevent diffuse light reaching the photoanode of the cell during IV and EIS characterization.

4.3. Outdoor aging procedure

The cells were put aging on 6th of October 2016 and they were kept there until 17th of November 2016, which corresponds approximately to 1000 h. The tilt angle of the cells was set to 70° that is about the optimal angle for autumn and winter time in Espoo, Finland (60.2° N, 24.8° E) and its azimuth is towards south. IV curves of the cells and weather parameters were recorded every 15 minutes. The weather parameters were recorded just before each IV measurement so that the recorded weather values match as well as possible to the weather conditions during the IV measurements. Technically, it is also possible to record the weather parameters continuously during the IV scan but it slows down slightly the scan speed and faster scan speed was preferred this time. This is because if the weather conditions change during a scan, it can be seen in the data as shown in Section 3.7.1.

The initial plan was to keep the test cells first in open circuit conditions and then change a share of the cells to age under load. However, due to high variations in cell performances (see Section 5.2.1) all cells were kept in open circuit conditions throughout the testing.

The IV curve was recorded from -0.1 V onwards until the output current passed -0.1 mA. It was decided not to use constant upper voltage limit to avoid collecting unnecessary data in dark. The voltage step size was also relatively high 0.02 V to make scan speed faster and to reduce the data size.

The amount of obtained IV data from the test was large, over 20 000 IV scans. Therefore, the IV parameters were estimated directly from the IV curves by simple calculations without fitting the diode model (eq 3) to each measured IV curve. The fitting would have taken too much computing power and time.

5. Test results and discussion

In this chapter, the results of the test are presented. First, the weather during the test is shown to provide information about possible causes for cell aging. After that, the results of the indoor characterization are shown and analyzed. Yet after that, the data of the outdoor station is shown and analyzed, and lastly some comments about the measurement quality of the outdoor station is given.

5.1. Weather during the test

Fig 20 show the weather conditions during the test. The conditions have varied significantly: the weather was first relatively warm and sunny, then one week rainy and chilly, then one week frosty and snowy, and lastly rainy and chilly again. During the snowy period the cells had occasionally been buried under the snow. The relative humidity was high throughout the test: mostly it was between 80 % and 100 % and only rarely below 60 %. Temperature and irradiance are shown in Fig 20. During that time, cumulative irradiance reached only 34 kWh/m² that corresponds to 34 hours of 1 sun illumination. This should not have caused degradation for the cells since the used cell type has proven to be stable for over 800 kWh/m² illumination doses [65].

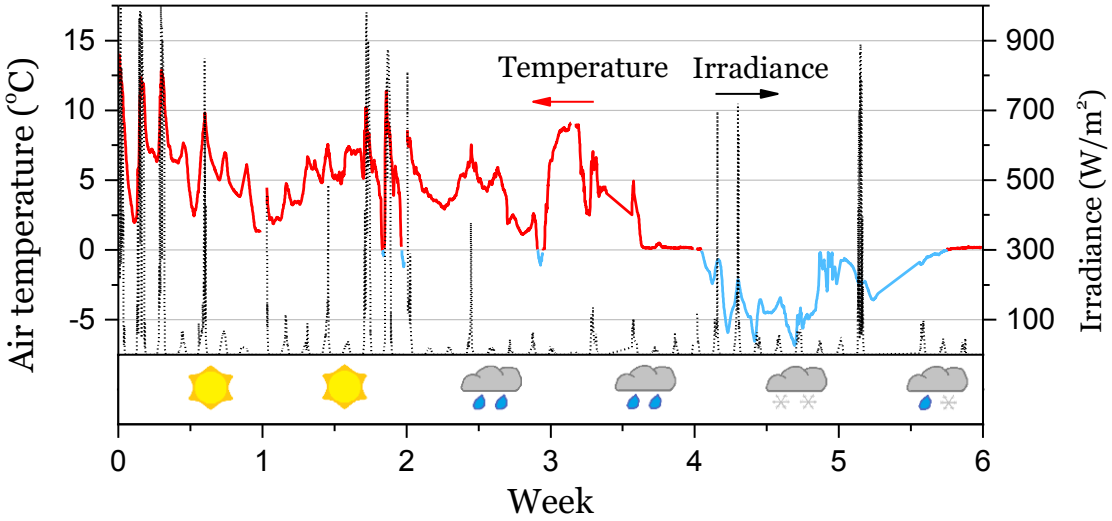

Figure 20. The temperature, irradiance and weather type during the test period.

5.2. Indoor measurements

The IV parameters of the test cell are shown in Fig 21. The results show high variances in performance as function of time and between each cell (more about the latter variations in Section 5.2.1.). There are two clear drops in the average cell efficiency: between weeks 2 and 3 and later between weeks 5 and 6, see Fig 21a. At those times the weather was rainy (not snowing) so extreme moisture is very likely causing degradation for the cells. The cell seems to be stable at sub-zero temperatures since they have rather stable efficiency over the freezing period. This is rather novel information. Only study [66] has previously reported that DSSCs do generate power *after* exposing to freezing temperatures without significant degradation, but operation *during* freezing has not been reported previously.

The reason for the decreased efficiency is that the cells generate less current, see Fig 21c. On both weeks, the short circuit current drops. On the other hand, the open circuit voltage increases significantly on the first rainy week. The average fill factor and series resistance are more stable parameters: fill factor slightly increases mainly due to decreasing current and series resistance has no clear trend.

The effect of water on the cell stability has been under debate and contradictory results have been presented previously. Study [67] obtained similar results as have been found in this work though they used hydrophilic N719 dye instead of hydrophobic Z907. They noticed that adding water to the electrolyte during the assembly increased the open circuit voltage and the fill factor of the cells, and slightly decreased the short circuit current density, resulting in slight increase of efficiency. They proposed that water shifts the lower band edge of TiO_2 nanoparticles higher such that less excited electrons are able to move from the LUMO level of the dye to the conduction band of the nanoparticles. This would increase the open circuit voltage (which is the potential difference between the conduction band of the TiO_2 and redox-electrolyte without any losses) and decrease the short circuit current density of the cell. In study [68] 10 vol-% water content in the electrolyte both increased slightly short circuit current density and open circuit voltage, which lead to the increase of cell efficiency. Furthermore, the cells with 10 vol-% water content were stable for 1000 h under simulated sunlight. They used the same Z907 dye as was used in this study. Study [69] examined the effect of water on some common dyes. They found that soaking photoanodes with hydrophilic N3 and N719 dyes in water-ethanol solution instead of pure ethanol did cause dye desorption during the soaking. For hydrophobic Z907 dye similar desorption was not observed. Again, cells prepared from water-ethanol soaked photoanodes had higher open circuit voltage but lower short circuit current density.

However, all these studies added most likely distilled water to the cells. Rainwater has numerous different impurities that may also penetrate through the cell sealing. Therefore, the increase in open circuit current could be due to the band edge shift proposed in [67], which would also decrease the short circuit current density. On the other hand, the penetration of impurities inside the cell may have also caused degradation, which have resulted in the decrease of short circuit current density.

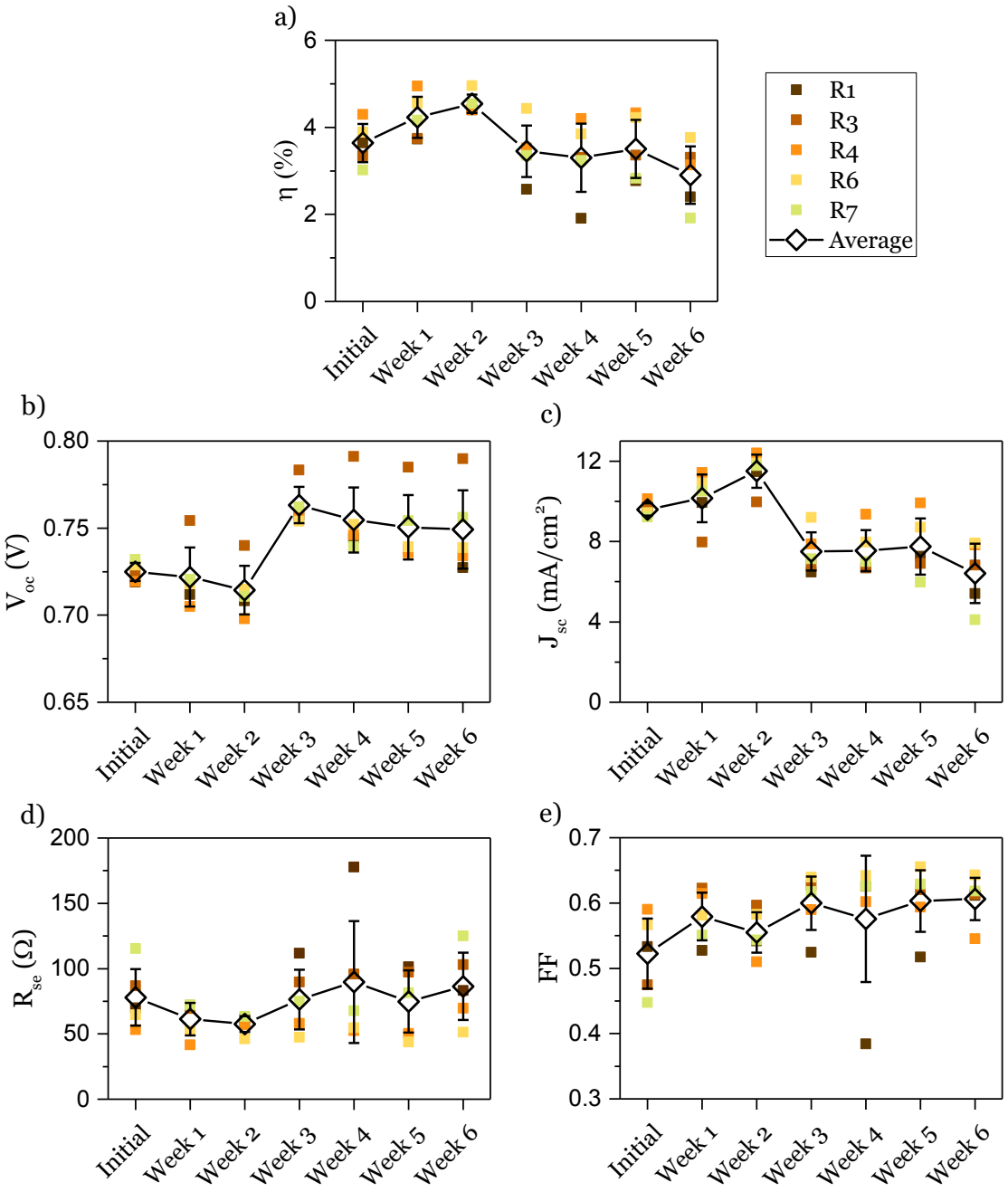

Figure 21. The figure shows a) efficiency, b) open circuit voltage, c) short circuit current density, d) series resistance, and e) fill factor measured under AM 1.5 G spectrum at 1 sun equivalent at 25 °C.

The EIS data is shown in Fig 22 data. The cell R1 is missing from the figure since the potentiostat was unable to measure the impedance of that particular cell. The reason for this failure remained unclear since there is nothing special visible neither in the IV parameters nor in the IV curves (latter not shown here) of that cell. There were no other failures in EIS measurements with the other cells. However, after the first rainy week, the EIS data readability became a problem: there were no more easily visible distinct semicircles in Nyquist plots but instead only one wide semicircle. This complicated the fitting of the equivalent circuit to the spectrum, and often the obtained parameters varied significantly between consecutive fits. These "faulty" parameters may have also ended up to the Fig 22, which could explain some of the high variations.

In overall, the average series resistance has decreased slightly while the other resistance components have remained stable within the error margins, see Fig 22. The decrease of the series resistance occurs in the beginning already before the rainy week so it is most likely due to that the cells had not yet reached their maximum performance after the assembly. It is typical that the performance of the cells increases initially and the exact reactions behind this are not understood. Otherwise the parameters are stable, at least for some cells, so the internal resistance may not have large contribution in the cell degradation, at least on all cells.

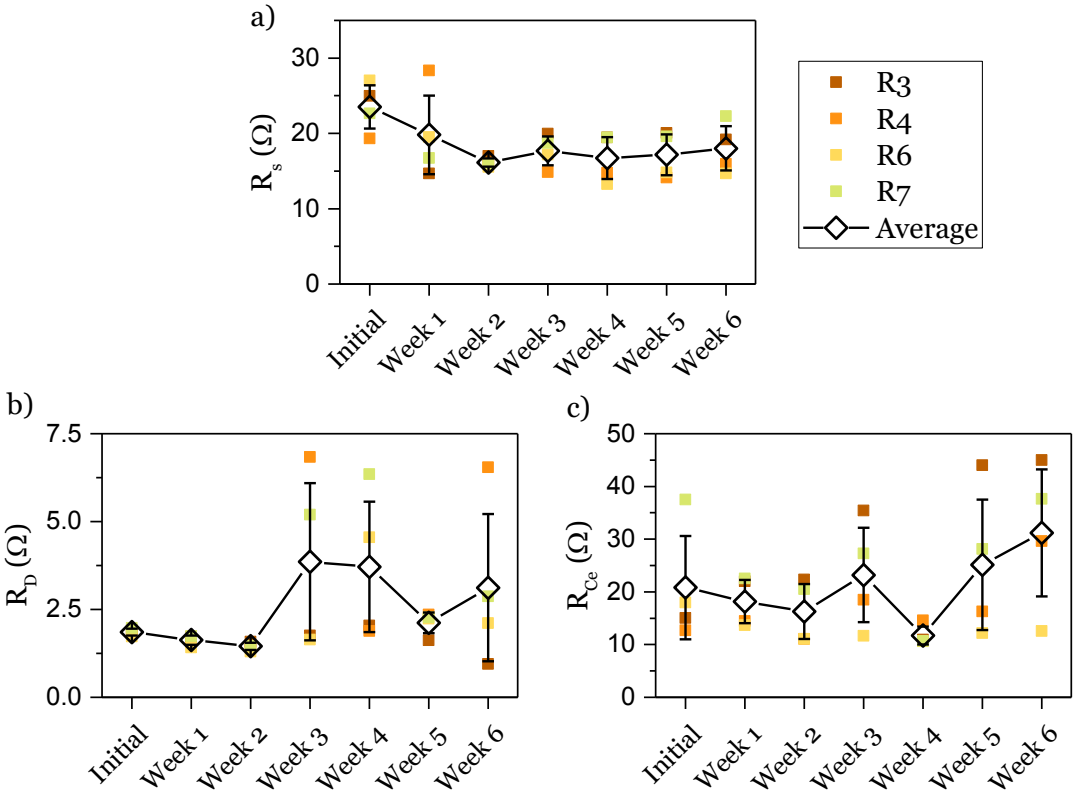

Figure 22. The figure shows a) series resistances of the cell, b) mass transport resistance at the counter electrode, and c) charge transfer resistance at the counter electrode-electrolyte interface. High variance in some values is most likely due to failed fitting of equivalent circuit to the spectrum. R1 is missing from the data since it experienced contact issues during the EIS scans, which prevented performing the measurements.

Initial and final photos of the cell are shown in Fig 23. The cells seem to have survived quite well from the outdoor environment. Cells R1 and R7 have suffered electrolyte leakage: there are yellow traces of iodine outside the electrolyte chamber in R7, and R1 was noticed to have become empty two weeks after the final measurements. The color of the dyed TiO_2 has remained quite stable during the test period, see Fig 24 a-b. The red pixel value has slightly increased and the blue pixel value decreased though the differences still fit inside the error margins. Instead, the color of the electrolyte changes from yellowish to more transparent during the testing period, see Fig 25 a. This increases the RGB blue pixel value of the electrolyte in the images at the electrolyte area, see Fig 25b. Initially, the average blue pixel value is 70 and after the testing it is 105. This corresponds to approximately 50 % decrease in the iodine concentration from 0.05 M to 0.025 M. However, the color change is not very even for all cells (R1, R4, R6) as is visible for R4 in Fig 25a where there is a clear color gradient between the upper and lower part. This also explains the increased variance of the blue pixel value. It is not clear why this happened. It should not be a leakage since the capillary forces should spread rest of the electrolyte evenly as happened during the cell assembly. On the other hand, moisture may have penetrated only into the upper end of the cell, which would have caused spatial bleaching of the electrolyte. Though diffusion should again balance the redox couple concentration gradient but this may take some time as was found in simulations for the movement of tri-iodide from the edges of the cell to the active area of the cell [70].

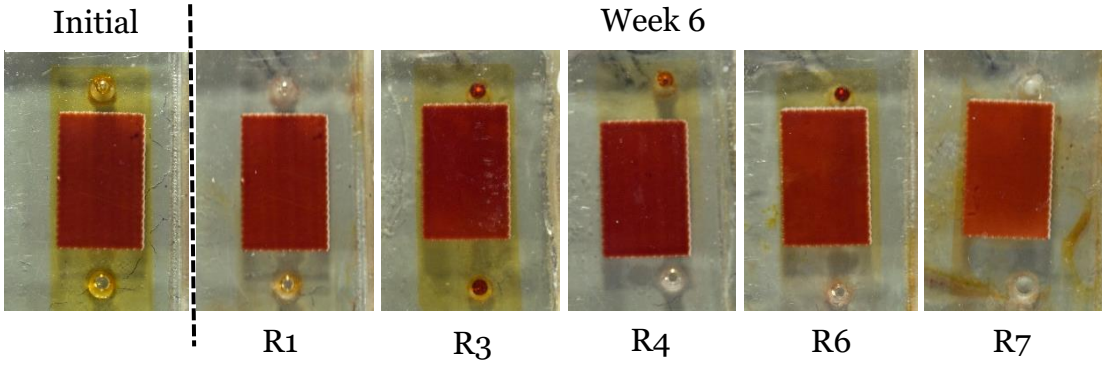

Figure 23. Photographs of the cells from front side. Initially, all cells looked like the one on left but in the end some cells had lost more electrolyte color than the others. R7 was also leaking electrolyte: there are yellow spots under the sealing.

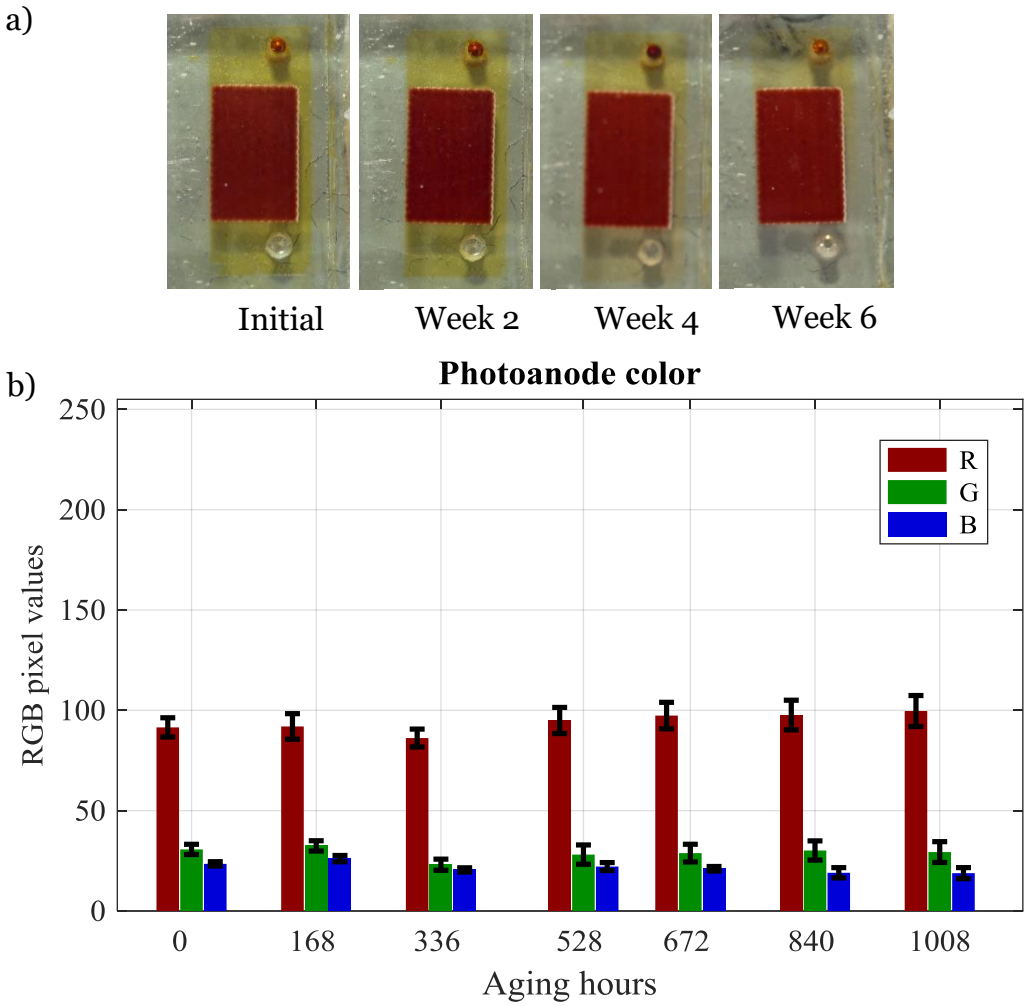

Figure 24. a) Cell R4 photographed from frontside during the test period, b) RGB pixel values of the photoanodes of all cells. The pixel values illustrate the whole photoanode area average and these values are average from all cells. The error bars describe the standard deviation of the values.

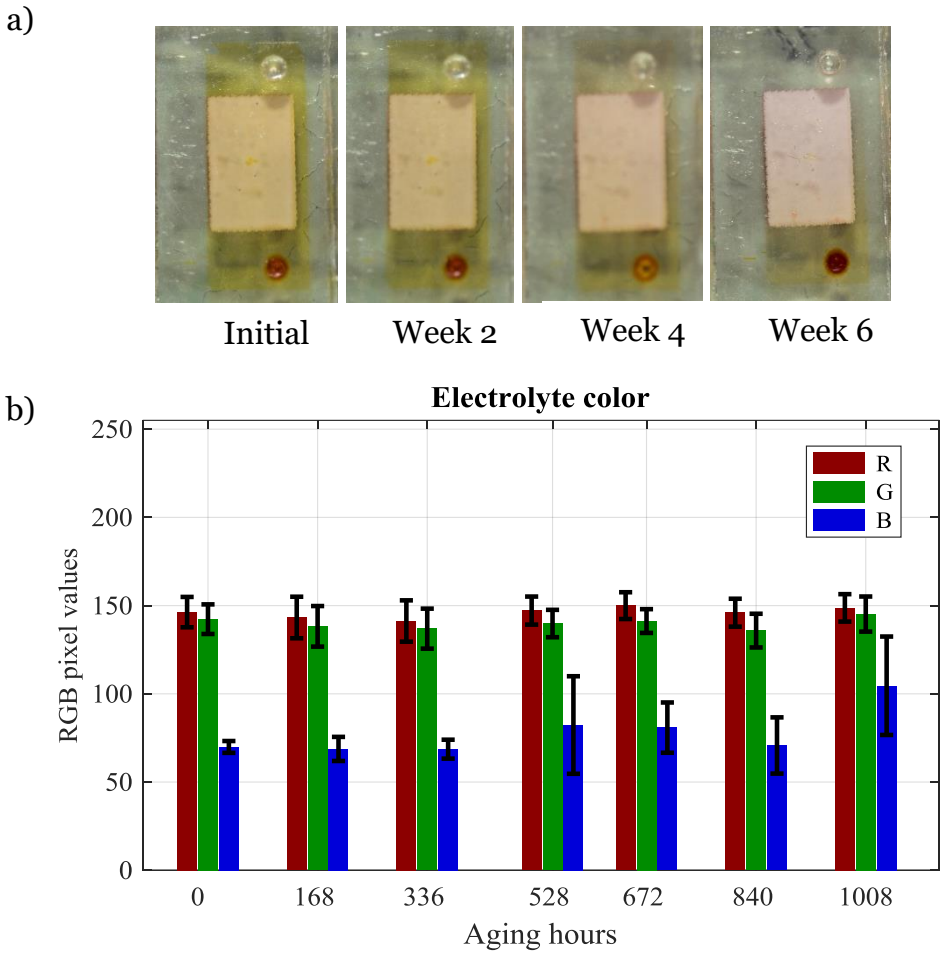

Figure 25. a) Cell R4 photographed from backside during the test period, b) average RGB pixel values of the electrolyte of all cells. The pixel values are obtained only from the upper part of the cells (upper in the picture) not over all the yellowish area and the values are average from all cells. Cells R1, R4, and R6 encountered partial color change of the electrolyte, which increased the standard deviation of the blue pixel value.

The loss of redox couple concentration in the cell have not had limiting effect on the short circuit current density on average in the whole cell. The saturation current measurements show that the short circuit current density does not reach maximum yet at 1 sun equivalent light intensity, see Fig 26 (R1 was again unmeasurable like with EIS so it is missing from the data). This means that there are more charge carriers available than is utilized under 1 sun illumination. Otherwise there would be a horizontal line beyond 1 sun illumination in Fig 26.

However, Fig 26 cannot reveal whether there are local areas where there are not enough charge carriers in the cells. This kind of partial lack of charge carriers would not stop the short circuit current density from increasing as intensity increases but instead only limit the increase, as is the case in Fig 26. The final current values increase less than the initial, which indicate that the cells cannot produce as much current as initially. However, cells R3 and R6 improve their current generation under high intensities, which indicates that at least these two cells do not suffer from charge carrier loss at all. Therefore, something else has to

limit the current generation of the cells in addition to that cells R4 and R7 may have locally limited electrolyte functionality.

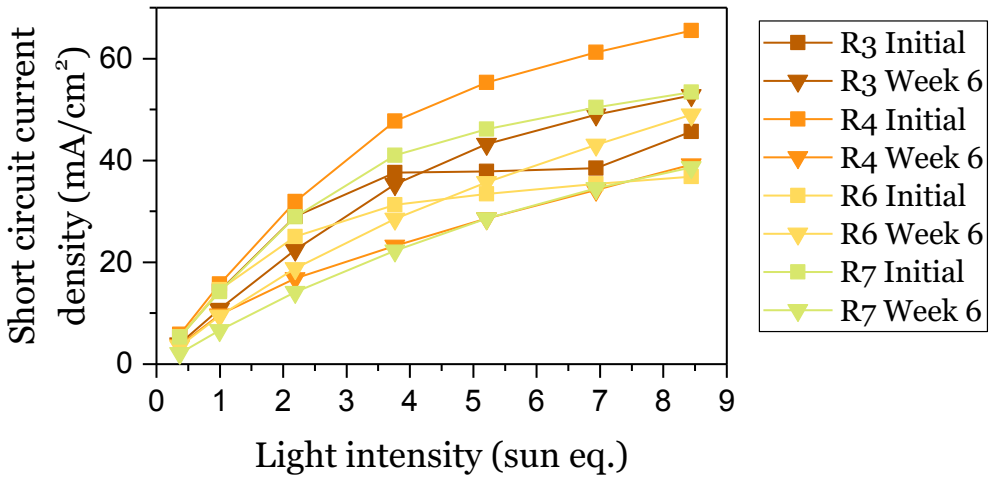

Figure 26. Short circuit current densities of the cells under different light intensities. The squares show the initial current densities and triangles the current densities measured after 6 weeks. R1 had similar issues as with EIS measurements and it could not be measured with this setup.

The IPCE measurements under low light intensity show that the cells have lost performance to convert photons to electrons, see Fig 27a. The IPCE has decreased on average about 35 to 40 %, which is about the same relative drop as the short circuit current density in Fig 21c. This confirms that the loss of short circuit current density is not due to resistive or charge carrier limitation but to some other factor. Moreover, the factor seems to be wavelength dependent: the IPCE has decreased relatively more in the long wavelength region, see Fig 27b. It is difficult to state which of the IPCE components of equation 6 are causing the decrease since all of the components are wavelength dependent in general, and only guesses can be made.

The study [67] stated that the electron injection efficiency decreased since the shift of TiO_2 band edge prevents electrons from moving from the LUMO level of the dye to the conduction band of the TiO_2. This phenomenon may well be wavelength dependent: photons with shorter wavelengths are more likely to excite electrons to higher energy levels of the dye, which allows them to move from the dye to the TiO_2 layer more often than electrons excited by lower wavelength photons. Thus, the IPCE results support this theory. On the other hand, the electron collection efficiency is lower for electrons excited by longer wavelengths: longer wavelengths penetrate deeper into the cell than shorter wavelengths. For that reason, the electrons generated by long wavelength photons have longer distance to the external circuit and thus have higher change for recombination. If the amount of recombination sites gets increased, the electrons generated by long wavelength photons encounters more likely the additional recombination sites, which explain why the IPCE has decreased more in the longer wavelength region. Lastly, the dye molecules may have also degraded due to chemical changes. It is possible that a part of the dye molecule

transforms into other form which may alter how the molecule responds to light which has an impact on light harvesting efficiency.

The variance of the IPCE spectrum is larger than the variance of short circuit current density. Furthermore, the cells are in different order in the IPCE spectrum than they are in the short circuit current density. Theoretically, integrating over IPCE spectrum should result in short circuit current density [14], which is not the case here. These findings may relate to how the IPCE of the cell was determined. Only a small spot of the cell was illuminated during the measurements. The cells may well have received some spatial differences in current generation since they have received at least spatial differences in redox couple concentrations as Fig 25a shows for R4. IPCE should not be reduced due to lack of charge carriers but something else instead since the used light intensity was small. Possibly, the shift of TiO_2 band edge is also spatial. This could introduce spatial differences in IPCE as well. However, this is a strong assumption and more evidence to support this theory is needed for its proving.

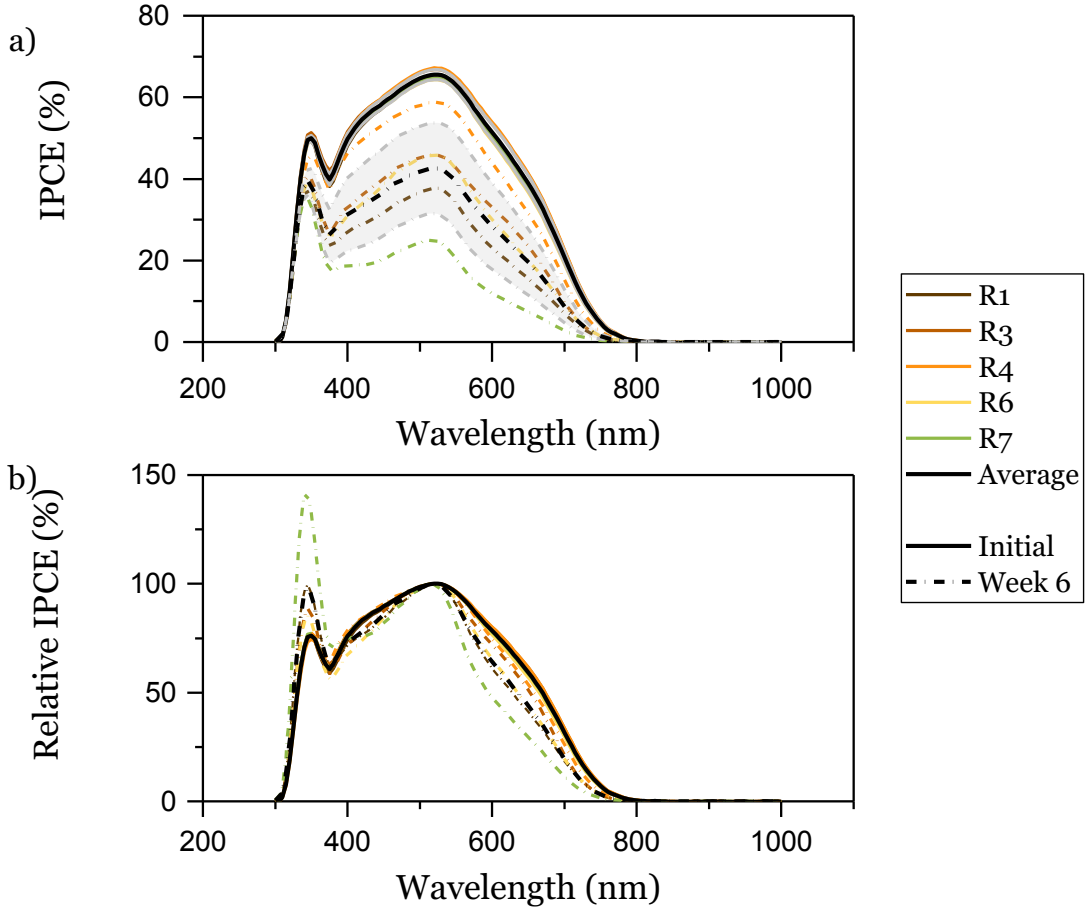

Figure 27. a) IPCE spectra of the cells. Initial measurements before the aging period are plotted with solid lines, and the measurements after the period are plotted with dashed lines. The grayed area represents the standard deviation of the final results. The data is measured from a spot in the middle of the cell, not over the whole active area. b) Normalized IPCE spectra. The spectra values are obtained by dividing the original spectra by its peak value near the 500 nm. For the sake of clarity, standard deviations are left out from b.

5.2.1. Conclusions on cell degradation

The cells have lost slightly performance during the aging period. The initial average cell efficiency was 3.6 % and after the aging period it was 3.0 % so there is a 17 % loss in the efficiency. The main reason for the cell aging is the decreased ability to convert photons into electricity: the average IPCE has decreased significantly, which decreases the cell current. The degradation occurred during the rainy periods so rainwater is expected to be the source of degradation. Freezing temperatures were not noticed to cause any additional degradation for the cells. Three possible reasons for the decreased IPCE were came up.

Most likely, lower edge of conduction band of TiO_2 particles shifted higher such that less photo-excited electrons had enough energy to move from the dye LUMO-level of the dye molecules to the conduction band of TiO_2 nanoparticles. This kind of shift was proposed in study [67] where water was added artificially to electrolyte and the test results were similar as in this work. In study [67], the open circuit voltage was higher for the cells with added water in comparison to reference cells and short circuit current was lower. In this work, water was not added artificially to the electrolyte but it might well have penetrated into the cells during the testing period increasing the open circuit voltage and decreasing the short circuit current.

Additionally, the penetrated rainwater may have contained different impurities that have increased the recombination electron-hole pairs via other routes than shift of conduction band edge. IPCE results showed that the electron collection efficiency may have decreased, and this could be due to the impurities. However, proving this theory requires material analyzation techniques such as XRD and deep theoretical knowledge about DSSC chemistry, so it was not attempted in this work. This alternative theory does not exclude the theory of band shifting so both of them may have had contribution on the decrease of short circuit current.

Lastly, local disappearing of iodine from the electrolyte was observed in this work, and it may have decreased slightly the short circuit current density. In total, the cells have had enough charge carriers in the electrolyte since the short circuit current density had not reached maximum yet at 1 sun illumination. However, it does not exclude the possibility that some areas in the cells have run out of charge carriers already at 1 sun or even lost them completely.

The cause of degradation can be the combination of these three, naturally, since they do not exclude each other, though the first theory explains the test results best. The cells are not similar together either. Cells R1 and R7 had imperfect sealing and they were noticed to be dried up two weeks after stopping the aging tests. R3 experienced the highest increase in open circuit voltage and highest decrease in short circuit current so it could have let most water penetrate inside it. Interestingly, R3 maintained its electrolyte color best. R4 and R6 lost least performance though they encountered partial bleaching or leaking of the electrolyte.

5.3. Outdoor measurements

Fig 28 shows outdoor IV data for cell R6 over the test period. The figure shows some similar degradation trends as the indoor measurements: open circuit voltage increases and efficiency and power density decreases. The fill factor seems also to increase at high intensities but to decrease at low intensities.

The data in Fig 28 is novel in a sense that no one has before reported the IV curves of DSSCs under winter conditions temperatures near -10 °C in literature. The cells seem to operate in freezing temperatures about as well as in non-freezing conditions. There is no clear drop in any of the IV parameters between 670 h and 950 h when it was freezing. During the darker days the cell temperature remained below zero throughout the day but on the sunnier days (near 750 h and 875 h) the sun heated the cells to temperatures between 5 °C and 15 °C (high variations were observed due to clouds and wind gusts on those days). To get idea about the cells performance under higher intensities when cell temperature is below zero even colder ambient temperatures are needed.

5.3.1. Effect of irradiance on IV parameters

The open circuit voltage is relatively independent on light intensity when irradiance is above 10 W/m^2: the open circuit voltage is only slightly higher for high intensities. The other parameters are much more dependent on the intensity. Higher light intensity increases quite linearly the current and power densities of the cell but decreases both efficiency and fill factor. The decrease of efficiency is due to decrease of fill factor, which again is due to increase of resistive losses caused by increased current.

The typical efficiency value in outdoor conditions is relatively high, around 10 % that is about twice as high as characterized for R6 indoors under 1 sun illumination. The reason for this is that typical irradiance value during the measurement was below 100 W/m^2. With such low intensities, the current generation is low and the resistive losses are small. This increases fill factor and efficiency.

The efficiency and power density of the cell R6 are plotted also as function of light intensity into Fig 29a-b and their correlation relations are shown in Table 10. The Fig 29a-b confirms that the efficiency is much higher for lower intensities and slightly higher for early scans due to degradation at later on. Interestingly, the variance of efficiency is also much higher at low intensities. This is most likely due to inaccuracy of parameter estimation from the IV scans, see Section 5.3.4. Power density seems also to be nearly linearly independent on light intensity. The consecutive scans (especially the cyan line on high intensities) show nearly linear increase when the sun is rising or setting during a clear sky day.

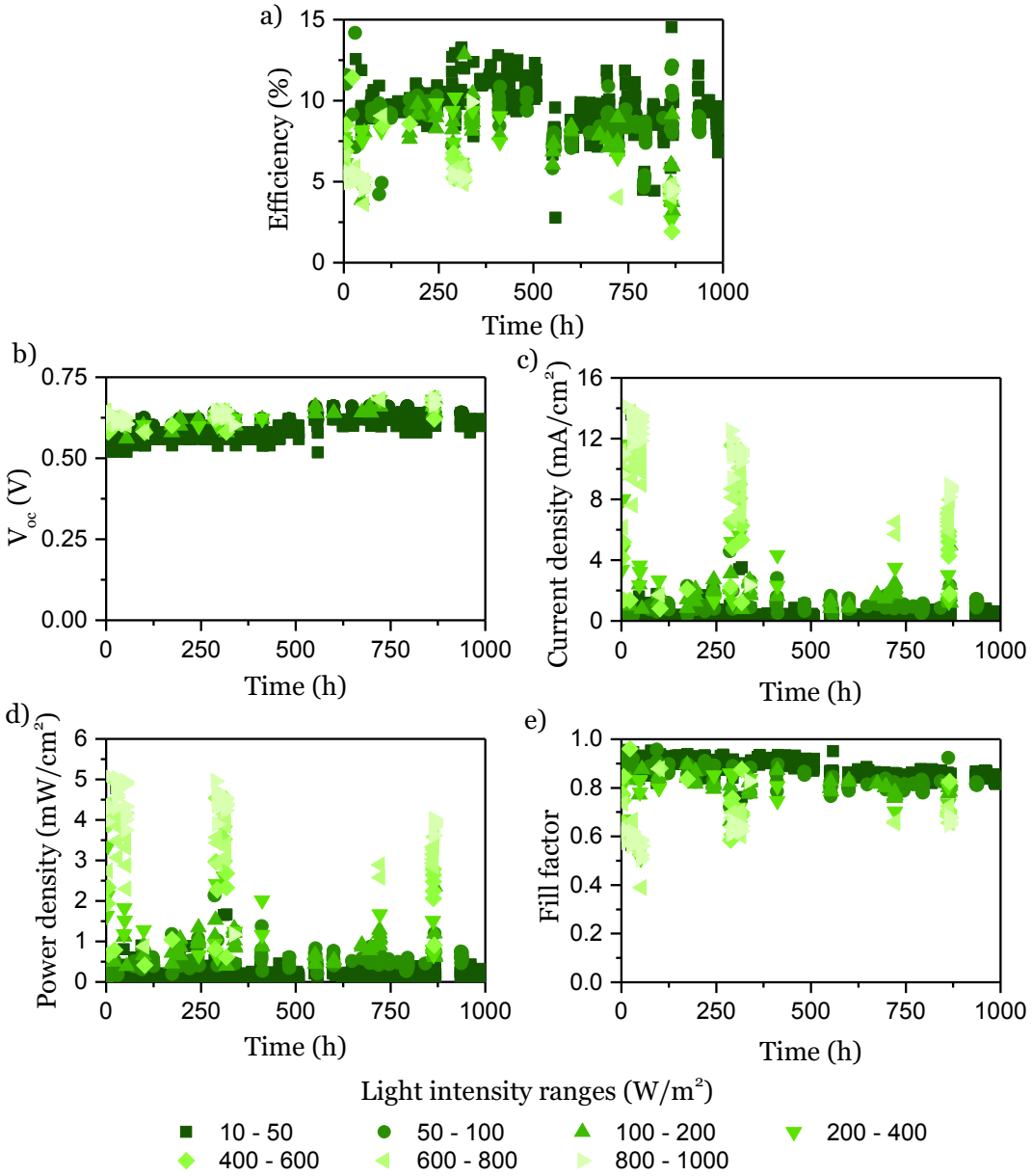

Figure 28. The figure shows a) open circuit voltage, b) efficiency, c) power density, and d) fill factor over the test period for cell R6. The lighter green the color of the data points the higher the light intensity during that scan. Between 670 h and 950 h the ambient temperature was below zero.

Table 10 Statistical correlation parameters of efficiency, power density, and weather parameters. The equation is for the linear fit into the variable pair and the R^2 value describe the goodness of the fit (0 bad fit, 1 perfect fit). In the variable pair the left variable is the explanatory variable (x) and the right one dependent variable (y). The units for variables are the same as in Fig 29.

Variable pair		Equation	R^2 value
Irradiance	Efficiency	y = - 0.006x + 9.98	0.36
Irradiance	Power density	y = 0.012x + 0.31	0.89
Temperature	Efficiency	y = 0.012x + 9.33	0.0005
Humidity	Efficiency	y = 0.055x + 4.89	0.12
Irradiance	Temperature	y = 0.006x + 2.56	0.10
Irradiance	Humidity	y = -0.046x + 86.8	0.45
Temperature	Humidity	y = -1.576x + 87.37	0.21

5.3.1. Effect of temperature and humidity on IV parameters

The immediate efficiency of the cell seems to be independent on both temperature and humidity, statistically. There are not clearly visible trends in Fig 29 c-d and the R^2 value is very low in both cases, see Table 10. Actually, the weather parameters are more dependent on each other (figures not shown here). When sun is shining it is warmer and dryer. Since high irradiance decreases the cell efficiency it also seems that higher temperature and lower humidity decreases cell efficiency if the irradiance is left out from the considerations. This makes the relations of the environment parameters and cell efficiency much more complicated and they cannot be modeled with simple linear model. Therefore, more advanced statistical analysis is needed for finding the effect of temperature and humidity on cell efficiency. Furthermore, the effect of degradation should be taken into account in the analysis. Alternatively, separate test measurements with fixed light intensity, temperature, and humidity levels would reveal the real relation of cell efficiency empirically to the environment parameters. However, both cases are beyond the scope of this work and are not considered any further here.

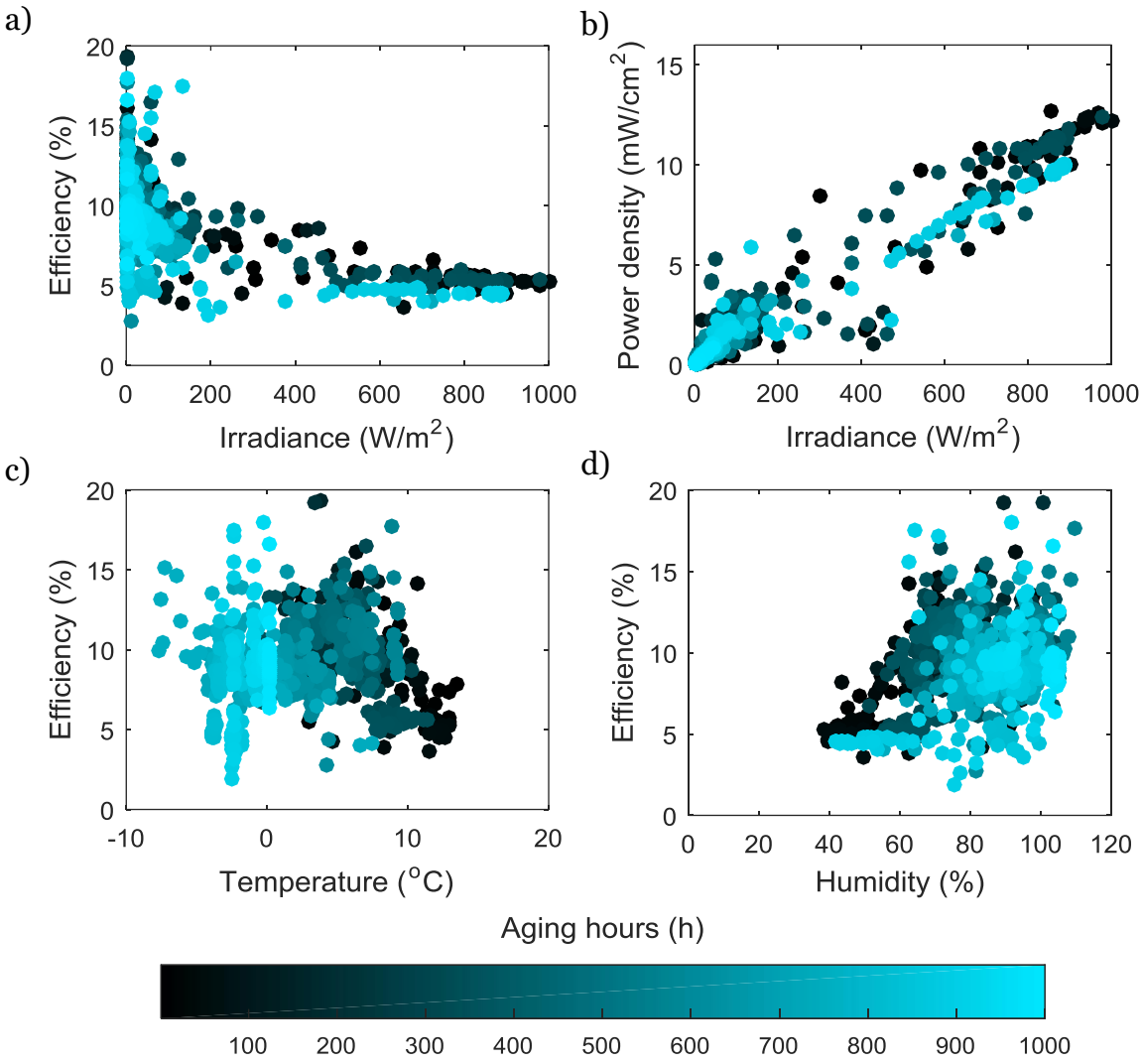

Figure 29. a) Efficiency as function of irradiance, b) power density as function of irradiance, c) efficiency as function of irradiance, and d) efficiency as function of humidity. Data includes IV data from cell R6. The darker blue the data point in the figures the earlier is the scan time.

5.3.1. Theoretical energy generation of cells

The cells were aged in open circuit conditions so they did not produce any energy. Fig 30 power shows the theoretical cumulative energy generation of each cell. The cumulative energy generation was calculated by integrating the maximum power point values obtained from the outdoor IV measurements over time. Next, the theoretical efficiencies of the cells were determined by calculating the ratio for cumulative power output and irradiance. These values describe how large a share of irradiance the cells could have converted into electricity during the test period. Interestingly, these efficiency values are higher than the ones obtained from the indoor IV characterizations. The cells perform better in the actual outdoor conditions than under simulated 1 sun AM 1.5 G irradiation. Only R4 performed

about at the same level both indoors and outdoors. However, contact issues were noticed on the particular channel to which the R4 was connected during the test. The contact was lost couple of times (possibly due to frost) and the resistance of the channel had increased to 6.5 Ω (cf. average 4.5 Ω).

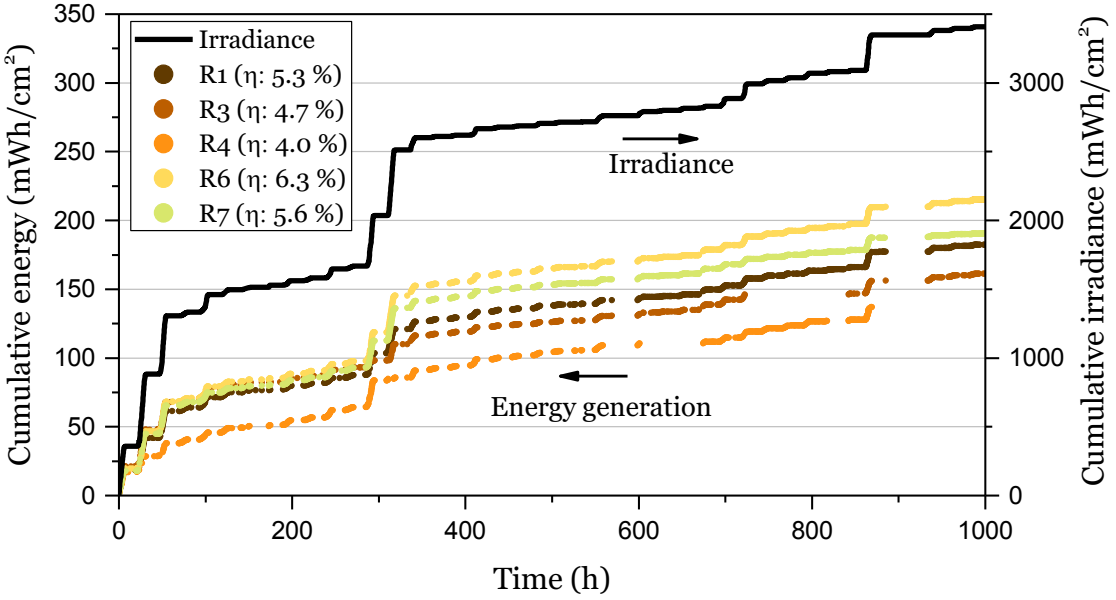

Figure 30. The cumulative energy generation of each test cell and cumulative irradiance during. The longer gaps in the data are due to either cell contact failure or system failure. The efficiency values visible in the legend describe how large share of the cumulative irradiance the cells could have converted to electricity.

5.4. Outdoor data quality issues and future improvements

The choice not to fit diode model to the outdoor IV data generates some errors into Fig 28. For example, the Fig 28e has impossibly high fill factor values near one: typical theoretical fill factor limits are below 0.9 at observed temperatures. On the other hand, the variance of efficiency is high at low intensities (see Fig 30). The simple estimation of short circuit current, open circuit voltage and maximum power point have larger error margins than the fit process. This results sometimes in impossibly high fill factor values and highly varying efficiency values at low intensities, apparently. Though, the results should be correct on average. Therefore, if time for the fitting process is available one should fit the diode model to each IV scan. Alternatively, fitting analysis could be implemented into the LabVIEW program where it could be performed in the process of collecting data.

Sometimes, the measured irradiance level did not correspond to the actual irradiance level on the test cell. Instead, either the cell or pyranometer was shadowed by an obstacle. If the cell was shadowed the recorded efficiency was significantly too low for the measurement and if the pyranometer was shadowed the opposite occurred. Fortunately, these events were so well visible in the data

and rare enough that they can be removed from the data manually afterwards. In future, the analysis could also be performed programmatically at the same stage where the unstable IV measurement due to cloud movements are filtered away.

One possible source of mismatch between indoor and outdoor IV data is the use of tape mask (see Section 4.2) indoors but not outdoors. Without tape mask, light may enter the cell also closer from the edges of the cell. If the light is non-perpendicular it may reflect back and forth inside the substrates and eventually reach the photoanode and generate current. In short, the effective active area of the cell appears larger than the actual area of the photoanode layer, which results in overestimated current density and efficiency values. To obtain precise results a similar mask should be used outdoors, too.

Unfortunately, the LabVIEW software environment (i.e. not the implemented measurement program but its execution software) crashed twice during the measurements. The reason for these events remained unsolved. On the first time, a short voltage drop in the grid might have caused the crash but on the second time no such drop in voltage was noticed. It may well be some programmatic error in the operating system or the LabVIEW software environment. Until reason for this failure is found it is good practice to check occasionally the status of the computer during the measurements.

6. Summary

Firstly, a sample type review on indoor aging study practices for DSSCs and Omh-PSCs was performed. The most popular study methods for these cell types are dark storage test and constant illumination test: there are numerous different studies in literature involving these methods. Within the sample of studies, most commonly the aging procedures followed the intermediate level ISOS standards. Typically, the most common mistake in the reviewed sample is poor environment reporting: in both common test types, the humidity is not reported, and additionally in the constant illumination method, the temperature is not reported properly, i.e. only ambient temperature is reported or the temperature is not reported at all. Additionally, cells are aged under open circuit conditions, so degradation due to current generation is not detected. On the other hand, the used light source typically matches the recommended IEC AM 1.5 G standard and the level of aging characterization reaches the ISOS advanced level. Many studies use also characterization methods that are not even required in any of the ISOS standard levels, such as EIS, to gain broader knowledge of the cell functionality.

The indoor aging study methods cannot comprehensively declare studied cells stable, and actual outdoor stability tests are needed for ensuring the stability of the studied cell. Therefore, another review was performed for outdoor measurements practices for DSSCs and Omh-PSCs in a similar way as was performed for indoor aging study methods. There are clearly less outdoor studies for these cell types than there are indoor studies: only 15 proper studies were found from literature. The reviewed studies followed again the intermediate ISOS level, typically. Like with the indoor sample, the most common deficiency was the improper reporting of environment conditions: most severely, the solar irradiance and temperature were not monitored. On the other hand, unlike with the indoor sample, the cell characterization was also performed more weakly: for example, only one study reported IPCE spectra of the cells. The most common advanced ISOS level practice of the studies was the operation regime of the tested cells: most studies kept their cells operating close to the maximum power point. Lastly, the practice to protect the test cells or panels from weather varied: the most protected cells were under a waterproof, UV filtering greenhouse like cover while some cells were left bare.

The New Energy Technologies group at Aalto University has lacked an outdoor testing station for their solar cell studies. Therefore, a new testing station was implemented in this work. It was designed to fulfill the advanced ISOS level for outdoor measurements (only wind speed monitoring was left for future) and the special requirements of the group, such as support for simultaneous testing of different cell types. It records automatically IV curves of the tested solar cells and key weather parameters: irradiance, temperature, and humidity. It also provides the possibility to age the cells either under open circuit, short circuit, or custom load voltage (e.g. at maximum power point).

The station was tested by inserting five DSSCs for open circuit aging. The aging test was performed for 6 weeks (1000 h) from October 6th to November 17th in Espoo, Finland. During that period, the weather varied from mildly warm and sunny to rainy and cold to freezing and snowy. The tested cells experienced

degradation only during the rainy, non-freezing conditions, so rainwater is the most likely source of degradation. The cells were not observed to lose any efficiency after they were exposed to freezing temperatures, and furthermore, the cells were able to produce power under freezing conditions about as well as in above zero temperature.

The degradation was mostly due to their decreased ability to generate current. Three possible theories were figured out to explain the reason. In the most supported theory, rainwater penetrated into the cells, which caused a shift in lower TiO_2 conduction band edge upwards and/or degradation of dye molecules. Alternatively, or additively, penetrated rainwater may have had different impurities that may have also increased the recombination in the cell. Lastly, local loss of iodine in the electrolyte (partial or complete) may have limited slightly the short circuit current of the cell though the total amount of iodine in the electrolyte was well sufficient at 1 sun illumination.

The produced outdoor IV data was also analyzed and some observations were made. Firstly, the open circuit voltage of the cells was noticed to be almost independent of light intensity. Above 10 W/m^2, the open circuit voltage stayed nearly constant. On the other hand, fill factor and efficiency were more dependent on the light intensity. Below 100 W/m^2 illumination the cells were about twice as efficient as under 1000 W/m^2 illumination (8 % vs. 4 %) and their fill factor was even between 0.8 and 0.9 instead of 0.6. As the current provided by the cell goes down, also the effect of the resistive losses decreasing the fill factor reduce tremendously. However, at those lower illumination levels, current is much smaller than under bright sun light, so the total power generation remains small. The immediate effect of temperature and humidity on the cell efficiency was statistically very small.

Based on measured maximum power point output values outdoors, the theoretical light to electricity conversion efficiency of the cells was on average 5 %, i.e. the cells would have converted about 5 % of the all received light into electricity were they kept at maximum power point instead of open circuit. This value is slightly over 1 % unit higher than the reported efficiency under standard measurement conditions of 1000 W/m^2, a good thing to keep in mind when estimating the energy production of a DSSC under real operating conditions.

7. References

[1] *Snapshot of Global PV Markets 2014*, IEA PVPS; ISBN 978-3-906042-32-9
[2] *Technology Roadmap Solar Photovoltaic Energy 2014*, IEA
[3] G. Hasmi, K. Miettunen, T. Peltola, J. Halme, I. Asghar, K. Aitola, M. Toivola, P. Lund; *Review of materials and manufacturing options for large area flexible dye solar cells*; Renewable an Sustainable Energy Reviews, 2011, vol 15, pp 3717-3732
[4] T. Toyoda, T. Sano, J. Nakajima, S. Doi, S. Fukumoto, A. Ito, T. Tohyama, M. Yoshida, T. Kanagawa, T. Motohiro, T. Shiga, K. Higuchi, H. Tanaka, Y. Takeda, T. Fukano, N. Katoh, A. Takeichi, K. Takechi, M. Shiozawa; *Outdoor performance of large scale DSC modules*; Journal of Photochemistry and Photobiology A: Chemistry, 2004, vol 164, pp 203-207
[5] A. Asghar, M. Emziane, H. K. Pak, S. Y. Oh; *Outdoor testing and degradation of dye-sensitized solar cells in Abu Dhabi*; Solar Energy Materials & Solar Cells, 2014, vol 128, pp 335-342
[6] M. Grätzel; *Photovoltaic performance and long-term stability of dye-sensitized meosocopic solar cells*; Comptes Rendus Chimie, 2006, vol 9, is 5-6, pp 578-583
[7] S. Mathew, A. Yella, P. Gao, R. Humphry-Baker, B. F. E. Curchod, N. Ashari-Astani, I. Tavernelli, U. Rothlisberger, Md. K. Nazeeruddin, M. Grätzel; *Dye-sensitized solar cells with 13% efficiency achieved through the molecular engineering of porphyrin sensitizers*; Nature Chemistry, 2014, vol 6, pp 242-247
[8] A. Kojima, K. Teshima, Y. Shirai, T. Miyasaka; *Organometal Halide Perovskites as Visible-Light Sensitizers for Photovoltaic Cells*; Journal of the American Chemical Society, 2009, vol 131, pp 6050-6051
[9] M. A. Green, K. Emery, Y. Hishikawa, W. Warta, E. D. Dunlop; *Solar cell efficiency tables (Version 45)*, Progress in Photovoltaics, 2015, vol 23, is 1, pp 1-9
[10] T. A. Berhe, W.-N. Su, C.-H. Chen, C.-J. Pan, J.-H., Cheng, H.-M., Chen, M.-C. Tsai, L.-Y. Chen, A. A. Dubale, B.-J. Hwang; *Organometal halide perovskite solar cells: degradation and stability*; Energy & Environmental Science, 2016, vol 9, pp 323-356
[11] L. Etgar, P. Gao, Z. Xue, Q. Peng, A. K. Chandiran, B. Liu, Md. K. Nazeeruddin, M. Grätzel; *Mesoscopic $Ch_3NH_3PbI_3$ Tio_2 Heterojunction Solar Cells*; Journal of the American Chemical Society, 2012, vol 134, pp 17396-17399
[12] J.-Y. Jeng, Y.-F. Chiang, M.-H. Lee, S.-R. Peng, T.-F. Guo, P. Chen, T.-C. Wen; *$CH_3NH_3PbI_3$ Perovskite/Fullerene Planar-Heterojunction Hybrid Solar Cells*; Advanced Materials, 2013, vol 25, pp 3727-3732
[13] H.-S. Kim, J.-W. Lee, N. Yantara, P. P. Boix, S. A. Kulkarni, S. Mhaisalkar, M. Grätzel, N.-G. Park; *High Efficiency Solid State Sensitized Solar Cell-Based on Submicrometer Rutile TiO_2 Nanorod and $CH_3NH_3PbI_3$ Perovskite Sensitizer*; Nano Letters, 2013, vol 13, pp 2412-2417
[14] J. Halme, P. Vahermaa, K. Miettunen, P. Lund; *Device Physics of Dye Solar Cells*; Advanced Energy Materials, 2010, vol 22, pp E210-E234
[15] N Koide, A. Islam, Y. Chiba, L. Han; *Improvement of efficiency of dye-sensitized solar cells based on analysis of equivalent circuit*; Journal of Photochemistry and Photobiology A: Chemistry, 2006, vol 182, pp 296–305
[16] M. I. Asghar, K. Miettunen, S. Mastroianni, J. Halme, H. Vahlman, P. Lund; *In situ image processing method to investigate performance and stability of dye solar cells*; Solar Energy, 2012, vol 86, pp 331-338
[17] M. I. Asghar, K. Miettunen, J. Halme, P. Vahermaa, M. Toivola, K. Aitola, P. Lund, *Review of stability for advanced dye solar cells*; Energy & Environmental Science; 2010, vol 3, pp 418-426
[18] S. Shalini, R. Balasundaraprabhu, T. Satish Kumar, N. Prabavathy, S. Senthilarasu, S. Prasanna; *Status and outlook of sensitizers/dyes used in dye sensitized solar cells (DSSC): a review*; International Journal of Energy Research; 2016, vol 40, pp 1303-1320
[19] S. Yun, P. Lund, A. Hinsch; *Stability assessment of alternative platinum free counter electrodes for dye-sensitized solar cells*; Energy & Environmental Science, 2015, vol 8, pp 3495-3514
[20] D. Wang, M. Wright, N. Kumar Elumalai, A. Uddin; *Stability of perovskite solar cells*; Solar Energy Materials & Solar Cells, 2016, vol 147, pp 255-275
[21] G. Niu, X. Guo, L. Wang; *Review of recent progress in chemical stability of perovskite solar cells*; Jouranl of Materials Chemistry A, 2015, vol 3, pp 8970-8980
[22] *Overcoming ultraviolet light instability of sensitized TiO_2 with meso-superstructured organometal tri-halide perovskite solar cells*; Nature Communications 2013, vol 4
[23] M. O. Reese, S. A. Gevorgyan, M. Jørgensen, E. Bundgaard, S. R. Kurtz, D. S. Ginley, D. C. Olson, M. T. Lloyd, P. Morvillo, E. A. Katz, A. Elschner, O. Haillant, T. R. Currier, V. Shrotriya, M. Hermenau, M. Riede, K. R. Kirov, G. Trimmel, T. Rath, O. Inganäs, F. Zhang, M .Andersson, K. Twingstedt, M. Lira-Cantu, D. Laird, C. McGuinness, S. Gowrisanker, M. Pannone, M. Xiao, J. Hauch, R. Steim, D. M. DeLongchamp, R. Rösch, H. Hoppe, N. Espinosa, A. Urbina, G. Yamna-Uzunoglu, J.-B. Bonekamp, A. J. J. M. van Breemen, C. Girotto, E. Voroshazi, F. C. Krebs; *Consensus stability testing protocols for organic photovoltaic materials and devices*; Solar Energy Materials & Solar Cells, 2011, vol 95, pp 1253-1267

[24] O. Haillant, D. Dumbleton, A. Zielnik; *An Arrhenius approach to estimating organic photovoltaic module weathering acceleration factors*; Solar Energy Materials & Solar Cells; 2011, vol 95, is 7, pp, 1889-1895
[25] T. J. McMahon, G. J. Jorgensen, R. L. Hulstrom, D. L. King, M. A. Quintana; *Module 30 Year Life: What Does it Mean and Is it Predictable/Achievable?;* National Center for Photovoltaics Program Review Meeting, 2000
[26] D. C. Jordan, S. R. Kurtz; *Photovoltaic degradation rates—an analytical review*; Progress in photovoltaics: Research and Applications, 2013, vol 23, is 1, pp 12-29
[27] F. Bella, S. Galliano, M. Falco, G. Viscardi, C. Barolo, M. Grätzel and C. Gerbaldi; *Unveiling iodine-based electrolytes chemistry in aqueous dye-sensitized solar cells*; Chemical Science, 2016, vol 7, pp 4880-4890
[28] A. Chiappone, F. Bella, J. R. Nair, G. Meligrana, R. Bongiovanni, C. Gerbaldi; *Structure–Performance Correlation of Nanocellulose-Based Polymer Electrolytes for Efficient Quasi-solid DSSCs*; ChemElectroChem, 2014, vol 1, pp 1350-1358
[29] S. J. Lue, Y.L. Wu, Y.L: Tung, C.M. Shih, Y.C. Wang; *Functional titanium oxide nano-particles as electron lifetime, electrical conductance enhancer, and long-term performance booster in quasi-solid-state electrolyte for dye-sensitized solar cells*; Journal of Power Sources, 2015, vol 274, pp 1283-1291
[30] R. Harikisun, H. Desilvestro; *Long-term stability of dye solar cells*; Solar Energy, 2011, vol 85, is 6, pp 1179-1188
[31] H. Petterson, T. Gruszecki, C. Schnetz, M. Streit, Y. Xu, L :sun, M. Gorlov, L. Kloo, G. Boschloo, L. Häggman, A. Hagfeld; *Parallel-connected monolithic dye-sensitised solar modules*; Progress in Photovoltaics, 2010, vol 18, is 5, pp 340-345
[32] D. Kuang, C. Klein, Z. Zhang, S. Ito, J.E. Moser, S. M. Zakeeruddin, M. Grätzel; *Stable, High-Efficiency Ionic-Liquid-Based Mesoscopic Dye-Sensitized Solar Cells*; Small, 2007, vol 3 pp 2094-2102
[33] A. Hinsch, J. M. Kroon, R. Kern, I. Uhlendorf, J. Holzbock, A. Meyer, J. Ferber; *Long-term Stability of Dye-Sensitized Solar Cells*; Progress in Photovoltaics, 2001, vol 9, pp 425-438
[34] S. Noda, K. Nagano, E. Inoue, T. Egi, T. Nakashima, N. Imawaka, M. Kanayama, S. Iwata, K. Toshima, K. Nakada, K. Yoshino; *Development of large size dye-sensitized solar cell modules with high temperature durability*; Synthetic Metals, 2009, vol 159, is 21-22, pp 2355-2357
[35] A. Agresti, S. Pescetelli, B. Taheri, A. E. Del Rio Castillo, L. Cinà, F. Bonaccorso; *Graphene–Perovskite Solar Cells Exceed 18 % Efficiency: A Stability Study*; ChemSuSChem, 2016, vol 9, is 18, pp 2609-2619
[36] J. A. Christians, P. A. Miranda Herrera, P. V. Kamat; *Transformation of the Excited State and Photovoltaic Efficiency of CH3NH3PbI3 Perovskite upon Controlled Exposure to Humidified Air*, Journal of the American Chemical Society, 2015, vol 137, pp 1530-1538
[37] Z. Zhu, Y. bai, X. Liu, C.-C. Chueh, S. Yang, A K.-Y. Jen; *Enhanced Efficiency and Stability of Inverted Perovskite Solar Cells Using Highly Crystalline SnO2 Nanocrystals as the Robust Electron-Transporting Layer*; Advanced Materials, 2016, vol 28, pp 6478 – 6484
[38] Y. Rong, X. Li, Z. Ku, G. Liu, H. Wang, M. Xu, L. Liu, M. Hu, P. Xiang, Z. Zhou, T. Shu, H. Han; *Monolithic all-solid-state dye-sensitized solar module based on mesoscopic carbon counter electrodes*; Solar Energy Materials & Solar Cells 2012, vol 105, pp 148-152
[39] X. Chen, J. Zhao, J. Zhang, L. Qiu, D. Xu, H. Zhang, X. Han, B. Sun, G. Fu, Y. Zhang, F. Yan; *Bis-imidazolium based poly(ionic liquid) electrolytes for quasi-solid-state dye-sensitized solar cells*, Journal of Materials Chemistry, 2012, vol 22, pp 18018-18024
[40] M. Bastianini, R. Vivani, M. Nocchetti, D. Costenaro, C. Bisio, F. Oswald, T. B. Meyer, L. Marchese; *Effect of iodine intercalation in nanosized layered double hydroxides for the preparation of quasi-solid electrolyte in DSSC devices*, Solar Energy, 2014, vol 107, pp 629-699
[41] M. Carne, D. Bryant, T. Watson, D. Worsley; *Photocatalytic Oxidation of Triiodide in UVA-Exposed Dye-Sensitized Solar Cells*, International Journal of Photoenergy, 2012
[42] Y. Han, S. Meyer, Y. Dkhissi, K. Weber, J. M. Pringle, U. Bach, L. Spiccia, Y.B. Cheng; *Degradation observations of encapsulated planar $CH_3NH_3PbI_3$ perovskite solar cells at high temperatures and humidity*, Journal of Material Chemistry, 2015, vol 3, pp 8139-8147
[43] S. Guarnera, A. Abate, W. Zhang, J. M. Foster, G. Richardson, A. Petrozza, H. J. Snaith; *Improving the Long-Term Stability of Perovskite Solar Cells with a Porous Al_2O_3 Buffer Layer*, Journal of Physical Chemistry Letters, 2015, vol 6, pp 432-437
[44] Q. Dong, F. Liu, M. K. Wong, H. W. Tam, A. B. Djurišić, A. Ng, C. Surya, W. K. Chan, A. M. C. Ng; *Encapsulation of Perovskite Solar Cells for High Humidity Conditions*, ChemSusChem, 2016, vol 9, pp 2597-2603
[45] M. Berginc, U. O. Krašovec, M. Topič; *Outdoor ageing of the dye-sensitized solar cell under different operation regimes*; Solar Energy Materials & Solar Cells, 2014, vol 120, pp 491-499
[46] C. Cornaro, S. Bartocci, D. Musella, C. Strati, A. Lanuti, S. Mastroianni, S. Penna, A. Guidobaldi, F. Giordano, E. Petrolati, T. M. Brown, A. Reale, A. Di Carlo; *Comparative analysis of the outdoor performance of a dye solar cell mini-panel for building integrated photovoltaics applications*; Progress in Photovoltaics, 2015, vol 23, pp 215-225

[47] A. Hinsch, H. Brandt, W. Veurman, S. Hemming, M. Nittel, U. Würfel, P. Putyra, C. Lang-Koetz, M. Stabe, S. Beucker, K. Fichter; *Dye solar modules for façade applications*: Recent results from project ColorSol; Solar Energy Materials & Solar Cells, 2009, vol 93, pp 820-824
[48] S. Mastroianni, A. Lanuti, S. Penna, A. Reale, T. M. Brown, A. Di Carlo, F. Decker; *Physical and Electrochemical Analysis of an Indoor–Outdoor Ageing Test of Large-Area Dye Solar Cell Devices*; ChemPhysChem, 2012, vol 13, pp 2925-2936
[49] F. Bella, G. Griffini, M. Gerosa, S. Turri, R. Bongiovanni; *Performance and stability improvements for dye-sensitized solar cells in the presence of luminescent coatings*; Jouranl of Power Sources, 2015, vol 283, pp 195-203
[50] H. Tanaka, A. Takeichi, K. Higuchi, T. Motohiro, M. Takata, N. Hirota, J. Nakajima, T. Toyoda; Long-term durability and degradation mechanism of dye-sensitized solar cells sensitized with indoline dyes; Solar Energy Materials & Solar Cells, 2009, vol 93, pp 1143-1148
[51] N. Kato, K. Higuchi, H. Tanaka, J. Nakajima, T. Sano, T. Toyoda; *Improvement in long-term stability of dye-sensitized solar cell for outdoor use*; Solar Energy Materials & Solar Cells, 2011, vol 95, pp 301-305
[52] J.-G. Knag, J.-H. Kim, H.-B. Jang, J.-T. Kim; *Characteristics of DSSC Panels with Silicone Encapsulant*; International Journal of Photoenergy, vol 2015
[53] D.K. Ivanou, R. Santos, J. Maçaira, L. Andrade, A. Mendes; *Laser assisted glass frit sealing for production large area DSCs panels*; Solar Energy, 2016, vol 135, pp 674-681
[54] N. Kato, Y. Takeda, K. Higuchi, A. Takeichi, E. Sudo, H. Tanaka, T. Motohiro, T. Sano, T. Toyoda; *Degradation analysis of dye-sensitized solar cell module after long-term stability test under outdoor working condition*; Solar Energy Materials & Solar Cells, 2009, vol 93, pp 893-897
[55] S. Dai, J. Weng, Y. Sui, S. Chen, S. Xia,, Y. Huang, F. Kong, X. Pan, L. Hu, C. Zhang, K. Wang; *The design and outdoor application of dye-sensitized solar cells*; Inorganica Chimica Acta, 2008, vol 361, pp 786-791
[56] Q. Dong, F. Liu, M. K. Wong, H. W. Tam, A. B. Djurišić, A. Ng, C. Surya, W. K. Chan, A. M. C. NgK; *Encapsulation of Perovskite Solar Cells for High Humidity Conditions*; ChemSusChem, 206, vol 9, pp 2579-2603
[57] X. Li, M. Tschumi, H. Han, S. S. Babkair, R. A. Alzubaydi, A. A. Ansari, S. S. Habib, M. K. Nazeeruddin, S. M. Zakeeruddin, M. Grätzel; *Outdoor Performance and Stability under Elevated Temperatures and Long-Term Light Soaking of Triple-Layer Mesoporous Perovskite Photovoltaics*; Energy Technology, 2015, vol 3, pp 551-555
[58] Background map from Wikimedia commons: *https://upload.wikimedia.org/wikipedia/commons/thumb/7/74/Mercator-projection.jpg/773px-Mercator-projection.jpg*; viewed on November 24th 2016
[59] Elevation data from: *elevationmap.net*; viewed on November 24th 2016
[60] Climate descriptions for study cities from Wikipedia: *en.wikipedia.org*; viewed on November 24th 2016
[61] A. Tiihonen; *Preparation of Dye solar cell aging test unit*, Bachelor's thesis at Aalto University, 2011
[62] P Holm; *Mobile solar cell test station*; special assignment at Helsinki University of Technology, 2009
[63] *Agilent 34980A User manual*
[64] T. Esram, P. L. Chapman; *Comparison of Photovoltaic Array Maximum Power Point Tracking Techniques*; IEEE Transactions on Energy Conversion, 2007, vol 22, no 2, pp 439-449
[65] Z. Zhang, S. Ito, J.-E. Moser, S. M. Zakeeruddin, M. Grätzel; *Influence of Iodide Concentration on the Efficiency and Stability of Dye-Sensitized Solar Cell Containing Non-Volatile Electrolyte*; ChemPhysChem, 2009, vol 10, pp 1834-1838
[66] S. G. Hashmi, P. Lund, Performance variations and recovery effects in dye sensitized solar cells during long term exposure to natural winter conditions, 31st European Photovoltaic Solar Energy Conference and Exhibition
[67] Y.-S Jung, B. Yoo, M. K. Lim, S. Y. Lee, K.-J. Kim; *Effect of Triton X-100 in water-added electrolytes on the performance of dye-sensitized solar cells*; Electrochemica Acta, 2009, vol 54, is 26, pp 6286-6291
[68] K. Zhu, S.R. Jang, A. J. Frank; *Effects of water intrusion on the charge-carrier dynamics, performance, and stability of dye-sensitized solar cells*; Energy & Environmental Science, 2012, vol 5, is 11, pp 9492-9495.
[69] M. Hahlin, E. M. J. Johansson, R. Schölin, H. Siegbahn, H. Resnmo; *Influence of Water on the Electronic and Molecular Surface Structures of Ru-Dyes at Nanostructured TiO_2*; The Journal of Physical Chemistry C; 2011, vol 115, is 24, pp 11996-12004
[70] K. Miettunen, J. Halme, A.-M. Visuri, P. Lund; *Two-Dimensional Time-Dependent Numerical Modeling of Edge Effects in Dye Solar Cells*; The Journal of Physical Chemistry C, 2011, vol 115, is 14, pp 7019-7031

A. Manual for outdoor testing station

In this chapter the system features are presented comprehensively. However, for better understanding of the instrument and software operation it is also advised to refer their manuals and guides [A1-A3] and also for previous works [A4-A5] in our group. In Appendix B is given short instructions for performing measurements.

A.1. Cell platform

The schematics of the outdoor cell platform is shown in Fig A1. It has same features as the indoor cell platform for SCATU expect it can be made weatherproof and it supports 32 cells. The cells are placed on the six cross beams such that their copper tape terminals are bent beneath the beam and pressed against the beam with the spring screws of the platform. The spring screws provide the electrical connection between the platform and the cell and they should press the tapes firmly against the beam for strong contact. The springs are marked either with "*P*" or "*C*" for corresponding to the copper tape terminals of the photo- and counter electrodes, respectively (i.e. the springs on the lower sides of the beams are for photo anodes and the springs on the upper sides of the beams are for counter electrodes in Fig A1.) The platform terminals are also numbered from 1 to 32. The terminals 1 to 16 are connected to cable 1 (marked to the connector head) and terminals 17 to 32 are connected to cable 2. An easy way to connect the cells to the platform is to press the springs with e.g. screwdriver and then squeeze the copper tape between the spring and beam.

When all cells for measurements are connected to the platform, the platform should be sealed with detachable plastic covers, see Fig A2. The covers are numbered from 1 to 6 (both lower and higher covers). This means that they are inserted against corresponding beams (beams are also numbered from 1 to 6, see Fig A1.) The shorter covers are placed on the photo anode side (lower in Fig A1) and the higher covers on the counter electrode sides (upper in Fig A1.). The rubber sealant comes between the beam and cover. It is easiest to place the both covers going into the same gap simultaneously. You may need to push slightly the cells out of the way to manage fit the covers in the gaps. Lastly, the covers should go all the way down to the bottom of the gap to ensure waterproofness.

A.2. Roof station

There is an aluminum stand on the roof where the cell platform will be inserted, see Fig A3. The platform is simply hanged to the uppermost beam of the stand close to the pyranometer (the small device with yellow wire in Fig A3). It is recommended to tie the platform to the stand since wind gusts may drop the platform if the tilt of the platform is high. The tilt of the platform is adjustable, ask helping hands from other group members for modifying the tilt.

The cell platform cables are connected to the connection terminal that is the grey electric junction box next to the stand. The terminal has room for several measurement

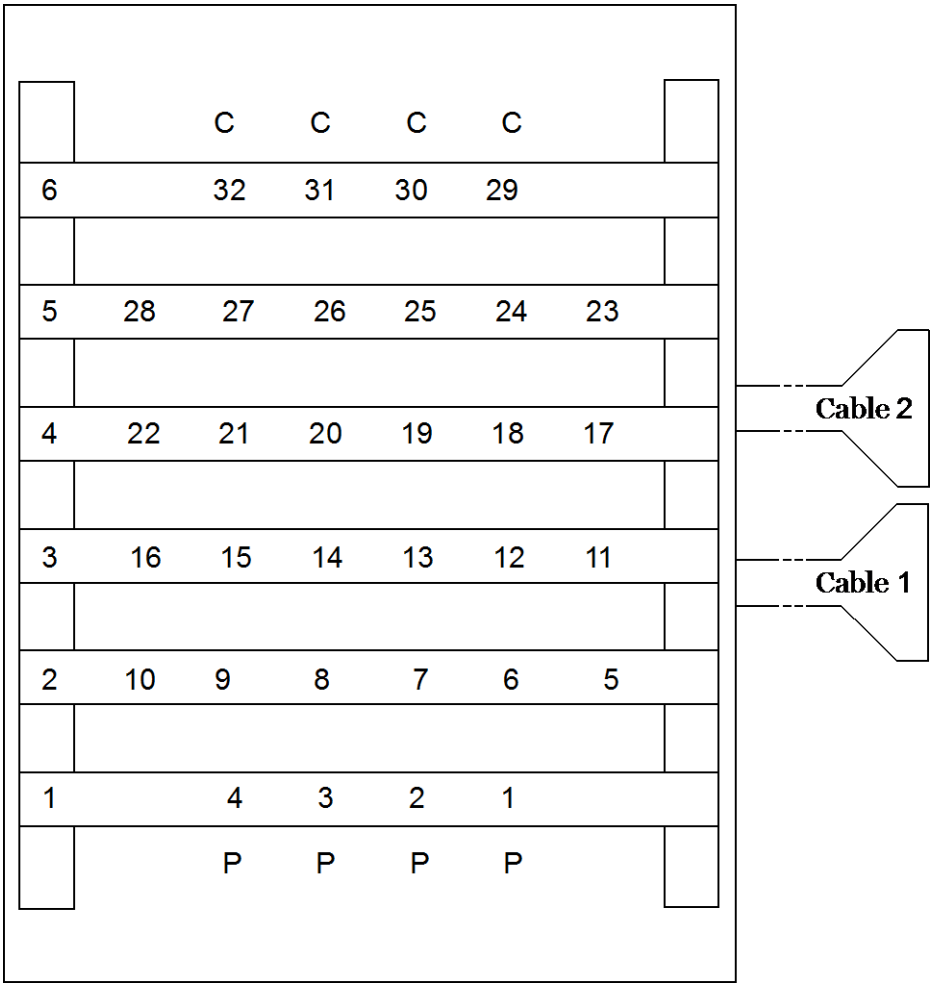

Figure A1. Positions of cells on the cell platform. Cells 1 to 16 are connected to cable 1 and the rest to cable 2. "*P*" indicates the side of photo electrode and "*C*" indicates the side of counter electrode. The numbers from 1 to 6 on left are the numbers of each beam.

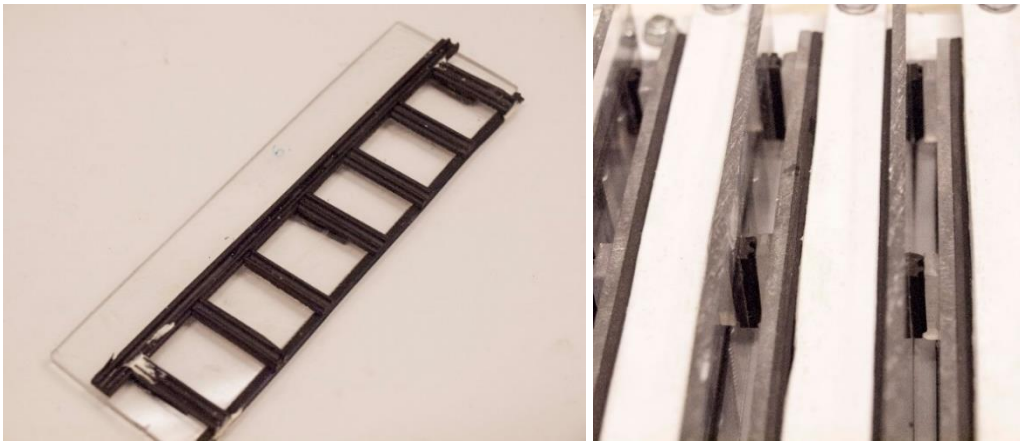

Figure A2. On the left is shown a detachable cover (higher one) and on the right is shown how the covers are placed against the beams.

cables, currently there are two extension cables going down to the lab. When connecting the cables also the ground cables (the metallic wires coming out of the cables) should also be closed. When connections are ready the cover can be closed. The measurement cables and all sensor cables should be fitted to the holes of the cover. Lastly, a sand bag should be placed gently on top of the terminal to prevent wind blowing the cover away. The box has holes in its bottom to ensure that water does not accumulate inside it and the cables are elevated slightly so they do not lie on the bottom of the box.

The connector terminal contains also connections for the weather instruments. At the moment, there are four T-type thermocouple extension wires coming up to the box and a black multicore telephone cable where several free positive/negative cable pairs are remaining for extra instruments. Currently, the black cable hosts the humidity sensor and pyranometer.

Figure A3. Roof station. The cell platform is hanged to the stand next to the pyranometer. The connection terminal is the grey box next to the stand.

A.3. Weather recording.

The pyranometer should be close to the cell platform so that the building southwest does not shadow the pyranometer and cell platform at different times. However, some margin (e.g. 20 cm) should be left between the pyranometer and platform so that the platform does not shadow the pyranometer at evenings.

The ambient temperature sensors (two free brown thermocouple wires with black heads) should be positioned behind the cell platform so they are not heated up by the sun light. The cell temperature sensors are integrated to the stand where the pyranometer is fixed. Sensing the actual cell temperature outdoors is difficult in practice: getting good thermal contact to very small cell is difficult. In addition, wind may cool down differently the thermocouple and the cell and ice may develop between the cell and sensor insulating them thermally from each other. Therefore, the sensors are let to heat up by sun light, which simulates the cell temperature. By a test measurement on a sunny day during 6th of October the difference of the cell temperature and sensor temperature was about ±2°C measured by an infrared camera. However, the current method for cell temperature measurement is still sensitive for wind that may cool down differently the cells and sensors so one should not assume exact relation between the cell temperature and sensor temperature. In future, a thermocouple could be fitted inside a solar cell for more accurate temperature sensing.

Humidity sensor is the small tube in the end of the grey wire and it is attached to the stand. It should not require any special attention during the measurements. Unlike the other sensors, the humidity sensor requires power that is provided by the source measure unit of the setup during the humidity scans.

A.4. Measurement instruments

The measurement system is composed of a source measure unit (SMU, Keysight U2722A), switch unit (Agilent 34980A) and a PC. The SMU takes care of the IV recording and sinks the load current of the cells. The switch unit connect the cell platform to the SMU such that the cells can be both loaded and measured automatically. PC controls the measurements and records the data.

The SMU has three separate channels in total. The first channel is dedicated for IV measurements (hereafter called IV channel) and the rest two for loading the cells (hereafter called load channels). The load channels can sink current simultaneously when the IV channel is performing an IV measurement. Thus, they can be used for constant loading of the test cells.

The switch unit has in total 8 slots for multiplexer cards. Each of these cards have two banks, which again have 20 positive/negative channel pairs. Each of these cards has a d-sub cable with female terminal where the extension wires from the roof station will be connected. These cables are divided into two such that the 16 cell connection wire pairs are connected to the both banks of the card, see Fig A4 for schematics. The bank with smaller channel numbers (hereafter called measurement bank) provides connection between the cell platform and the IV channel of the SMU. The bank with larger channel numbers (hereafter called load bank) provides connection to a load channel of the SMU. When a certain cell is being IV scanned, the switch unit closes the corresponding channel on the measurement bank and opens the corresponding channel on the load bank[5]. When the IV scan is finished, the corresponding channel is reopened on the measurement bank and reclosed on the load bank.

The switch unit cards can be modified to support two separate measurements, too. The modification happens by removing the female d-sub cable from one of the banks of the card and inserting another female d-sub cable to the remaining bank. With this setup, a single card can have a total of 32 cells instead of 16 but the cells cannot be loaded.

The weather sensors are also connected to the switch unit. They are connected to the channels 17-19 of the measurement banks. The switch unit can read the analog voltage signal of these sensors. For thermocouples, the switch unit has a reference temperature junction so it is able to read the thermocouple voltage signals and directly convert them into temperature values.

The banks of the switch unit are numbered such that slot 1 has banks 1 and 2, slot 2 has banks 3 and 4, and so on. The channels are numerated also according to the slots. In slot one there are channels 1001 – 1040 such that channels 1001 – 1020 are in bank 1 and channels 1021 – 1040 are in bank 2. In slot 2 the corresponding channels are 2001 – 2040 and so on.

[5] here, closing a channel means that it is electrically closed, i.e. an electric contact is made and opening is the opposite

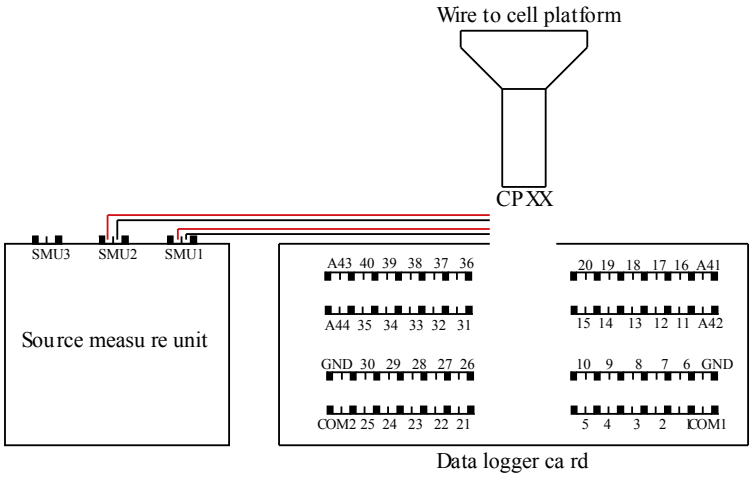

Conne ction scheme

1 -> CP 01	21 -> CP 01
2 -> CP 02	22 -> CP 02
3 -> CP 03	23 -> CP 03
4 -> CP 04	24 -> CP 04
5 -> CP 05	25 -> CP 05
6 -> CP 06	26 -> CP 06
7 -> CP 07	27 -> CP 07
8 -> CP 08	28 -> CP 08
9 -> CP 09	29 -> CP 09
10 -> CP 10	30 -> CP 10
11 -> CP 11	31 -> CP 11
12 -> CP 12	32 -> CP 12
13 -> CP 13	33 -> CP 13
14 -> CP 14	34 -> CP 14
15 -> CP 15	35 -> CP 15
16 -> CP 16	36 -> CP 16
17 -> (free)	37 -> (free)
18 -> (free)	38 -> (free)
19 -> (free)	39 -> (free)
20 -> SMU 1	40 -> SMU 2 (3)
A41 -> (fee)	A43 -> (fee)
A42 -> (fee)	A44 -> (fee)
COM1 -> (fee)	COM2 -> (fee)
GND -> CP GND	GND -> (fee)

Switching p rocedu re du ring measu reme nts

1. Start: every channel open
2. Close channels 22 - 36 and 40
3. Close channels 1 and 20
4. Perform measu reme nts
5. Open channels 1 and 20
6. Close channel 21
7. Open channel 22
8. Close channels 2 and 20
9. Repe at the p rocedu re for every channel
10. Open channels 16 and 20
11. Close channel 36
12. Open channel 21
13. Move to step 3

Figure A4. Connection scheme of the data logger card. The switching procedure of the measurements are also shown in the schematics.

A.5. Connections between instruments

The extension cable is connected similarly to the switch unit as is the cell platform to the extension cable on the roof (also ground cables). For SMU connections there are two alligator clip contacts, see Fig A5. The first one is for IV channel and the second one is for a load channel. The black wires are connected together and red wires are connected together. The humidity sensor also receives its power during the humidity scans from the SMU IV channel. When connections are ready, the instruments can be switched on. The switch unit and computer are switched on from their stand-by switches and the SMU is switched on by inserting its power cable to its power card.

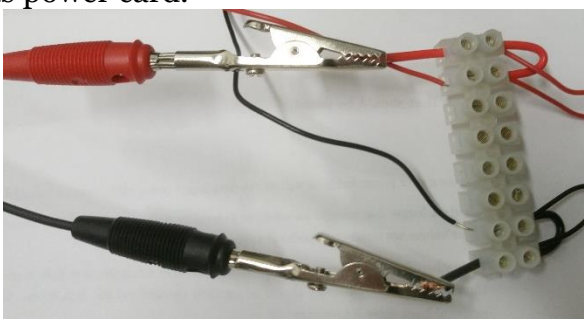

Figure A5. Connection rib for SMU and switch unit. The different measurement banks are connected in parallel to the connection rib. In the SMU measurement channel, there are also wires for the humidity sensor powering.

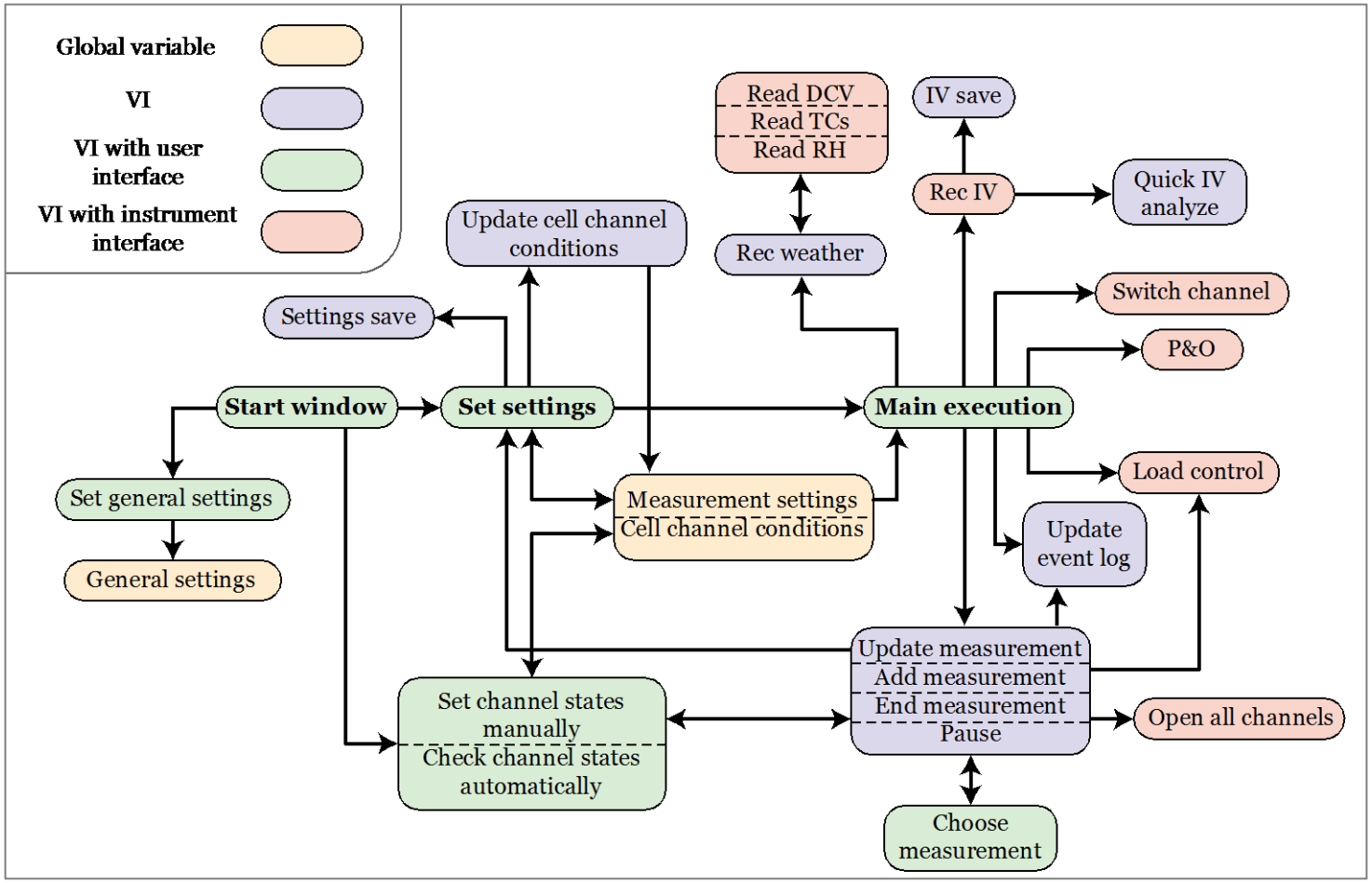

Figure A6 The structure of the measurement program. The rectangles represent single or multiple VIs (similar VIs are combined into one rectangle and are separated by dashed lines.) The arrows represent communication and data flow between different VIs. For example, "Set settings" VI transfers measurement setting parameters to "Settings Save" VI and commands it to save them into a text-file. Double-headed arrows represent situations where a VI commands another VI to execute a task, reads the result from that VI, and continues its own execution according to the obtained result.

A.6. Measurement program

The measurement program is developed with LabVIEW software environment and it is built by modifying the SCATU measurement program. It is composed of several virtual instrument (VI) subprograms that handle different tasks in the measurement program such as writing measurement results into a file or controlling measurement instruments, see Fig A6. The main VIs of the program are “Start window”, “Set settings”, and “Main Execution”. These VIs provide the main user windows and contains the main code for the program. They are presented later in this chapter.

Another important part of the code are the global variables “General settings”, “Measurement settings”, and “Cell channel conditions”. The “General settings” variable contains all the system related parameters that may need to be modified if the system is modified in future, for example a broken sensor is replaced by a different one. These parameters are presented in Table A1. The “Measurement settings” variable contains measurement related parameters that may be unique for each measurement. These parameters are presented later in this chapter. Lastly, the “Cell channel conditions” variable contains the states of each switch unit channel. These channels can be in four different states: “Not connected”, “Connected”, “Measuring”, and “Loading”. The “Not connected” state means that the channel contains no cell and the “Connected” means that the channel has a cell but it is not yet included in a measurement. The “Measuring” state indicates that the channel is dedicated for IV measurements and “Loading” means that the channel is dedicated for electrical loading of the cell. The other VIs shown in Fig A6 are for more specific task and they are presented later in this chapter with the three main VIs.

The program is launched by opening the “Start window” VI, see Fig A7, and pressing the white arrow in the upper left corner of the window. There, the user can launch different settings initialization sub VIs by pressing the corresponding buttons. “Set measurable channels manually” and “Check measurable channels automatically” opens pop-up windows where user can modify which channel contains cells and which not. The given values are updated to the “Cell channel conditions” variable. In the former window the values are given manually and in the latter window the program determines automatically which channels contain cells. This happens by a resistance measurement: if the channel has resistance less than 500 kΩ it has a cell, otherwise not. The automatic version skips all those channels that already have ongoing measurements or are dedicated for loading so their states are not modified with this VI. In the manual version, the channels marked as “Measuring” or “Loading” can also be altered to repair situations where the program has crashed due to some error. The ”Set general settings” button opens another pop-up window where user can modify the parameters shown in table A1. These parameters should be changed only after making modifications to the measurement system and when there are no running measurements.

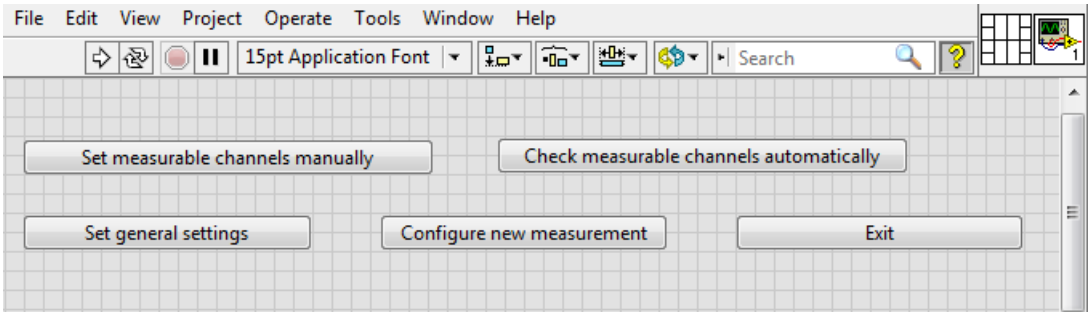

Figure A7. Start window of the measurement program.

Table A1. The values and parameters of the general settings of the measurement program. The default values are the ones used in this work.

Parameter/value	Default value	Comments
U2722A address	(none)	Use NI device finder if the USB port of the instrument is changed for new value.
34980A address	(none)	
Pyranometer sensitivity	70.2 µV	Update after recalibration.
Thermocouple Type	T-type	Update if changed. NOTE, only one thermocouple type allowed at the moment.
Pyranometer channel	1018	Channel of pyranometer signal.
Humidity sensor channel	1019	Channel of humidity sensor signal.
Ambient temp TC channels	2018,2019	Separate multiple channels by comma.
Cell temp TC channels	1017,2017	
SMU Current Range	10 mA	Current and voltage operation ranges of SMU for providing power for the humidity sensor. Check these if sensor is changed.
SMU Voltage Range	20 Volts	
Humidity sensor input (V)	5	Voltage input for humidity sensor.
Sensor start up time (s)	1	Start-up time of the humidity sensor.
Aging voltage step size (V)	0.01	Resolution of the maximum power point tracking voltage. Small values slow down the tracking.

When all the initialization settings are complete, the "Configure new measurement" button can be pressed, which opens the "set settings" VI and its window shown in Fig A8. There, the user can give several parameters and values for the measurement to be started. These possible selections and entries are presented in Table A2. On the next tab, "Aging scheme", the user can define the aging region of the cells during the test. There are four possible options: "Open circuit", "Short circuit", "Constant voltage", "Maximum power point tracking", and "External diode tracking". In open circuit, the cells are not connected to the SMU loading. In short circuit and constant voltage, the cells are connected in parallel by the switch unit and the formed array is kept under 0 V or a set constant

voltage aging, respectively. In maximum power point tracking, the cell array maximum power point is tracked by so-called perturb and observe algorithm (see Chapter 3.8 for the algorithm description). The last option, the external diode tracking, enables replacing the active SMU loading by passive diode loading. The SMU load channel is simply disconnected from the switch unit and a separate passive circuit is inserted in the released connection. On “Test Channels” tab the user can select, which channels will be measured. There, the channel list shows the states of all channels according to the “Cell channel conditions” variable and only channels marked as “Connected” can be selected for new measurement. The channels that will load the cells will be automatically selected later so they should not be marked at this point. On the last tab, “Test sequence” user can define in which order the IV and weather will be recorded.

When all the parameters and values are given, “Save settings” button opens the “Main execution” VI and its window is opened. At the same time, the given parameters and values are added to the “Measurement settings” variable and saved to a text-file and the selected channels and corresponding load channels are updated to the “Cell channel conditions” variable. The values given in this “set settings” window are unique for each measurement so there can be different measurements running at the same time (how to add measurements is described later).

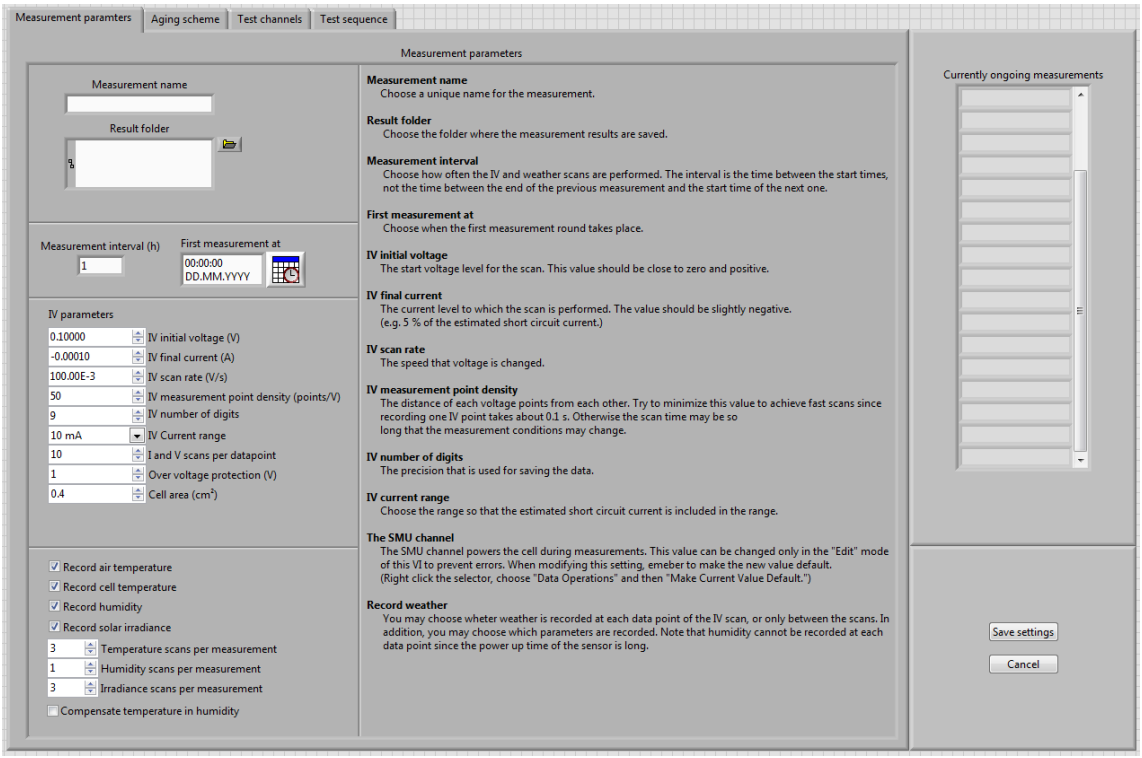

Figure A8. The window of ”set settings” VI.

Table A2. The measurement parameter values and their descriptions. These parameters are unique for each measurement.

Parameter/value	Comments
Measurement name	The name of the measurement is used for distinguish multiple simultaneous measurements from each other.
Result folder	Folder where results are saved. Use unique folder for each measurement
Measurement interval (h)	Interval of the measurements. Describes the time difference between the start time of the executed measurement round and the start time of the next round.
First measurement at	When first measurement will be performed.
IV initial voltage (V)	The start voltage of the IV scan. Should be positive (voltage is decreased in the scan).
IV final current (A)	The lower current limit of the IV scan. Should be negative .
IV scan rate (V/s)	How fast voltage is decreased in the IV scan.
IV measurement point density (points/V)	The density of the measurement points in the scan.
IV number of digits	The accuracy of voltage value in saved text-file. E.g. 9 means that the values are saved with accuracy of 1 nA/nV.
IV Current range	The upper limit of estimated short circuit current.
I and V scans per datapoint	How many times current and voltage are recorded and averaged per data point.
Over voltage protection	A voltage limit to handle situations where lower current limit is never reached for instance due to cell failure.
Cell Area	The active area of the cell.
Record air temperature	Disable if the sensor is not in use or the value is not needed.
Record cell temperature	
Record humidity	
Record solar irradiance	
Temperature scans per measurement	How many times each parameter is read and averaged.
Humidity scans per measurement	
Irradiance scans per measurement	
Compensate temperature in humidity	Filter effect of temperature out from relative humidity value. Actual relative humidity has non-linear dependence on temperature, this compensation is only linear.

The window of "Main execution" VI (referred hereafter shortly as "main VI") is shown in Fig A9. On its first tab is shown the details of all ongoing measurement. There are also buttons "Pause a measurement", "Continue a measurement", "Update a measurement", "Add a measurement", and "End a measurement" whose functions are described in more detail in the following chapter. On the next tab, "Program state" is shown the current state of the program. On the remaining tabs are shown graphs from latest IV graphs and IV parameters for each cell in every measurement and the weather value charts and the event log of the program execution history.

The over mentioned buttons all opens a pop-up window after a while (see next chapter for details for the delay). The window informs that the instruments are released from the program execution and modifications to the system can be made. At this point, the user should add or remove the cell platform(s) what are needed elsewhere or returned to the measurement. Then, user should continue the execution of the program by pressing "Continue measurements" so that the measurement execution will be continued.

In case of "Pause a measurement" another pop-up window opens where the user can select a measurement(s) that will be suspended from continuing execution. This way, the other measurements can continue while some will be left paused. The paused measurement can be continued with the "Continue a measurement" button where the user can simply select what measurements will be continued. A measurement can be ended permanently with the "End a measurement button". There, the same measurement selection pop-up window appears, and it tells to choose the measurement(s) to be ended. In case of "Add a measurement" or "Update a measurement" the "Set settings" window will be opened where the user can modify the settings in similar way as described earlier.

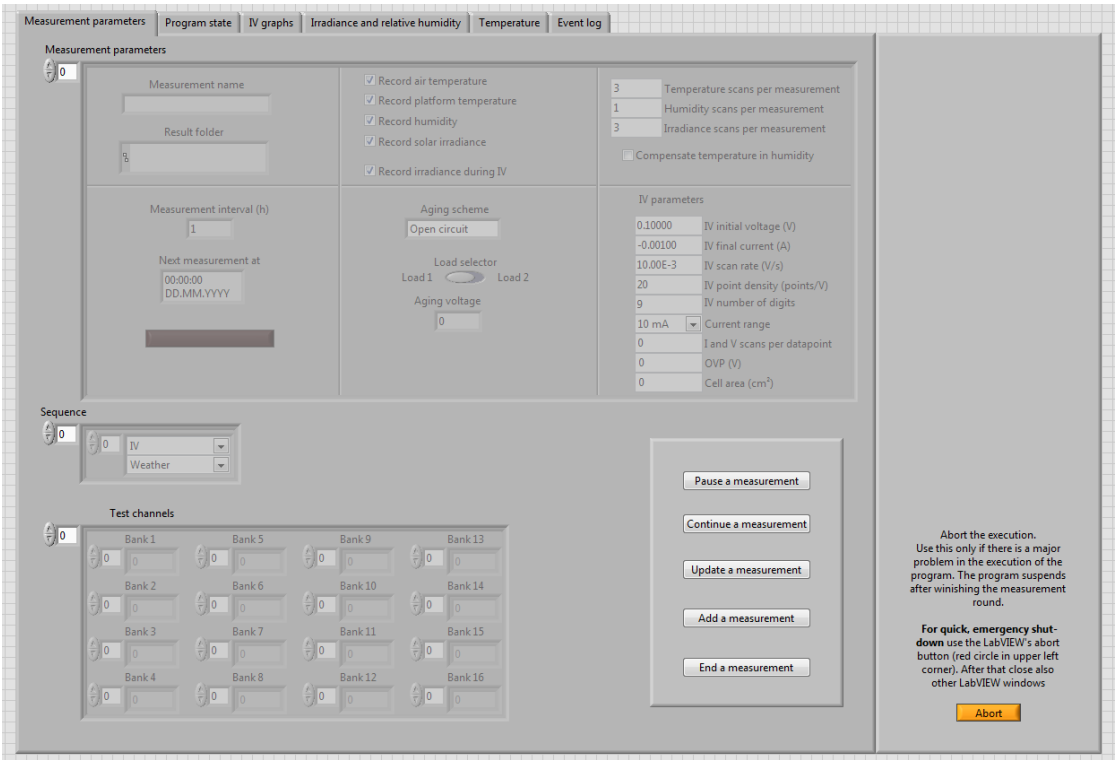

Figure A9. The main window of the measurement program.

The event log on the last tab of the main VI window shows all recent, non-regular activity on the measurement execution. For example, it records if the measurement execution has been paused or a new measurement to the system is added and when this happened. The event log is saved also on a text-file after each event so it is not lost even though the program would crash. The event log is useful if one needs to trace back the time of some event.

In case of an error, there is the orange "Abort" button in the lower right corner of the main window. It allows the user to quickly shut down the measurement execution but in a controlled manner. It still finishes the measurement execution loop (see next chapter). It allows the user to select whether the ongoing measurements can be continued in future. In case of more urgent error, there is a red circle in the upper left corner of the main window next to the white arrow that was used to start the measurement program initially. This immediately stops the measurement execution. It does not stop the operation of the instruments so the SMU will be left sinking current from the loaded cells. In this case, the user should run "Reset instruments" from the desktop of the computer for resetting the instruments.

A.6.1. Description of the main measurement execution

The main VI contains also the main measurement execution loop that handles all the sub-VIs controlling different sub tasks. It has two stages: collect and apply the user given modifications (I) and execute the measurements (II), see Fig 10A for schematics. In the first stage, the main VI checks if user wishes to make modifications to the program execution (described in the previous chapter) and has pressed the corresponding button. If a button has been pressed during the previous round of the loop[6], the corresponding pop-up window is opened and the user can make all the needed modifications. After that, the modifications are loaded from the global variables and the code moves to the second stage.

During the second stage, all the applied measurements are looped through and they are executed. The loop goes through the applied measurement from oldest to newest. First, the loop checks whether the measurement of the iteration is paused or not and whether the defined interval time has passed since its last start moment. If the measurement is either paused or not enough time has elapsed, the loop continues to the next measurement. Otherwise, it begins to measure the cell of the corresponding measurement one by one. For each cell, weather and IV scans are performed according to the selections made during the "set settings" window on the fourth tab "Test sequence".

For weather recording, a "Rec weather" VI is opened. This VI handles the collection of data from the sensors and saving the data into a text file. The VI collects the data from all available sensors with three different VIs. The irradiance data is collected with the "Read DCV" VI that simply performs voltage scans for the pyranometer and converts the voltage signal to irradiance value. The temperature data is collected with the "Read TCs" VI that simply measures the

[6] The program cannot record the modifications in advance and apply them automatically at this point. The reason for this was to save time in programming: the task is not very easy in LabVIEW environment.

thermocouple voltage and converts the voltage reading to temperature. Lastly, the relative humidity value is collected with the “Read RH” VI. This VI first powers up the sensor and then performs the voltage scan for it and converts the voltage reading to humidity. The obtained weather values are converted to text-format and saved into the text file. The values are also sent back to the main VI where they are plotted on chart plots to show the recent weather history.

For IV recording, the main VI first disconnect the cell from loading (if it is being loaded) and connects it to the SMU measurement channel using the “Switch channel” VI. Next, the “Rec IV” VI is launched. This VI performs the IV scan both forward and reverse directions. Then, it saves the data as a text-file using the “IV save” VI and performs an analyze for the obtained IV curve using the “Quick IV analyze VI[7]. It determines the open circuit voltage, short circuit current, fill factor and efficiency of the IV curve if the forward and reverse scans match each other closely and returns the obtained values and the whole IV curve to the main VI. There the IV curve is plotted on a graph and the obtained IV parameters are shown as values.

When all cells are measured, the main VI schedules the start time for the next round for this measurement and moves to the next measurement if there is a one. Otherwise, the main VI moves back to stage one and starts the loop from the beginning. If there are no ongoing measurements (i.e. all measurements are either paused or waiting for next measurement round), the loop simply keep skipping the stage 2 repeatedly until there is again an ongoing measurement.

The maximum power point of the loaded channels is tracked occasionally in the program. If there are ongoing measurements, the maximum power point is tracked using the “P&O” VI after each cell measurement. Otherwise, the tracking is executed once in each round of the program loop. The tracking method is presented in Chapter 3.8 of this work.

A.6.2. About data saving

The weather and IV data is saved each time into a separate text-file with tab-delimiting. This method was chosen to avoid generation of large files. Were each scan appended into a single data file, even for one cell per file, the file sizes could have grown to tens of megabytes. Reading such large files may cause issues during the data analyzation. However, thousands of separate text-files take more space on disk so it is advised to store them in zipped folders.

To distinguish the generated files conveniently, the files were named according to the measurement name, the measurement (weather or IV), channel number, and date. The resulting name could look like “Measurement1_IV_ch2001_on20-11-2016_at14-36-25.txt”.

[7] The ”Quick IV analyze” VI is currently used only for monitoring cell parameters. In future, it is easy to add more sophisticated IV analyzation tools here like diode model fitting.

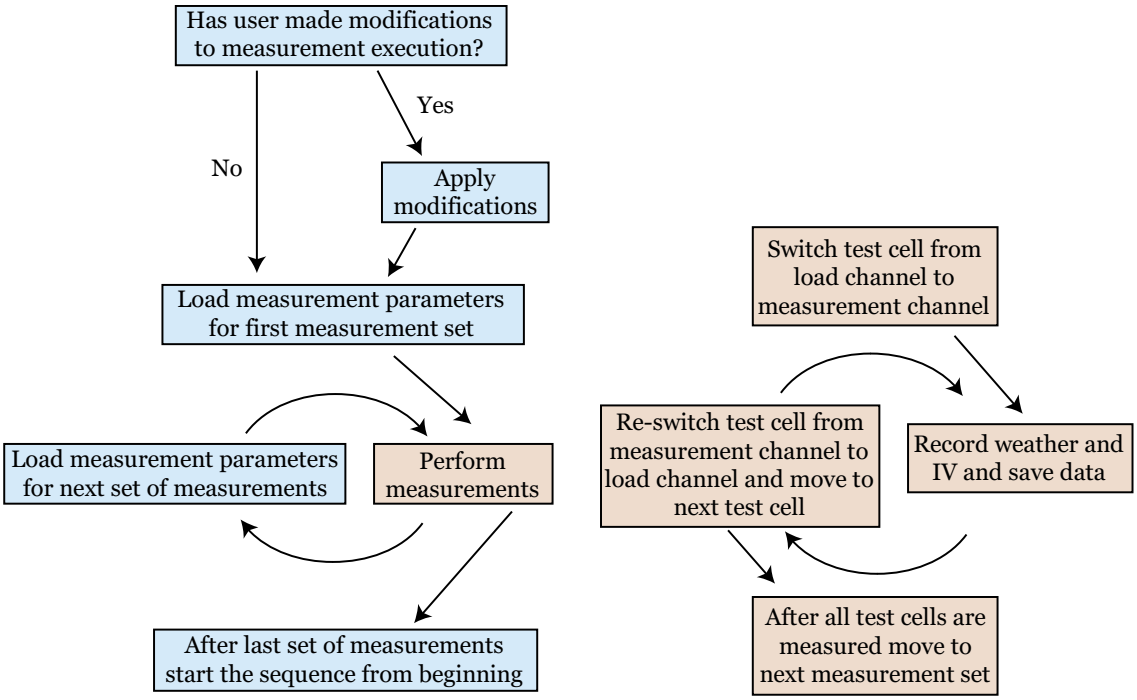

Figure A10. The measurement execution sequence. The program loop starts with the interactive part of the VI. If user wishes to make modifications to the measurement execution (e.g. update measurement parameters of an existing measurement or add a new one) the modifications are performed at this point. Next, the VI starts taking measurements a channel by channel, a set by set.

A.7. Appendix A references

[A1] User manual Keysight U2722A Source measure unit
[A2] User manual Agilent 34980A
[A3] NI LabVIEW Skills Guide: http://www.ni.com/labview/skills-guide/, viewed last on December 15th 2016
[A4] P Holm; Mobile solar cell test station; special assignment at Helsinki University of Technology, 2009
[A5] A. Tiihonen; Preparation of Dye solar cell aging test unit, Bachelor's thesis at Aalto University, 2011

B. Quick instructions

1. Connect the cells to the cell platform (photo electrode to “P” side) and insert the cover sealings to their numbered positions.
2. Connect the cell platform to the connection terminal and connect the ground wireas and close the terminal cover and add a sand bag on top of it gently so the cover does not break. When exiting the roof make sure that the latch closes after you.
3. Check the connections of the switch unit
    a. Connection between extension cables and switch unit (ground cables connected, too)
    b. Connection between switch unit and SMU measurement channel
    c. Optionally, if cells will be aged under load, the connection between switch unit and SMU loading channel has to be connected.
4. Power up the devices and turn on the PC. Password is “solar”
5. Open the “Start Window”. First, check that general settings are OK.
6. Apply the channels with cells into the program by pressing “Set measurable channels manually” or “Check measurable channels automatically” If you know what channels will be measured, use the manual one since it is faster, otherwise use the automatic one.
7. Next, press “Configure new measurement” and apply the parameters on the first tab. On the second tab choose the aging regime. On the third tab, choose the cell channels for measurement. Choose only the channels within the odd banks if you will perform measurement with loading. On fourth tab choose the order of the measurement techniques. It is recommended to make weather scan first so that the program can automatically show real time efficiency values.
8. When all settings are given, press the Save settings button in lower right corner and the program execution starts.

Adding, updating, pausing, continuing, or ending a measurement

- Press the corresponding button on the first tab. If there are ongoing measurements, the program finishes them first before reacting to the button.
- A pop-up window appears telling that the execution is paused and modifications to the system can be made. At this point, insert or remove any cell platforms if needed.
- Next, choose the measurement that will be updated, paused, continued or ended. The measurement execution will continue for those measurements that were not paused or ended. In case of update or adding, the settings window appears. Give the settings and save them and the measurement execution will continue.

Finishing the measurements

- If last measurement was ended, the program execution will stop automatically. After that, press “Exit” also at the start window. Close also the LabVIEW program. Zip your data and transform it to your computer (the zipping may take some time)
- Shut down the computer and the devices.

Error handling

- If a pop-up window appears, and it tells about an error, stop the program execution. The continue option may crash the LabVIEW program, which may leave the instruments in operational state even though the communication is lost. Run the “Reset instruments” from desktop and after that close the LabVIEW software. Restart the computer and instruments. After that, continue the measurements by pressing “Continue measurements after crash”. The program will continue making measurements. Inform others about the occasion.
- For other types of errors, find the appropriate way to close the LabVIEW if possible and continue following the steps above. Otherwise, just find a way to shut down the computer and restart it.